Investigating ER Body Localization and the Splice Variant Function of HOTHEAD in *Arabidopsis thaliana*

by

Therese Marie Francom

A thesis
presented to the University Of Waterloo
in fulfillment of the
thesis requirement for the degree of
Master of Applied Science
in
Biology

Waterloo, Ontario, Canada, 2020

Author's Declaration

I hereby declare that I am the sole author of this thesis. This is a true copy of the thesis, including any required final revisions, as accepted by my examiners.

I understand that my thesis may be made electronically available to the public.

Abstract

Plants live in constantly changing, often unpredictable environments and have evolved diverse strategies to adapt to these changes. The first line of defense for land plants is the cuticle – a layer which covers the epidermis of above ground organs and serves to protect them from desiccation, irradiation, and pathogens. In addition to playing a key role in defense, the cuticle mediates organ separation and expansion. Many genes involved in regulating cuticle formation and function have been identified through forward genetic screens and one such gene is *HOTHEAD* (*HTH*). Plants harboring mutant *hth* alleles show ectopic organ fusion, a phenotype resulting from changes in cuticle permeability. Transgenic plants expressing HTH translationally fused to fluorescent reporter gene constructs fully restore *hth* mutants to wild-type and show that the HTH protein is associated with the endoplasmic reticulum (ER). This study confirmed HTH localization to a specific set of stress inducible ER-derived organelles known as "ER bodies". To further investigate the role of HTH in stress response pathways through its localization to ER bodies, *HTH* transcript and protein expression patterns were examined under stress conditions and were found to respond to both salt shock and methyl jasmonate exposure. In addition, HTH localization to ER bodies was confirmed through subcellular fractionation immunoblot analysis and the examination of the HTH localization pattern within the cells of an ER body mutant plant. The aforementioned studies focused on the full-length HTH protein, however, there are two known isoforms of HTH. The splice variant isoform (SV) is characterized by a 27 amino acid deletion in the fifth exon of HTH which occurs in the middle of a predicted GMC oxidoreductase substrate binding domain. The two isoforms may possess differing functions and expression patterns within the plant. Transgenic plants expressing the SV translationally

fused to fluorescent reporter gene constructs did not restore *hth* mutants to wild-type, thus the confidence level at which conclusions on the function and expression pattern of the SV protein are not high. Expression studies with the SV protein translationally fused to fluorescent reporter gene constructs show that the SV isoform may be associated with the endoplasmic reticulum (ER) as well as ER bodies. Determining the roles that these two isoforms play in cuticle formation/function or stress response could provide insight into pathways by which the stress response or the cuticles of crop plants may be altered to withstand harsher or non-native environmental conditions. If these pathways can be elucidated, mechanisms for global food security could be expanded.

Acknowledgements

I would like to express my gratitude and thanks to my supervisor, Dr. Susan Lolle for her support and guidance throughout my graduate studies. She is an excellent mentor to young scientific minds. I would also like to thank my thesis committee members Dr. Barbara Moffatt and Dr. Simon Chuong for their invaluable expertise and input throughout my thesis studies.

Special thanks to the Holyoak, Craig, Chuong, and Moffatt labs for the use of their lab equipment and guidance.

I would also like to acknowledge the Natural Sciences and Engineering Research Council of Canada (NSERC) for the financial support of this research.

Finally, I would like to thank my friends, family, co-workers and fellow students for their unending support and enthusiasm for my studies. In no particular order; the Francom family, James Bannister, Eric Le Dreff-Kerwin, Nilanth Yogadasan, Quinn Abram, Dr. Mike Mansfield, Katherine Mansfield, Monica Gromala, Louis Pfeifer, Ivan Cadonic, Saeer Adeel, Aranksha Thakor, Alyssa Overton, Delaney Nash, Nikhil George, Alex Ng, Nathan Bennoit, Angus Hilts, Dr. Aaron Frenette, Heather Ikert, Adrian Van Dyk, Carmen Wong, Erica Cushnie, Elizabeth Copley, Jessica Panadero, Maeve Semple, Angela Dangelo and many others.

Table of Contents

List of Figures

List of Tables

List of Abbreviations

Absorbance at 664 nanometers (A_{664})

Absorbance at 647 nanometers (A_{647})

Actin 7 (ACT7)

Adenosine diphosphate (ADP)

Adenosine triphosphate (ATP)

Adenosine triphosphate-binding cassette (ABC)

Adhesion of calyx edges (ACE)

Agrobacterium tumefaciens (*A. tumefaciens*)

Alcohol dehydrogenase (ADH)

Amino acid (aa)

Arabidopsis thaliana (*A. thaliana*)

Base pair (bp)

Basic leucine zipper (bZIP)

β-glucosidase (BGLU)

β-glucuronidase (GUS)

Binding immunoglobulin protein (BiP)

Bodyguard (BDG)

Bovine serum albumin (BSA)

Carbon (C)

Centimeter (cm)

Centrifugal force (xg)

Chopping buffer (CB)

Coat protein 2 (COPII)

Coefficient of variance (CV)

Coenzyme A (CoA)

Columbia ecotype (Col)

Complementary deoxyribonucleic acid (cDNA)

Concentration of a solution – volume by volume percent (v/v)

Concentration of a solution – weight by volume percent (w/v)

Constitutively expressed ER bodies (cER bodies)

Cycle threshold (C_T)

Cytochrome P450 77 (CYP77)

Days after flowering (DAF)

Degrees celsius (°C)

Deoxyribonucleic acid (DNA)

Derived cleaved amplified polymorphic sequences (dCAPS)

Embryo sac development arrest 17 (EDA17)

Endoplasmic reticulum (ER)

Endoplasmic reticulum-retention signal: Lysine (K) - Aspartic acid (D) - Glutamic acid (E) - Leucine (L) (KDEL); Histidine (H) - Aspartic acid (D) - Glutamic acid (E) - Leucine (L) (HDEL); Arginine (R) - Glutamic acid (E) - Glutamic acid (E) - Leucine (L) (REEL)

Endoplasmic reticulum-retention signal KDEL-like: Lysine (K) - Aspartic acid (D) - Glutamic acid (E) - Lysine (K) (KDEK); Lysine (K) - Lysine (K) - Glutamic acid (E) - Leucine (L) (KKEL); Lysine (K) - Asparagine (N) - Glutamic acid (E) - Leucine (L) (KNEL)

Enhanced chemiluminescence substrate (ECL)

Enhanced yellow fluorescent protein (EYFP)

Escherichia coli (*E. coli*)

Ethylenediaminetetraacetic acid (EDTA)

Ethyl methanesulfonate (EMS)

Excitation/emission wavelengths (ex/em)

Fatty acid elongase (FAE)

Fatty acyl ω-hydroxylase (FAH)

Flavin adenine dinucleotide (FAD)

Fructosidase 4 (AtFruct4)

GDSL lipase-like protein (GLL)

Glabra (GL)

Glucose-methanol-chlorine oxidoreductase (GMC oxidoreductase)

Glyceraldehyde-3-phosphate dehydrogenase C-2 (GAPC2)

Glycerol 3-phosphate acyltransferase (GPAT)

Glycosylphosphatidylinositol (GPI)

Grams (g)

Green fluorescent protein (GFP)

HEAT SHOCK PROTEIN 70 (Hsp70)

Honestly significant difference (HSD)

Hothead (HTH)

HOTHEAD promoter driven expression of *HOTHEAD* translationally fused to *G3 GREEN FLOURESCENT PROTEIN* (*HTH_{pro}:HTH-G3GFP* and *HTH_{pro}:HTH-GFP*)

HOTHEAD promoter driven expression of *HOTHEAD* translationally fused to ENHANCED *YELLOW FLOURESCENT PROTEIN* (*HTH_{pro}:HTH-EYFP*)

HOTHEAD promoter driven expression of the splice variant form of HOTHEAD translationally fused to ENHANCED *YELLOW FLOURESCENT PROTEIN* (*HTH_{pro}:SV-EYFP*)

Hydrogen (H)

Hydrogen cyanide (HCN)

Hydroxynitrile lyase (HNL)

Immunoglobulin G (IgG)

Independently transformed transgenic lines (ITL)

Induced ER bodies (iER bodies)

Inositol-requiring enzyme1 (IRE1)

Jacalin-related lectin (JAL)

Kilobase (kb)

Kilodalton (kDa)

Lipid transfer proteins (LTP)

Litre (L)

Leaf endoplasmic reticulum bodies (L-ER bodies)

Long-chain acyl-coenzyme A (LACS)

Long-chain fatty acid (LCFA)

Mandelonitrile lyase (MDL)

Mandelonitrile lyase 2 of *Prunus dulcis* (PdMDL2)

Membrane of endoplasmic reticulum body (MEB)

Messenger ribonucleic acid (mRNA)

Meter (m)

Methyl jasmonate (MeJA)

Microgram (µg)

Microlitre (µl)

Micrometer (µm)

Micromole (µmol)

Milligram (mg)

Millilitre (ml)

Millimolar (mM)

Minute (min)

Molar (M)

Murashige and Skoog basal medium (MS)

Nanograms (ng)

Nanometer (nm)

Nanomole (nmol)

Nicotinamide adenine dinucleotide phosphate (NADPH)

Nitrogen (N)

ω-hydroxy fatty acyl dehydrogenase (HFADH)

ω-oxo fatty acyl dehydrogenase (OFADH)

Ovule inner integuments (ii1, ii1', ii2)

Ovule outer integuments (oi1, oi2)

Pellet (P)

Polymerase chain reaction (PCR)

Polyvinylidene difluoride (PVDF)

Protein kinase C (PKC)

PYK10 binding protein 1 (PBP1)

Pyranose dehydrogenase of *Agaricus meleagris* (AmPDH)

Quantitative real time polymerase chain reaction (qRT-PCR)

Rate of chlorophyll extraction (RCE)

Reactive oxygen species (ROS)

Responsive-to-desiccation 21 (RD21)

Reverse transcription (RT)

Ribonucleic acid (RNA)

Root apical meristem (RAM)

Second (sec)

Shoot apical meristem (SAM)

Sodium (Na)

Sodium chloride (NaCl)

Sodium dodecyl sulphate (SDS)

Sodium hydroxide (NaOH)

Spectinomycin (Spec)

Splice variant isoform of HOTHEAD (SV)

Supernatant (S)

Toluidine blue O (TBO)

Tonsoku-associated protein 1 (TSA1)

Total (T)

Transformed generation (T)

Transparent testa glabra 1 (TTG1)

Trisaminomethane (Tris)

Trisaminomethane-buffered saline (TBS)

Trisaminomethane-buffered saline with Tween 20 (TBS-T)

Trisaminomethane-chloride (Tris-Cl)

Ultraviolet (UV)

Unfolded protein response (UPR)

Unit of an enzyme's catalytic activity (U)

Upstream open reading frame (uORF)

Very long-chain fatty acid (VLCFA)

Wassilewskija ecotype (Ws)

Water-soluble chlorophyll-binding protein (WSCP)

Alpha (α)

Beta (β)

Omega (ω)

DNA code

Adenine (A)

Cytosine (C)

Guanine (G)

Thymine (T)

Protein code

Alanine (A)

Arginine (R)

Asparagine (N)

Aspartic acid (D)

Cysteine (C)

Glutamic acid (E)

Glutamine (Q)

Glycine (G)

Histidine (H)

Isoleucine (I)

Lysine (K)

Methionine (M)

Phenylalanine (F)

Proline (P)

Serine (S)

Threonine (T)

Tryptophan (W)

Tyrosine (Y)

Valine (V)

Chapter 1: General Introduction

1.1 The Cuticle

1.1.**1** Cuticle function

The main function of the cuticle is protection; the cuticle serves as the interface between the plant and its external environment (Riederer and Schreiber, 2001). It is a hydrophobic layer found external to the cell walls of shoot epidermal cells - e.g. leaves, trichomes, floral tissues, and the stem - of most plants (Bessire et al., 2007; Hegebarth et al., 2016; Hegebarth and Jetter, 2017; Li-Beisson et al., 2009; Xue et al., 2014). The cuticle prevents dehydration, allows for the movement of select molecules (i.e. signalling molecules and charged molecules), reduces the negative effects of UV irradiation, and limits attacks from insects and pathogens (Eigenbrode and Jetter, 2002; Kerstiens, 1996; Lolle and Pruitt, 1999; Ziv et al., 2018). Over the past couple decades, research into the cuticle has uncovered unexpected associations between the cuticle, development, and defense.

The cuticle protects the plant from many environmental stressors, but also plays a principal role in maintaining distinct organ boundaries during plant development (Ingram and Nawrath, 2017; Lolle et al., 1992). Mutations that affect cuticle composition or structure generally give rise to plants with ectopic organ fusions (Bird et al., 2007; Ingram and Nawrath, 2017; Lolle et al., 1992; Sieber et al., 2000; Wellesen et al., 2001). The fusion zones between organs in these mutants often have a disrupted or malformed cuticle layer; in wild-type plants, the cuticle layer would normally serve as an inert barrier between the epidermal cell walls of the respective organs involved thereby maintaining organ separation (Ingram and Nawrath, 2017; Sieber et al., 2000). Taken together, these studies demonstrate a role for the cuticle in organ partitioning.

During sexual reproduction, the cuticle is involved in cell-cell signaling and acts as a selectively permeable barrier. The cuticle acts as a water diffusion barrier regulating pollen germination on stigma papillary cells; this results in pollen adhesion followed by recognition of compatible pollen, hydration, and pollen tube growth (Lolle and Pruitt, 1999; Sieber et al., 2000). Small (< 1 kilodalton), water-soluble molecules can diffuse through organ fusion zones separated by the cuticle (Ingram and Nawrath, 2017; Siegel and Verbeke, 1989; Verbeke and Walker, 1986).

The cuticle is the plant's first line of defence against pathogen invasion and/or tissue damage through insect herbivory. In order to invade plants, pathogens must break through the cuticle layer; most pathogens employ a two-part attack consisting of an initial mechanical rupture of the cuticle layer followed by excretion of enzymes such as cutinase to hydrolyse cutin polymers creating an opening into the plant (Deising et al., 2000; Longhi and Cambillau, 1999). The hydrolysis of cutin polymers results in the production of cutin monomers which can elicit plant defense responses such as hydrogen peroxide production (Schweizer et al., 1996; Ziv et al., 2018). This demonstrates the cuticle's essential role in physically defending the plant as well as its role in triggering the plant defense pathway.

1.1.**2** Cuticle structure and composition

The cuticle is a heterogeneous structure made up of waxes, cutin polymers, and polysaccharides, however, the composition of the cuticle can differ between plant species, developmental stages, and in response to environmental stimuli. The prevailing model of cuticle structure describes the cuticle as being composed of the "cuticular layer" and the "cuticle proper" (Fernández et al., 2016; Yeats and Rose, 2013) (Figure 1.1 A). The cuticular layer is located between the epidermal polysaccharide cell wall and the cuticle proper; the cuticular layer is mainly composed

of cutin polymers and polysaccharides (Heredia-Guerrero et al., 2014) (Figure 1.1 A). The cuticle proper is located at the surface of the plant and directly interfaces with the external environment; this region is composed of cutin polymers and is enriched in waxes (Yeats and Rose, 2013) (Figure 1.1 A). Waxes found within the cutin matrix - intracuticular waxes - are surrounded by cutin polymers forming dense regions; waxes deposited on the surface of the matrix - epicuticular waxes - form a waxy film that acts to protect the plant against environmental assaults (Yeats and Rose, 2013).

The wax compounds found in the cuticle are highly hydrophobic and are present in a mixture of very long-chain fatty acids (VLCFA) (C24-C34), alcohols, alkanes, esters, and triterpenoids (Fernández et al., 2016; Samuels et al., 2008) (Figure 1.1 B). Long-chain fatty acids (LCFAs) (C16-C18) are converted to coenzyme A (CoA) thioesters in the plastid of epidermal cells by a long-chain acyl-coenzyme A synthase (LACS) (Lue et al., 2009) (Figure 1.1 B). The LCFA acyl-CoA's are transported to the endoplasmic reticulum (ER) where the fatty acid elongase (FAE) complex adds carbons to LCFA acyl-CoA resulting in VLCFAs (Haslam and Kunst, 2013) (Figure 1.1 B). Waxes are thought to be transported to the plasma membrane into the cuticle proper through Golgi-dependent or -independent exocytosis, adenosine triphosphate-binding cassette (ABC) transporters, or with the help of glycosylphosphatidylinositol (GPI)-anchored or apoplastic lipid transfer proteins (LTP) (McFarlane et al., 2010; Shi et al., 2018; Yeats and Rose, 2008).

Cutin compounds in the cuticle are less hydrophobic than waxes and are mainly composed of interesterified hydroxy fatty acids and dicarboxylic acids with a low abundance of glycerol and phenylpropanoids (Pollard et al., 2008). The main hydroxy fatty acids found in the cuticle are ω-

hydroxy fatty acids consisting of midchain hydroxyl, oxo, or epoxy groups; these groups may be esterified to form linkages with other cutin monomers resulting in branched structures (Pollard et al., 2008; Yeats and Rose, 2013). The cutin found in the floral organs of *A. thaliana* adheres to the norm with a ω-hydroxy fatty acid dominant cuticle (Li-Beisson et al., 2009). The cutin found in the leaves and stems of *Arabidopsis thaliana* (*A. thaliana*) deviate from this norm; the main hydroxy fatty acids found in the leaf and stem cuticle are α-ω-dicarboxylic acids (Bonaventure et al., 2004; Pollard et al., 2008).

Cutin monomers, like waxes, begin their synthesis within the plastid of epidermal cells; the LCFAs are transported to the ER where LACS enzymes synthesize the acyl-CoA chain which undergoes ω-hydroxylation by fatty acyl ω-hydroxylase (FAH) and midchain hydroxylation by enzymes in the CYTOCHROME P450 77 (CYP77) family (Li-Beisson et al., 2009; Lü et al., 2009) (Figure 1.1 B). From here, ω-hydroxy fatty acyl dehydrogenase (HFADH) and ω-oxo fatty acyl dehydrogenase (OFADH) can convert hydroxy fatty acids to dicarboxylic fatty acids (Yeats and Rose, 2013) (Figure 1.1 B). Glycerol 3-phosphate acyltransferase (GPAT) synthesizes 2-monoacylglycerol esters of hydroxy fatty acid or dicarboxylic fatty acid cutin monomers (Yang et al., 2012) (Figure 1.1 B). These compounds may be transported across the plasma membrane, into the cuticular layer and cuticle proper utilizing a pathway like that described for cuticular wax export (Bessire et al., 2011; McFarlane et al., 2010; Panikashvili et al., 2011). It has been proposed that the glycerol moiety of the 2-monoacylglycerol esters allow the compounds to move through the hydrophilic cell wall of epidermal cells (Yeats et al., 2012). Alternatively, cutin monomers may bind to polysaccharides within the cell wall to facilitate movement from the cell into the cuticle layers (Yeats and Rose, 2013).

Polysaccharides are the third main class of compounds found within the cuticle; these compounds are hydrophilic and have a high instance of H-bonding within the cuticle. Originally, the cuticle was believed to be free of polysaccharides (Fernández et al., 2016; von Mohl, 1847), however, many studies have found evidence of their presence throughout the cuticle layer (Fernández et al., 2016; Guzman et al., 2014). Polysaccharides such as pectin, cellulose, and hemi-cellulose are thought to originate from the epidermal cell wall and are essential in providing a base for cuticle formation during development (Guzman et al., 2014; Lopez-Casado et al., 2007). The cuticular layer carries a net negative charge which is thought to be due to the presence of polysaccharides; this charge gradient allows the cuticle to regulate the transport of ions and charged molecules (Domínguez et al., 2011; Heredia and Benavente, 1991). Polysaccharides also play a role in regulating water transport and retention within the cuticle (Zwieniecki et al., 2001).

1.1.**3** The seed coat

In *Arabidopsis*, the embryo and endosperm are encased in a seed coat; the seed coat regulates the growth of the embryo and endosperm during development (Beeckman et al., 2000; Creff et al., 2015) and acts as a protective layer once the embryo has fully developed (Beeckman et al., 2000; Raviv et al., 2017). The seed coat, unlike the embryo and endosperm, is maternally derived - it is composed of five cell layers that are derived from ovule integuments that are of epidermal origin (Beeckman et al., 2000; Raviv et al., 2017; Robinson-Beers et al., 1992). There are two ovule integuments - the outer (oi) and inner (ii) integument - each is made up of two cell layers - an outer (2) and an inner (1) layer - however, the ii has an additional internal layer (ii1') between the ii2 and ii1 layers (Figure 1.2). At the one-cell stage of embryo development, cells in the ii1

layer develop vacuoles (Beeckman et al., 2000). Additionally, an electron-dense layer is found to border cells of the ii1 layer that are in direct contact with the embryo sack (Beeckman et al., 2000). This electron-dense layer is thought to be a cuticle layer and is present throughout embryo development (Beeckman et al., 2000). At the torpedo-stage, the periclinal walls of the oi1 layer cells thicken with an electron-dense substance - this thickened wall is referred to as "wall 3" and represents a zone of fusion between the oi1 and ii2 layers (Beeckman et al., 2000; Creff et al., 2015) (Figure 1.2). The oi1 layer is thought to respond to the mechanical stress of embryo expansion pushing on the seed coat (Creff et al., 2015). This results in the deposition of cutin-like material from the oi1 layer into wall 3 (Creff et al., 2015; Ingram and Nawrath, 2017; Luo et al., 2005). The deposition of cutin-like monomers thickens wall 3 which has been shown to regulate seed size (Creff et al., 2015; Luo et al., 2005). The electron-dense layers found in wall 3 and ii1 are thought to be primarily composed of cutin-like material typical of shoot epidermal cuticles (Beeckmann et al., 2000; Creff et al., 2015; Molina et al., 2008). Conversely, it was found that the oi2 layer was also electron-dense, although it was composed of suberin-like materials rather than cutin (Beisson et al., 2007; Molina et al., 2008).

The seed coat is essential in maintaining seed dormancy. The oi2 layer is specially designed for rupture and mucilage release upon contact with water under the right environmental conditions (Dean et al., 2007). However, it is unknown whether this oi2 layer is responsible for seed coat permeability or whether a cutin layer within the seed coat such as the one found in wall 3 or ii1 regulates permeability.

1.2 Plant Stress Responses

1.2.**1** The role of the endoplasmic reticulum in stress

The ER is a complex membrane system found in both plants and animals; it is important in the synthesis, folding, modification, and transport of proteins, it is also involved in detecting and responding to stress (Deng et al., 2013; Ellgaard and Helenius, 2003; Schroder and Kaufman, 2005). Proteins produced by ribosomes fold into a unique three-dimensional structure within minutes, however, aberrant, or misfolded, proteins can occur. These aberrant proteins accumulate in the ER which can lead to a variety of diseases and/or cell death (Llamas et al., 2017; Ohta and Takaiwa, 2014). There are two main processes that the ER employs to deal with aberrant proteins. The first involves protein folding using molecular chaperones, and the second, protein degradation using proteasomes (Ohta and Takaiwa, 2014). There are many molecular chaperons, one of which is HEAT SHOCK PROTEIN 70 (Hsp70) which belongs to the HSP70 molecular chaperone system (Mayer, 2013). Hsp70 binds exposed hydrophobic regions within misfolded proteins; Hsp70 folds the misfolded protein into the correct configuration by complexing with the co-chaperone Hsp40 and a nucleotide exchange factor (Mayer, 2013). If misfolded proteins are not correctly folded, they are degraded by proteasomes (Ohta and Takaiwa, 2014).

Under conditions of stress, misfolded proteins aggregate within the ER. This aggregation overwhelms the ER's quality control system which triggers a state of ER stress (Ellgaard and Helenius, 2003; Schroder and Kaufman, 2005). ER stress is communicated to the nucleus through the unfolded protein response (UPR), a response designed to increase the ER's capacity to degrade large amounts of aggregated proteins that accumulate under stress (Fontes et al., 1991; Ruberti and Brandizzi, 2018, Vitale and Boston, 2008). If the ER is not able to combat the

stress of mounting unfolded proteins, the cell will undergo programmed cell death (Howell, 2013).

There are two main pathways by which ER stress is sensed. The first involve membrane-associated basic leucine zipper (bZIP) transcription factors bZIP28 and bZIP17, and the second, the membrane-associated protein kinase/ribonuclease INOSITOL-REQUIRING ENZYME1 (IRE1) (Koizumi et al., 2001; Liu et al., 2008; Srivastava et al., 2013). Under conditions of stress, the molecular chaperone binding protein - binding immunoglobulin protein (BiP) - is localized to misfolded proteins, this releases BiP associated bZIP17/28 proteins (Gao et al., 2008; Srivastava et al., 2013). Free bZIPs cluster with coat protein 2 (COPII) vesicle elements in the ER membrane and are transported from the ER to the Golgi where they are cleaved, releasing the N-terminal domain which is transported to the nucleus and activates UPR target genes (Liu et al., 2007; Srivastava et al., 2012).

The other pathway by which ER stress is sensed is through IRE1 activation. Activated IRE1 splices bZIP60 mRNA resulting in mRNA encoding a bZIP60 variant with a nuclear targeting signal (Deng et al., 2011; Liu and Howell, 2016). Once in the nucleus, these bZIP transcription factors dimerize forming homo- (bZIP60 with bZIP60) or hetero- (bZIP60 with bZIP17 dimers which act to upregulate stress responsive genes (Liu et al., 2007; Liu and Howell, 2010).

1.2.**2** ER bodies

The ER is instrumental in processing proteins and packaging some of those proteins for transport. The ER forms many bodies containing various proteins, these bodies bud off the ER and are transported around the cell (Hara-Nishimura et al., 2004). There are two types of ER-derived organelle, those involved in storage and those involved in plant defensive (Hara-

Nishimura et al., 2004). Most of the ER-derived organelles involved in housing defensive proteins are similar in shape and content; they are spherical, small - ranging from 0.05-2 μm in diameter - and enriched in proteases (Chrispeels and Herman, 2000; Hara-Nishimura et al., 2004; Hayashi et al., 2001). However, in plants belonging to the order Brassicales, an entirely different ER-derived organelle, known as the ER body, is formed. ER bodies are spindle-shaped, large - ~5-10 μm in length and ~1 μm in diameter - and contain high amounts of a β-glucosidase known as PYK10/BGLU23 - a member of the β-glucosidase (BGLU) family of proteins (Matsushima et al., 2003b; Sherameti et al., 2008).

ER bodies are found constitutively expressed (commonly referred to as cER bodies where 'c' indicates constitutive) in the epidermal cells of young *A. thaliana* seedlings and in the roots of mature *A. thaliana* plants (Hayashi et al., 2001). More recently, another type of constitutively expressed ER body has been identified that is limited to only three different types of leaf cells and have been designated as L-ER bodies where the 'L' stands for leaf (Nakazaki et al., 2019a). *De novo* formation of ER bodies is induced upon methyl jasmonate (MeJA) and/or wounding stress (Matsushima et al., 2002) and is commonly referred to as iER bodies where 'i' indicates induced; iER bodies are found within the rosette leaves of mature, wounded *A. thaliana* plants (Ogasawara et al., 2009) whereas constitutively expressed ER bodies (cER bodies) are absent (Hayashi et al., 2001; Matsushima et al., 2002). The expression of iER bodies in response to wounding or MeJA - a wounding hormone involved in plant defense - indicates a role for ER bodies in plant defence.

Mutants with altered or no cER bodies have aided in elucidating the pathway by which cER bodies are formed (Matsushima et al., 2003; Nagano et al., 2008; Yamada et al., 2008; Yamada et al., 2013). NAI1 is a basic helix-loop-helix transcription factor which regulates the formation

of cER bodies in *A. thaliana* seedlings (Matsushima et al., 2004). NAI1 regulates the expression of genes involved in ER body formation such as *NAI2*, *PYK10*, *MEMBRANE OF ER BODY* (*MEB*) *1* and *MEB2* (Matsushima et al., 2004). NAI2 aggregates PYK10 proteins which initiates the formation of cER bodies from the ER (Yamada et al., 2008) (Figure 1.3). A study by Yamada et al. (2020) showed that when NAI2 and PYK10 are expressed simultaneously in onion cells, spindle-shaped ER bodies were formed indicating that NAI2 and PYK10, when expressed together, are sufficient to trigger ER body formation in non-Brassicaceae plant cells (Yamada et al., 2020).

In addition to PYK10, NAI2 also complexes with MEB1 and MEB2 directing these proteins to the budding cER body membrane (Yamada et al., 2013) (Figure 1.3). Once enough PYK10 and other cER body resident proteins have accumulated, the cER body will bud off from the ER (Yamada et al., 2008) (Figure 1.3).

NAI1 regulates genes encoding proteins that do not localize to ER bodies such as *JACALIN-RELATED LECTIN* genes (*JAL22, 23, 31*, and *JAL30/PYK10 BINDING PROTEIN 1* (*PBP1*)) and *GDSL LIPASE-LIKE PROTEIN* genes (*GLL23* and *GLL25*) (Nagano et al., 2005, 2008; Nakano et al., 2012). JAL proteins are believed to localize to the cytosol while GLL proteins localize to the vacuole; under cell disruption JAL, GLL, and PYK10 form a large aggregate and become insoluble (Nagano et al., 2005, 2008). This insoluble PYK10 complex has higher enzyme activity (Nagano et al., 2005, 2008).

PYK10 is the major protein component of cER bodies, however, there are other proteins that reside within ER bodies. RESPONSIVE-TO-DESICCATION 21 (RD21) and FRUCTOSIDASE 4 (AtFruct4) are both vacuolar enzymes which remain inactive until the ER fuses with the

vacuole (Hayashi et al., 2001; Rojo et al., 2003). WATER-SOLUBLE CHLOROPHYLL-BINDING PROTEIN (WSCP) has also been shown to localize to cER bodies (Takahashi et al., 2012). It is believed that upon mechanical wounding, WSCP is released into the cytosol where it binds chlorophylls within damaged thylakoid membranes preventing the chlorophylls from generating reactive oxygen species (ROS) (Takahashi et al., 2012). It is also hypothesized that upon fusion of the ER body with the vacuole, WSCP may act as a serine protease inhibitor to inhibit proteases within the vacuole (Takahashi et al., 2012). Other proteins that are suspected of localizing to ER bodies are BGLUs 18-25 (Xu et al., 2004). This is based on comparing the sequence similarity between these BGLUs and PYK10, additionally, these BGLU protein all contain an ER retention signal at their C-terminus just like PYK10 (Xu et al., 2004). Interestingly, it was determined that BGLU21 does localize to cER bodies (Nagano et al., 2009; Yamada et al., 2020) and BGLU18 localizes to iER bodies (Ogasawara et al. (2009).

The study by Ogasawara et al. (2009) showed that protein constituents differ between iER bodies and cER bodies. In this study, they showed evidence of BGLU18 localization to iER bodies, but not cER bodies while PYK10 localized only to cER bodies, but not iER bodies. This supports the predictions made by Xu et al. (2004) and indicates that there are two distinct types of ER bodies with different protein compositions: cER bodies and iER bodies. Recent studies have found that a close homolog of NAI2 plays a role in the formation of iER bodies – TONSOKU-ASSOCIATED PROTEIN 1 (TSA1) (Geem et al., 2019). This further supports the idea that cER bodies and iER bodies are distinct.

1.2.**3** ER bodies and the glucosinolate pathway

PYK10 is a myrosinase, and like other myrosinases, is involved in plant defence against

herbivory and fungal infection through the production of toxic compounds upon exposure to the substrate glucosinolate (Rask et al., 2000; Sherameti et al., 2008). Glucosinolates are stored within the vacuole of the cell (Shirakawa and Hara-Nishimura, 2018). Under stress conditions Hayashi et al. (2001) showed that ER bodies fuse to the vacuole, bringing glucosinolates into contact with myrosinases resulting in the production of toxic compounds (cyanogenesis) (Yamada et al., 2020). Myrosinases catalyze the conversion of thioglucosides to thiocyanates, isothiocyanates, nitriles, or epithionitriles which are all toxic compounds (Halkier and Gershenzon, 2006; Wittstock and Halkier 2002).

The products of glucosidase breakdown by myrosinases depends heavily on the surrounding environment; under a neutral pH the main product is isothiocyanate; under a pH less than 5, or in the presence of ferrous ions, the main product is nitrile (Halkier and Gershenzon, 2006; Lambrix et al., 2001). Hydroxynitriles produced from this reaction can be further catalyzed by hydroxynitrile lyases to produce hydrogen cyanide (Brabban and Edwards, 1995; Kissen and Bones, 2009).

The hydrogen cyanide produced through the breakdown of glucosinolates contributes to plant defence, deterring herbivory as its toxicity acts as a natural insecticide (Machingura et al., 2016). However, this build up of cyanide is also toxic to the plant. Most of the cyanide is detoxified through β-cyanoalanine synthase leaving any remaining cyanide at non-toxic concentrations (Gleadow and Møller, 2014; Machingura et al., 2016). Interestingly, at these low, non-toxic concentrations, there is evidence to suggest that cyanide plays a role as a signalling molecule in breaking seed dormancy, modifying responses to biotic stress, nitrate assimilation, and the inhibition of root hair elongation (Bethke et al., 2004; Chivasa and Carr, 1998; Grossmann,

1996; Siegień and Bogatek, 2006; Solomonson and Barber, 1990). Cyanide has characteristics that are common among other signalling molecules such as low molecular weight, high solubility in water, and the ability to modify specific targets through post-translational modifications - specifically cysteines (Gotor et al., 2019; Siegień and Bogatek, 2006).

1.3 *HOTHEAD*

1.3.1 The *HOTHEAD* gene

The *HOTHEAD* (*HTH*) gene was discovered through a forward genetic screen aimed at identifying genes involved in cuticle formation/function (Lolle et al., 1998). The *HTH* gene maps to chromosome 1 in *A. thaliana* at the locus AT1G72970 (Lolle et al., 1998; Krolikowski et al., 2003). The *HTH* gene is preceded by a 5' upstream region of 1905 bp and contains twelve upstream open reading frames (uORF). uORFs are known to regulate translation of the downstream gene, typically in a negative aspect (Merchante et al., 2017; Morris and Geballe, 2000). The characteristics of these uORFs determine how effective they are at inhibiting translation (Liu et al., 2013; Merchante et al., 2017; von Arnim et al., 2014). The length of the uORF is moderately tied to its efficacy – uORFs longer than 48 bp are expected to be more efficient (von Arnim et al., 2014), the 5' upstream region of *HTH* contains six uORFs longer than 48 bp. Additionally, the more uORFs, the stronger the translational inhibition (Liu et al., 2013); the 5' upstream region of *HTH* contains twelve uORFs. This indicates that the *HTH* gene may be a tightly regulated gene.

Mapping by Krolikowski et al. (2003) revealed that the *HTH* gene resides in the same location as the *ADHESION OF CALYX EDGES* (*ACE*) gene (Nakatani et al., 1998). The *ace* mutant shares a

similar organ fusion phenotype with *hth* mutants which lead to the mislabeling of *HTH* as *ACE*, however, sequence analysis indicates that *ACE* and *HTH* encode the same gene (Araki et al., 1998; Nakatani et al., 1998; Krolikowski et al., 2003). A novel allele of *HTH* was discovered during a forward genetic screen using transposon mutagenesis to uncover genes involved in female gametophyte development (Pagnussat et al., 2005) (Figure 1.4). This screen identified a mutation in the *EMBRYO SAC DEVELOPMENT ARREST 17* (*EDA17*) gene (Pagnussat et al., 2005). This mutation resulted in arrested development at the two-nuclear stage of megagametogenesis (Pagnussat et al., 2005).

There are 14 other *hth* mutant alleles some of which were generated through ethyl methanesulfonate (EMS) mutagenesis (*hth-1* to *hth-11*) (Table 1.1), transposon mutagenesis (*hth-12*), or T-DNA insertion mutagenesis (*hth-13* to *hth-15*) (Krolikowski et al., 2003; Kurdyukov et al., 2006b; Lolle et al., 1998) (Figure 1.4 A). It is important to note that the *hth-5* and *hth-11* mutant alleles were independently isolated but were eventually shown to harbor the same point mutation (Krolikowski et al., 2003) (Table 1.1). Mutant *hth* alleles generated through EMS mutagenesis resulted in a single nucleotide change - these mutations lead to the identification of the eight-key functional amino acids (aa) of the HTH protein (Figure 1.4 A) (Table 1.1). The *hth-1* and *hth-9* mutant alleles likely encode protein truncations - the *hth-1* mutation introduces a stop codon in the fourth exon and the *hth-9* mutation alters the splice site junction in the second intron - these do not provide insight into key functional aa's of the HTH protein (Figure 1.4 A) (Table 1.1).

All *hth* mutant plants share a common floral organ fusion phenotype suggestive of a defect in cuticle formation/function, however, the severity of these mutant phenotypes varies between *hth* mutant alleles. This variance is dependent on the accession this mutation is in (Landsberg vs

Columbia vs Wassilewskija). Mutants in a Landsberg accession show tightly closed flowers, mutants in a Columbia accession show a moderate floral organ fusion, and mutants in a Wassilewskija (Ws) accession show a floral phenotype that falls in the middle (Chang, 2016; Krolikowski et al., 2003; Lolle et al., 1998). All *hth* mutants retain the ability to self-fertilize, while pollen adhesion, germination, and growth on the vegetative tissues is commonly observed (Krolikowski et al., 2003; Lolle et al., 1998). The seeds of *hth* mutants are also affected; *hth* mutant seeds are approximately 1.5-2 times larger than the wild-type seed (Chang, 2016). All *hth* mutant seeds show variation in seed shape and size and have a higher seed coat permeability as compared to wild-type seeds (Chang, 2016). They have also been shown to adhere to one another, although this occurs infrequently (Chang, 2016).

1.3.2 The HOTHEAD protein

The *HTH* gene is 2834 base pairs (bp) in length in the Columbia (Col) ecotype background and consists of six exons that are predicted to translate into a 65.3 kilodalton (kDa) protein (AT1G72970.1) (Figure 1.4 B) (Appendix A). An expressed sequence tag of an *HTH* splice variant (AT1G72970.2) was identified by a sequence analysis of *A. thaliana* chromosome 1 (Theologis et al., 2000). This sequence analysis used two bacterial artificial chromosome libraries and one yeast artificial chromosome library generated from Col *A. thaliana* (Theologis et al., 2000). The splice site of this splice variant *HTH* sequence occurs in the middle of the fifth exon giving rise to an isoform of HTH that is missing 27 aa and is consequently 62.2 kDa in size (AT1G72970.2) (Figure 1.4 B).

Analyses on the AT1G72970.1 protein model have identified a putative N-terminal signal peptide, five putative N-glycosylation sites and four putative Protein Kinase C (PKC)

phosphorylation sites (Figure 1.4 B) (Chang, 2016). The N-terminal signal peptide indicates that HTH may localize to the ER or it may be a secreted protein; N-glycosylation can be crucial to the stability, structure, and functionality of some proteins; PKC phosphorylation sites allow the function of proteins to be changed by PKC activity (Shental-Bechor et al., 2008; Xiao et al., 2019). The putative glycosylation of HTH was confirmed through a deglycosylation immunoblot analysis of the HTH protein by Chang (2016), however much about HTH protein structure, its subcellular localization, and post-translational modification remain unknown.

Bioinformatic, phylogenetic, and experimental analysis suggest that HTH may function as either an alcohol dehydrogenase (ADH) involved in the formation of cutin monomers, or as a mandelonitrile lyase (MDL) involved in cyanogenesis (Chang, 2016; Krolikowski et al., 2003; Kurdyukov et al., 2006b). A study by Kurdyukov et al. (2006b) proposed that HTH may act as a fatty acid ω-alcohol dehydrogenase, catalyzing the biosynthesis of α-, ω-dicarboxylic fatty acids in the fatty acid ω-oxidation pathway leading to the formation of cuticular polyesters (Figure 1.1). These cutin building blocks would be synthesized within the ER before being transported to the cuticle layer - the method by which is, for the most part, unknown (Fich et al., 2016). Bioinformatic analyses has predicted the presence of two putative glucose-methanol-choline (GMC) oxidoreductase conserved domains; an N- and a C-terminal domain (Figure 1.4 B) (Krolikowski et al., 2003). The N-terminal domain is proposed to act as the FAD ADP-binding domain while the C-terminal domain putatively acts as the substrate binding domain (Bannwarth et al., 2004; Vrielink et al., 1991).

1.3.**3** HOTHEAD protein localization

The expression of HTH has been examined using a variety of approaches. Krolikowski et al.

(2003) used reverse transcription-polymerase chain reaction (RT-PCR) and *in situ* mRNA hybridization analyses to show the expression of *HTH* in the leaf, inflorescence, siliques, and root tissues. They reported that expression was not limited to the epidermal cells and that *HTH* mRNA could also be detected in subepidermal cells (Krolikowski et al., 2003). Through native *HTH* promoter driven expression of β-glucuronidase (GUS) and *in situ* mRNA hybridization analyses, Kurdyukov et al. (2006b) identified *HTH* expression in the emerging true leaves, the shoot apical meristem (SAM), and emerging lateral roots of seedlings, however, they found that *HTH* expression was restricted to epidermal cells.

Protein expression studies using native *HTH* promoter driven expression of a fluorescently tagged HTH fusion protein (*HTH_{pro}:HTH-GFP* or *HTH_{pro}:HTH-EYFP*) identified HTH expression at the chalazal end of the developing embryo sac, in the oi1 and oi2 layers of the seed coat, floral buds, sepals, petals, stamens and ovaries of *A. thaliana* (Chang, 2016). Expression of fluorescently tagged HTH was found in the vasculature of the primary root, lateral roots, the hypocotyl, and the cotyledons, as well as in the epidermal cells of emerging true leaves, the hypocotyl, and cotyledons of young *A. thaliana* seedlings (Chang, 2016). Expression of fluorescently tagged HTH was also found in the SAM, trichomes, and guard cells of young *A. thaliana* seedlings (Chang, 2016). Within the cells of young seedlings, fluorescently tagged HTH was expressed in a reticular network as well as in spindle-shaped bodies that were ~5-10 μm in length, ~1 μm in diameter, highly mobile (0.5-1 μm/sec), and of ER origin (Chang, 2016). These structures were proposed to be ER bodies.

1.3.**4** HOTHEAD association with stress response

Using quantitative real time polymerase chain reaction (qRT-PCR), Chang (2016) found that the

HTH gene was responsive to MeJA treatment. Additionally, large (~5-10 µm in length, 1 µm in diameter), fluorescent, spindle-shaped structures were observed in the midrib cells of HTH_{pro}*:HTH-GFP* and HTH_{pro}*:HTH-EYFP* rosette leaves following exposure to MeJA (Chang, 2016). These bodies were assumed to be ER bodies and thus it was determined that HTH localizes to ER bodies formed in response to MeJA exposure (Chang, 2016). The localization of HTH, a putative MDL, to ER bodies which house PYK10, a β-glucosidase, suggests the involvement of HTH in plant defense. However, the possibility that HTH functions as a putative fatty acid ω-alcohol dehydrogenase suggests the involvement of HTH in cuticle formation/function. Experimental evidence has not been found to resolve either putative enzymatic function.

There is no canonical ER retention motif (KDEL, HDEL, or REEL) within the HTH protein. HTH does contain three KDEL-like sequences KDEK, KKEL, and KNEL at aa positions 270, 310, and 387, respectively (Appendix B). However, these KDEL-like sequences within HTH have not been examined experimentally for targeting to ER-derived structures. There is a growing amount of evidence to suggest that KDEL sequences are not the only motifs that signal ER-retention (Masumura et al., 2015; Torrent et al., 2009). Torrent et al. (2009) identified an N-terminal tandem repeat (PPPVHL) ER retention signal in maize γ-zein; Masumura et al. (2015) identified the ER retention signal for a rice prolamin that was located in the middle and C-terminus of the prolamin. This indicates that there are many deviations in ER-retention motifs. In addition, some proteins found within cER bodies, such as RD21, AtFruct4, and WSCP, lack a KDEL sequence; these proteins are thought to be retained in cER bodies through association with PYK10 (Hayashi et al., 2001; Rojo et al., 2003; Takahashi et al., 2012). This strategy for ER retention has been observed with other proteins (Vitale and Ceriotti, 2004).

1.4 Research Rationale

Plants experience many adverse conditions, as they are not able to remove themselves from the sources of these stressors, they have developed a multitude of intricate signalling and response pathways to mount their defense systems against the stress. Many of the response pathways, cellular structures, genes, and proteins involved in defence of the plant have been identified, however, much remains unknown (Aljbory et al., 2016; Berens et al., 2017; Moon and Park, 2016). HTH has been associated with both cuticle formation/function and stress responses - both crucial for plant survival. Although the role of HTH in these processes is unclear, it is hypothesised that the full-length HTH protein may act as an alcohol dehydrogenase while the splice variant isoform of the HTH protein may act as a mandelonitrile lyase.

This splice variant isoform of the HTH protein is missing a 27 aa peptide from the middle of one of HTH's exons. The functional role of the HTH isoform is also unknown. The research outlined in the present study offers opportunities to better understand the role, if any, of the two HTH isoforms in the model organism *Arabidopsis thaliana*. In understanding the role that HTH and its isoform play in cuticle formation/function and response to biotic or abiotic stressors, we may identify strategies for crop improvement and global food security.

1.5 Experimental Objectives

Chapter 2

1. Validate HTH protein localization to ER bodies using various approaches.
2. Determine changes in *HTH* gene expression in response to salt shock.
3. Investigate whether HTH from ER bodies act as a mandelonitrile lyase using a mandelonitrile lyase enzymatic assay.

Chapter 3

1. Develop transgenic plants containing *HTH* promoter driven expression of fluorescently tagged HTH splice variant recombinant protein.
2. Determine whether the splice variant recombinant protein complements the *hth* mutant phenotype.
3. Investigate the HTH splice variant protein localization pattern in transgenic plant tissues and cells.

Figure 1.1. Schematic representation of the plant cuticle and the biosynthesis pathways for waxes and cutin monomers.

A. The cuticle is composed of the cuticle layer, cuticle proper, and epicuticular waxes. The cuticle proper is composed mainly of intracuticular waxes and cutin monomers. The cuticular layer is composed mainly of cutin monomers and polysaccharides. The cell wall contains polysaccharides. Two epidermal cells are shown below the cuticle. Putative transporters are represented by yellow boxes in the plasma membrane. These facilitate cutin and wax movement from the cell to the cuticle layers.

B. The wax and cutin biosynthesis pathway begins in a plastid (pink circle) and is carried out within the ER cisternae (brown outlined oddly shaped structure). Once the waxes and cutin monomers are synthesized in the ER, they are transported to the epicuticular/cuticle proper and cuticle proper/cuticular layer respectively through various pathways indicated by the black arrows.

Image modified from Chang (2016).

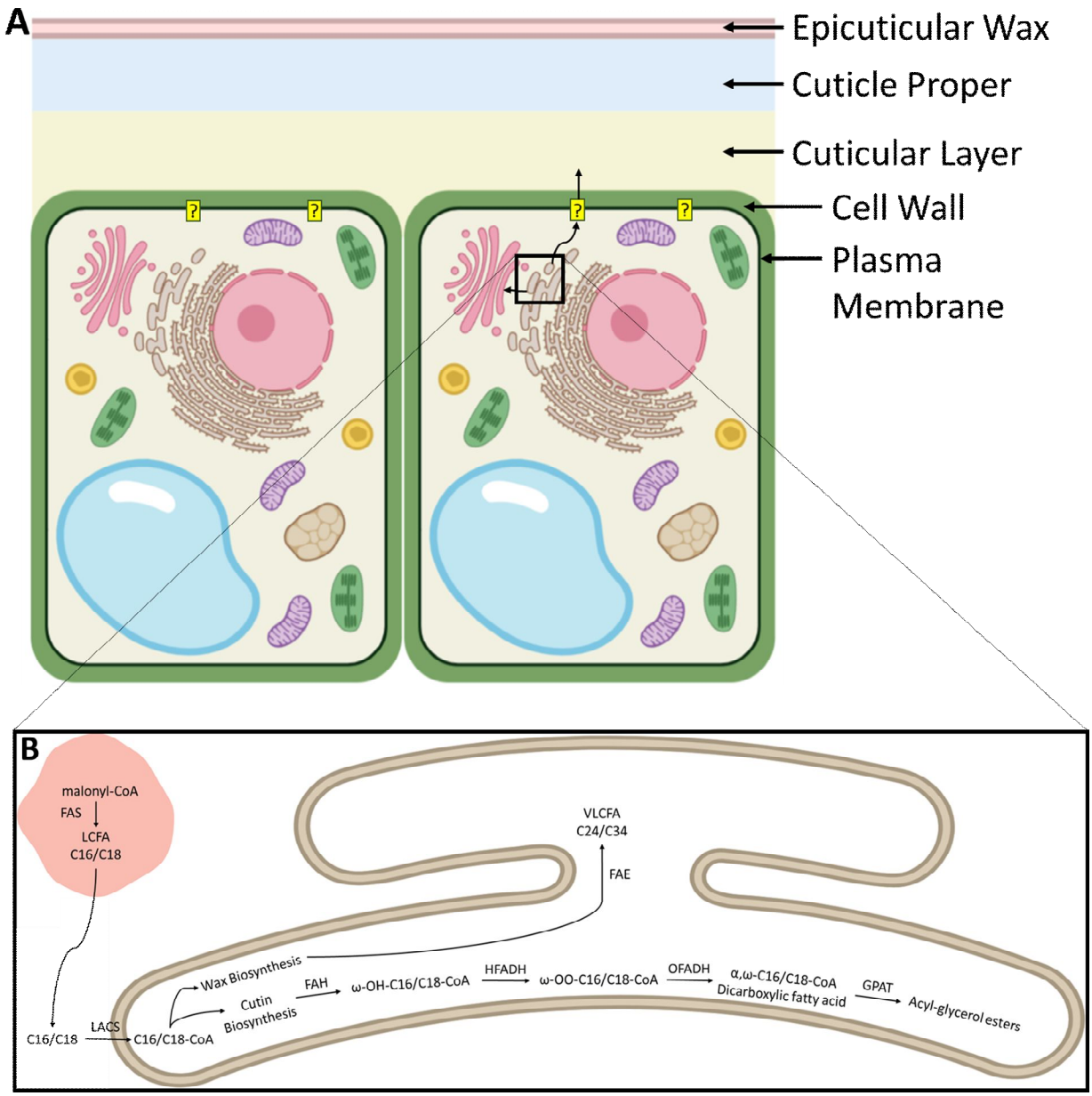
A
Epicuticular Wax
Cuticle Proper
Cuticular Layer
Cell Wall
Plasma Membrane
?
B
malonyl-CoA
FAS
LCFA
C16/C18
VLCFA
C24/C34
FAE
Wax Biosynthesis
Cutin
Biosynthesis
FAH
ω-OH-C16/C18-CoA
HFADH
ω-OO-C16/C18-CoA
OFADH
α,ω-C16/C18-CoA
Dicarboxylic fatty acid
GPAT
Acyl-glycerol esters
C16/C18
LACS
C16/C18-CoA

Figure 1.2. Schematic representation of the seed coat of *Arabidopsis thaliana*. There are five cell layers that make up the seed coat. An inset of the seed coat is outlined by a black box and shown in more detail to the right. The outer integuments consist of outer integument 1 and 2 (oi1 and oi2). The inner integuments consist of inner integuments 1 and 2 with a layer between known as 1' (ii1, ii2, and ii1'). Wall 3 represents a zone of fusion between the oi1 and ii2 layers. There are two layers containing cutin-like monomers in the seed coat. One is wall 3, the other is located between ii1 and the developing embryo.

Image modified from Chang (2016).

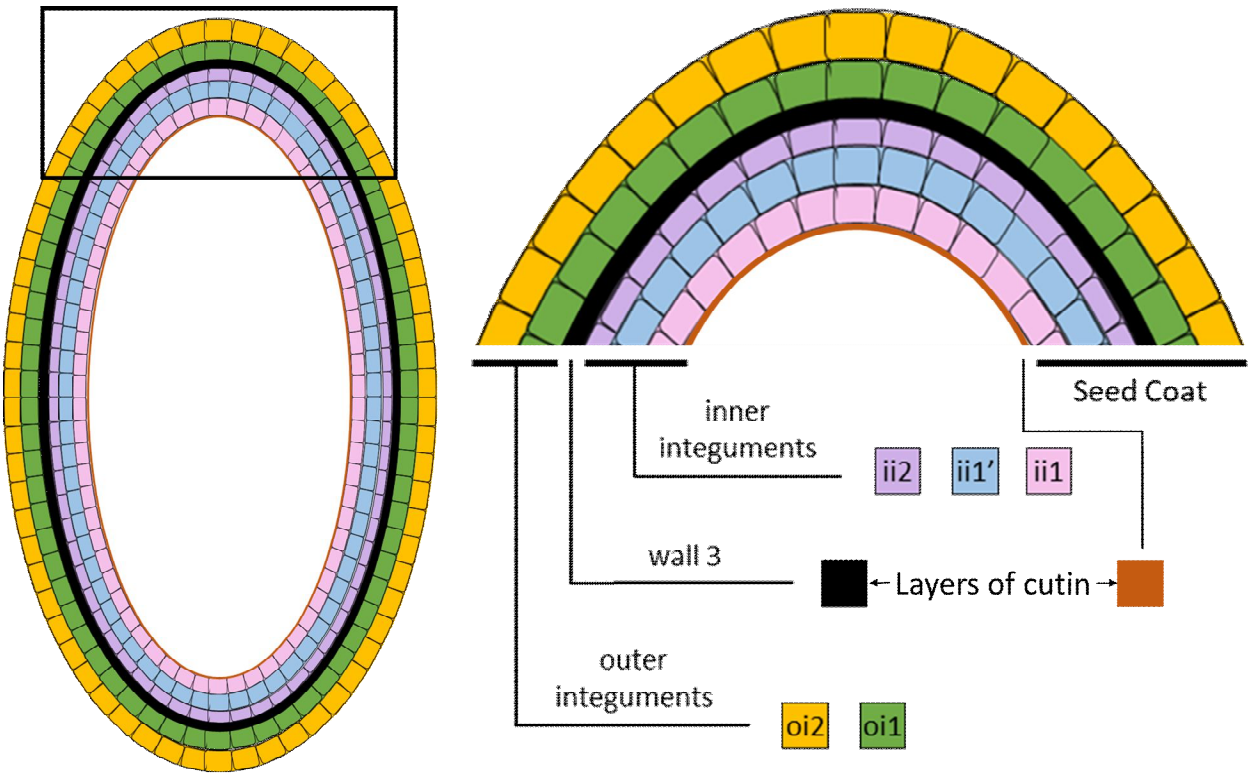
Seed Coat
inner
integuments
ii2
ii1'
ii1
wall 3
Layers of cutin
outer
integuments
oi2
oi1

Figure 1.3. Schematic representation of the formation of endoplasmic reticulum bodies. NAI2 recruits PYK10 to the ER membrane to initiate budding. NAI2 also recruits MEB1 and MEB2 which are ER body membrane proteins. Once a sufficient amount of PYK10 has accumulated, the ER body will bud off from the ER membrane. Image modified from Nakano et al. (2014).

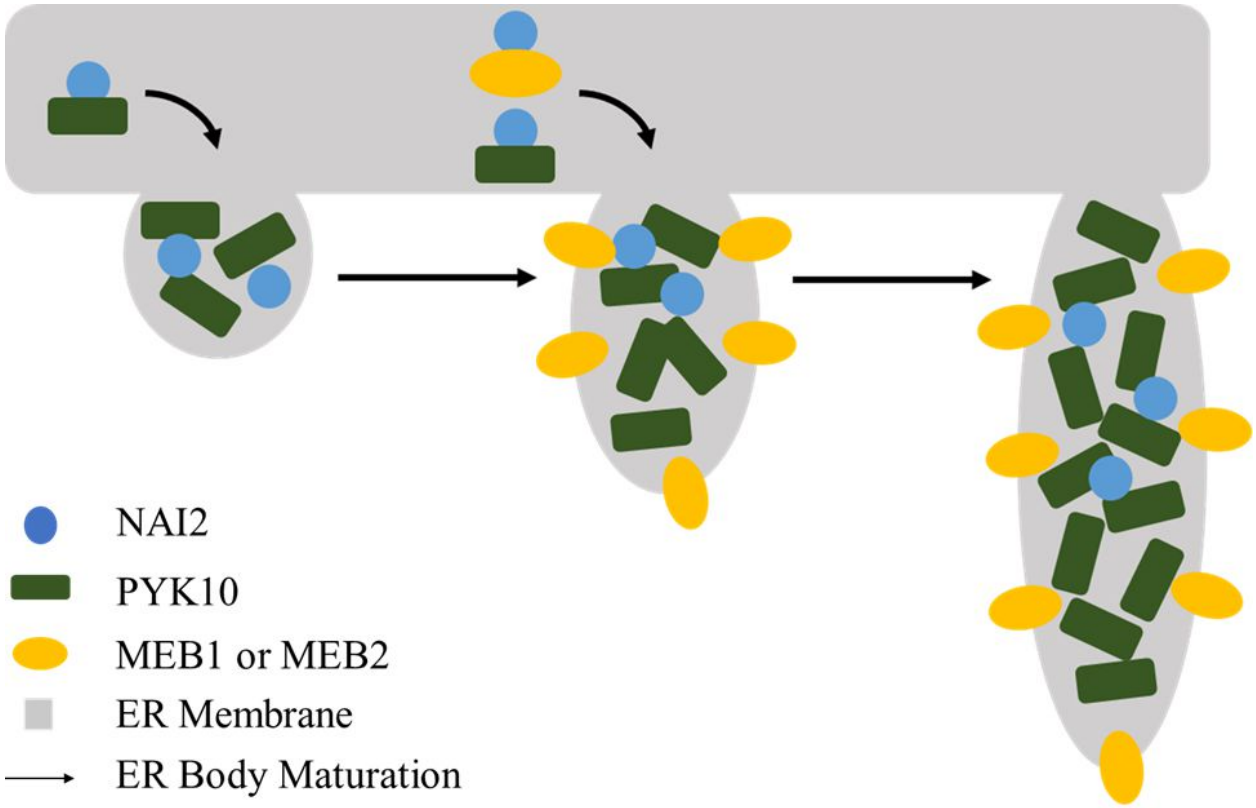
NAI2
PYK10
MEB1 or MEB2
ER Membrane
ER Body Maturation

Table 1.1. Point mutations of *hothead* mutant alleles. The DNA mutation is listed along with the position relative to the start of the coding sequence. The amino acid change is listed along with the position of the amino acid in the theoretical protein sequence of AT1G72970.1. Modified from Chang (2016).

Allele	Genetic Background	DNA Mutation	Amino Acid Change
hth-1	Landsberg *erecta*	$C_{1937} \rightarrow T$	$Q_{353} \rightarrow$ Stop
hth-2	Landsberg *erecta*	$G_{1761} \rightarrow A$	$G_{294} \rightarrow E$
hth-3	Landsberg *erecta*	$G_{2267} \rightarrow A$	$G_{435} \rightarrow R$
hth-4	Landsberg *erecta*	$C_{1472} \rightarrow T$	$R_{227} \rightarrow C$
hth-5, -11	Landsberg *erecta*	$C_{2654} \rightarrow T$	$P_{564} \rightarrow S$
hth-6	Landsberg *erecta*	$G_{1445} \rightarrow A$	$G_{218} \rightarrow S$
hth-7	Landsberg *erecta*	$C_{2661} \rightarrow A$	$T_{566} \rightarrow I$
hth-8	Landsberg *erecta*	$G_{2657} \rightarrow A$	$G_{565} \rightarrow R$
hth-9	Wassilewskija	$G_{1257} \rightarrow A$	Splice Site
hth-10	Landsberg *erecta*	$G_{1947} \rightarrow A$	$G_{356} \rightarrow E$

Figure 1.4. HOTHEAD.

A. The 5' upstream region and coding region of *HTH*. There are six exons (blue rectangles) and five introns (line). The location of the fifteen characterized genetic lesions found in *HTH* mutant alleles are indicated with *hth-1* to *hth-11* representing the point mutations derived from EMS (*hth-5* and *hth-11* describe the same point mutation derived independently), *hth-12* and *eda17* are sites of transposon insertion, *hth-13* to *hth-15* are sites of T-DNA insertion. The 81 base pairs missing in the splice variant transcript of *HTH* is shown by the black box outline. Scale bar ~ 1 kilobase (kb).

B. The HTH protein has six *HTH* exons (blue arrows) composed of 594 amino acids (aa) giving rise to a 65 kilodalton protein. Predicted glucose-methanol-choline (GMC) oxidoreductase domains (grey boxes) and signal peptide motif (yellow box) are above their putative positions on the HTH protein. The positions of the eight essential aa residues determined through genetic analysis are shown below the protein model (black line) along with the positions of the three putative catalytic residues (orange line). Above the putative GMC oxidoreductase domains are putative N-glycosylation (N yellow line) and protein kinase C phosphorylation (P green line) sites for posttranslational modification. The 27 aa missing from in splice variant isoform are indicated by the black outlined rectangle. Scale bar ~ 50 aa.

Modified from Chang (2016).

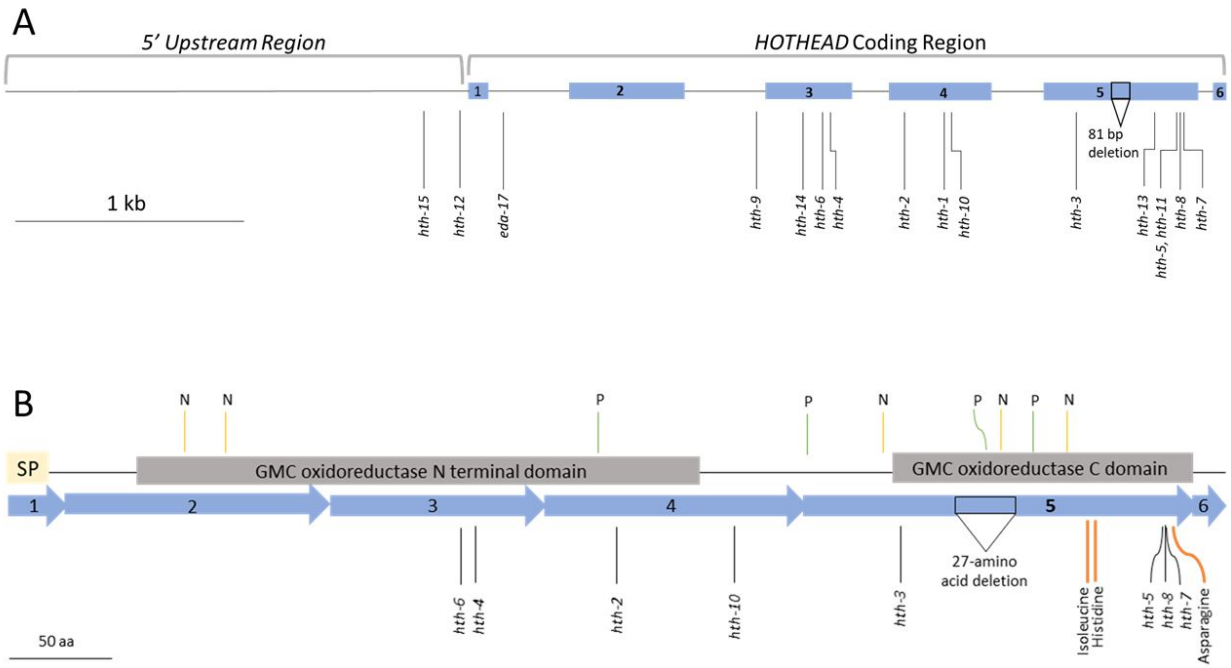
A
5′ Upstream Region
HOTHEAD Coding Region
1
2
3
4
5
6
81 bp deletion
1 kb
hth-15
hth-12
eda-17
hth-9
hth-14
hth-6
hth-4
hth-2
hth-1
hth-10
hth-3
hth-13
hth-5, hth-11
hth-8
hth-7
B
N
N
P
P
N
P
N
P
N
SP
GMC oxidoreductase N terminal domain
GMC oxidoreductase C domain
1
2
3
4
5
6
27-amino acid deletion
hth-6
hth-4
hth-2
hth-10
hth-3
Isoleucine
Histidine
hth-5
hth-8
hth-7
Asparagine
50 aa

Chapter 2 HOTHEAD Localization to ER Bodies

2.1 Introduction

Under conditions of stress, misfolded proteins aggregate within the ER. This aggregation overwhelms the ER's quality control system which triggers the UPR (Ruberti and Brandizzi, 2018). Autophagy or cell death is triggered if the ER is not able to combat the stress thus, the ER forms organelles filled with various proteins to defend the cell against the stress (Hara-Nishimura et al., 2004; Howell, 2013). Most ER-derived organelles involved in defence are spherical, small - ranging from 0.05-2 μm in diameter - and enriched for proteases (Chrispeels and Herman, 2000; Hara-Nishimura et al., 2004; Hayashi et al., 2001). However, there is one ER-derived organelle that differs; ER bodies are large - ~5-10 μm in length and ~1 μm in diameter - spindle-shaped structures that are enriched for a β-glucosidase known as PYK10 (Matsushima et al., 2003b; Sherameti et al., 2008).

cER bodies are found constitutively expressed in the epidermal cells of young *A. thaliana* seedlings and in the roots of mature *A. thaliana* plants (Hayashi et al., 2001). Upon exposure to MeJA or wounding stress, iER bodies are induced in rosette leaves, where they are normally absent (Hayashi et al., 2001; Matsushima et al., 2002; Ogasawara et al., 2009). The formation of cER bodies is regulated by NAI1 - a basic helix-loop-helix transcription factor (Matsushima et al., 2004). Mutant n*ai1-1* plants lack cER bodies and induce abnormal, tube shaped iER bodies, but do not have any other discernible mutant phenotypes (Matsushima et al., 2004). NAI1 regulates the expression of genes involved in cER body formation such as *NAI2*, *PYK10*, *MEB1* and *MEB2* (Matsushima et al., 2004). Mutations in these genes can also result in cER body

deficiency or abnormality; cER bodies are rarely found in *nai2* mutants (Yamada et al., 2008), cER bodies of *pyk10* and/or *bglu21* mutants are much longer than wild-type cER bodies (Nagano et al., 2009), and cER bodies of *meb1* or *meb2* mutants seem to resemble wild-type cER bodies (Yamada et al., 2013). The study of these mutants identified the mode of cER body formation (Figure 1.3). As shown in Figure 1.3, cER bodies mature and bud off from the ER after NAI2 directs the recruitment of PYK10 and MEB1/2 membrane proteins, populating the ER body lumen and membrane with these proteins respectively (Yamada et al., 2008) (Figure 1.3).

Ogasawara et al. (2009) showed that iER bodies are devoid of PYK10 and instead accumulate BGLU18. They also showed that iER bodies are expressed under conditions of wounding in *nai1-1* mutants (Ogasawara et al., 2009). This indicated that the formation of cER bodies and iER bodies differed as iER bodies were not regulated by NAI1 whereas cER bodies were. Geem et al. (2019) confirmed that the formation of cER bodies and iER bodies are regulated separately; they found that TSA1 directed the recruitment of BGLU18 to the ER membrane in the formation of iER bodies while NAI2 directed the recruitment of PYK10 to the ER membrane in the formation of cER bodies (Geem et al., 2019). This indicates that there are two distinct types of ER bodies with different protein compositions; this could indicate that these two ER bodies perform differing functions within the plant.

The major component of any ER body are BGLUs; BGLUs are myrosinases which are known to be involved in plant defence against herbivory and fungal infection (Rask et al., 2000; Sherameti et al., 2008). Myrosinases catalyze the breakdown of glucosinolates which are stored within the vacuole. Under stress conditions, ER bodies fuse to the vacuole bringing the BGLUs to the glucosinolates within the vacuole (Hayashi et al., 2001). This reaction produces nitriles which

can be further catalyzed by hydroxynitrile lyases to produce HCN - a toxic compound (Brabban and Edwards, 1995; Halkier and Gershenzon, 2006; Wittstock and Halkier 2002).

Using bioinformatic, phylogenetic, and experimental analyses, HTH has been suggested to function as an MDL (also known as a hydroxynitrile lyase) (Chang, 2016; Krolikowski et al., 2003) while other studies suggest that HTH may function as an ADH (Chang, 2016; Krolikowski et al., 2003; Kurdyukov et al., 2006b). Both MDLs and ADHs belong to the same superfamily of oxidoreductases; GMC (Dreveny et al., 2001; Sützl et al., 2019). Bioinformatic analysis has predicted the presence of two putative GMC oxidoreductase conserved domains; an N- and a C-terminal domain (Figure 1.4) (Krolikowski et al., 2003). The N-terminal domain is proposed to act as the FAD ADP-binding domain while the C-terminal domain putatively acts as the substrate binding domain (Bannwarth et al., 2004; Vrielink et al., 1991).

Protein expression studies using HTH_{pro}*:HTH-GFP* or HTH_{pro}*:HTH-EYFP* transgenic plants identified HTH expression in floral buds, sepals, petals, stamens and ovaries (Chang, 2016). Expression of HTH was also found in the vasculature of primary and lateral roots, the hypocotyl, and cotyledons, as well as in the epidermal cells of the hypocotyl, cotyledons, and emerging true leaves of seedlings (Chang, 2016). Expression of HTH was also found in the SAM, trichomes, and guard cells (Chang, 2016). Within the cells of these transgenic seedlings, HTH was expressed in a reticular network as well as in spindle-shaped bodies that were ~5-10 μm in length, ~1 μm in diameter, highly mobile (0.5-1 μm/sec), and of ER origin (Chang, 2016). These structures were proposed to be ER bodies. The transgenes used in these studies fully rescue the *hth-9* mutant phenotypes suggesting that the localization of these HTH translational fusions reflect that of the native HTH protein (Chang, 2016).

The localization of HTH to ER bodies suggested a link between HTH and plant stress responses. To test this, transgenic plants were exposed to MeJA and *HTH* gene transcriptional responses assayed (Chang, 2016). *HTH* transcript levels were shown to significantly increase in response to these treatments (Chang, 2016). Additionally, HTH was found to localize to structures proposed to be iER bodies as they formed in response to MeJA exposure (Chang, 2016).

In the present study, the localization of HTH to ER bodies was investigated using salt shock as an abiotic stress, by employing subcellular fractionation techniques and genetic analyses. Preliminary experiments aimed at testing cellular fractions containing HTH-GFP for MDL activity were also undertaken. The results described here are consistent with previous findings linking *HTH* expression to stress and confirming HTH localization to ER bodies but did not provide definitive evidence regarding enzymatic function.

2.2 Materials and Methods

2.2.**1** Growth conditions

A. thaliana plants used in this study included the wild-type accession Ws, the *hth-9* and *nai1-1* mutants (AT2G22770.1), and transgenic lines HTH_{pro}*:HTH-GFP*. Seeds were sown on pre-wet LC1 Sungro Sunshine (Sungro Horticulture) potting mix or ASB Greenworld Grower with Pearlite (ASB Greenworld) potting mix in 5 cm pots arranged in 40 cm x 20 cm flats and stratified at 4°C for 3-4 days. Flats were moved from 4°C to growth chambers maintained at 20 ± 4°C, with 40-60% relative humidity, and illuminated with a mixture of incandescent and fluorescent lights (140-170 µmol m^{-2} sec^{-1}) over a either a long day cycle (16/8-hour light/dark) or with continuous light (24 hour cycle) (Econoair AC60; Ecological Chambers Inc.). Plants were watered every three days, or as needed, with distilled water supplemented with 0.01 g/L 20:20:20 fertilizer (Plant-Prod Inc.).

For growth in sterile conditions, ~5 layers of seeds were placed in an open microcentrifuge tube and sterilized with chlorine gas made from mixing 50 ml of bleach (Javax, 5.25 % NaOCl) with 2 ml of concentrated HCl. Seeds were sterilized for 1-1.5 hours in an airtight chamber and plated on half-strength Murashige and Skoog (MS) media (M5519-50L; Sigma-Aldrich) at a density of 20-25 seeds/plate for subcellular fractionation studies or 10-15 seeds/plate for microscopy and salt shock studies. Seeds were stratified at 4°C for three days before being moved to the growth chamber. Seedlings grown on plates were positioned vertically and covered by four layers of cheesecloth to attenuate light intensity. Plants used for salt shock studies were grown with continuous light (24-hour cycle) while plants used for cER body isolation studies were grown under a long day cycle (16/8-hour light/dark).

2.2.**2** Quantitative reverse transcription polymerase chain reaction

Salt shock

Eleven-day-old plants from Ws and *HTH$_{pro}$:HTH-GFP* lines were transferred, under sterile conditions, from ½ MS plates to either fresh ½ MS plates (to control for mechanical manipulations) or ½ MS plates containing 100 mM NaCl. Transferred plants were plated at a density of 10 plants/plate and the plates returned to the growth chamber for 6-, 12-, and 24-hours. At each of the three timepoints, plates were removed from the chamber and approximately 100 mg of Ws tissue was collected and flash frozen in liquid nitrogen. Concurrently, *HTH$_{pro}$:HTH-GFP* plants were mounted on glass slides in water and viewed using a fluorescent microscope (Zeiss Axio Imager D1; Carl Zeiss Inc.) under the following filters (ex/em): GFP – 470/525 nm and autofluorescence – 550/570 nm, to examine any changes in expression patterns. This protocol was optimized by Carmen Wong (an undergraduate thesis student).

cDNA synthesis

Plant tissue was pulverized using 1/8" diameter stainless steel beads (Abbott Ball Company). Total RNA was extracted from samples using the RNeasy Plant Mini Kit (74904; Qiagen). The total RNA concentration was determined using the NanoDrop 2000 spectrometer (ND-2000C; Thermo Fisher Scientific). Total RNA (0.063 µg/µl) was DNase treated as outlined in the Turbo DNA-*free*™ kit (Am1907; Ambion). The RNA concentration following DNAse treatment was determined using the NanoDrop 2000 spectrometer (Thermo Fisher Scientific). RNase free water was used to dilute aliquots of DNase treated RNA to 0.0375 µg/µl. One of these aliquots was reverse transcribed (RT) using random hexamer primers (1-034-731; Roche) and SuperScript III Reverse Transcriptase (18080-093; Invitrogen); SuperScript III Reverse Transcriptase

(Invitrogen) was not added to the second aliquot and served as a no-RT control. This protocol was optimized by Carmen Wong (an undergraduate thesis student).

Quantitative RT-PCR

Primer efficiencies were determined through the generation of a standard curve in which the log of the starting template was plotted against cycle threshold (C_T) values. The template used in the generation of this curve included cDNA from both NaCl-treated and untreated samples for all three timepoints. A ten-fold serial dilution of pooled cDNA was made over six points and subjected to a qRT-PCR amplification. Each reaction contained nuclease free water, 300 or 500 nM primers, cDNA, and SsoFast EvaGreen Supermix (172-5200; Bio-Rad). qRT-PCR was performed in a Real-Time Thermal Cycler CFX96 (Bio-Rad). The program began with a denaturing step at 95°C for 30 seconds (sec), then 39 cycles of 95°C for 3 sec, and 60°C for 5 sec (Chang, 2016). Melt curve analysis followed each PCR cycle with temperature increasing from 65°C to 95°C at 0.5°C increments for 0.05 sec; the fluorescence in each sample was also measured following each cycle (Chang, 2016). Each qRT-PCR plate contained two controls: a no RT control, and a no template control. Standard curves were generated in triplicate for each primer pair and had to meet an amplification efficiency of 90-110% with a coefficient of determination greater than 0.98. The primer pairs used in this study are listed in Table 2.1 along with their efficiencies and coefficients of determination. Housekeeping genes were assessed for gene stability using the CFX Maestro™ software (Bio-Rad), and used to normalize *HTH* gene expression.

HTH and housekeeping gene expression in NaCl-treated and untreated samples for all three timepoints was quantified as stated above, however, the cDNA samples were not pooled, and

were diluted 20x in nuclease free water before being loaded onto the qRT-PCR plate. Three biological, and three technical replicates were used. Relative normalized expression of *HTH* was calculated through the delta delta C_T method (Livak and Schmittgen, 2001), plotted, and a two-way anova utilized to assess for significance. Specific significant interactors were determined using a post hoc test - Tukey's HSD (Honestly Significant Difference).

2.2.**3** Subcellular fractionation and immunoblot analysis

Subcellular fractionation

Roots harvested from 11-day-old *HTH_{pro}:HTH-GFP* plants (1-1.5 g) were chopped using a fresh single-edged razor blade in 1 ml of chopping buffer (CB) (50 mM Hepes-NaOH (pH 7.5), 5 mM EDTA, 0.4 M sucrose, and protease inhibitor cocktail (P2714; Sigma-Aldrich)) in a pre-cooled glass Petri dish and maintained on ice during processing (Matsushima et al., 2003b). The homogenate was filtered through four layers of cheesecloth. An aliquot of the filtrate (~200 µl) was set aside and designated as the "Total".

The remaining filtrate was subjected to centrifugation as follows. The initial filtrate was centrifuged in a 5810 R (Eppendorf) centrifuge with the A-4-62 rotor (Eppendorf) at 1000 xg for 20 minutes (min) at 4°C (Matsushima et al., 2003b) and the pellet harvested.

The pellet was large (~500 µl) and slightly diffuse, thus it was harvested by carefully pipetting off the supernatant. A small amount of supernatant (~50 µl) was left between the pellet and the atmosphere. The pellet was resuspended gently in the remaining supernatant by gently flicking the tube. This pellet was designated as the "Pellet 1 (P1) Fraction". The supernatant was then centrifuged in an accuSpin™ Micro 17 (Fisher Scientific) centrifuge at 8000 xg for 20 min at 4°C.

The resulting pellet was resuspended in 500 µl of CB and designated as the "Pellet 8 (P8) Fraction". The remaining supernatant was centrifuged at 17000 xg for 90 min at 4°C. The resulting pellet was resuspended with 500 µl of CB and designated as the "Pellet (P17) Fraction". The remaining supernatant was designated as the "Supernatant 17 (S17) Fraction" (Figure 2.1) (Matsushima et al., 2003b).

Immediately following collection, the protein concentration within each pellet and supernatant fraction was identified through the Quick Start™ Bradford Protein Assay (5000201; Bio-Rad) with BSA (2 mg/ml) as the standard (Quick Start™ Bradford Protein Assay Instruction Manual, Bio-Rad). The standard protocol was used for the microplate assay (Quick Start™ Bradford Protein Assay Instruction Manual, Bio-Rad). Aliquots from each fraction were transferred to 5x Laemmli sample buffer (60 mM Tris-Cl pH 6.8, 2% SDS, 10% glycerol, 5% β-mercaptoethanol, 0.01% bromophenol blue) to a final concentration of 20 µg/µl and boiled for 10 min.

The presence or absence of fluorescence in each sample was determined using a Zeiss Axiophot epifluorescence microscope (Zeiss Axio Imager D1; Carl Zeiss Inc.) under the following filters (excitation/emission wavelengths); GFP - 470/525 nm; autofluorescence - 550/570 nm.

Immunoblot Analysis

Protein obtained from each cell fraction and total homogenate was size separated on a 10% SDS-polyacrylamide gel with a Spectra™ multicolor broad range protein ladder (26623; ThermoFisher Scientific). Protein was transferred from the gel onto a 0.45 µm polyvinylidene difluoride (PVDF) membrane (75696E; Pall Life Sciences) using a Trans-Blot® SD Semi-Dry Electrophoretic Transfer Cell (Bio-Rad). Protein transfer was validated by Ponceau-S staining the PVDF membrane. Following staining, membranes were rinsed with distilled water and

blocked with 5% skim milk in Tris-buffered saline (TBS) with Tween-20 (TBS-T) (5% skim milk, 20 mM Tris pH 7.5, 300 mM NaCl, 0.1% Tween-20). Following blocking, membranes were incubated with 1° antibody – either rabbit anti-GFP polyclonal antibody (1:5000; Bio-Rad, AHP2984) or rabbit anti-PYK10 polyclonal antibody (1:2000; PhytoAB, PHY0984S) – diluted in 5% skim milk TBS-T and left overnight at 4°C. Membranes were washed with TBS-T and incubated for 1-2 hours with the 2° antibody – anti-rabbit IgG polyclonal antibody conjugated to horseradish peroxidase (1:50000; Sigma-Aldrich, A0545). Following incubation, the membrane was washed with TBS-T, cross-reactive proteins visualized using Clarity™ western enhanced chemiluminescence (ECL) substrate (1705060; Bio-Rad). Chemiluminescent bands were viewed using the Image Lab (Bio-Rad) software on a Chemi Doc™ MP imaging system (Bio-Rad) at 1-600 sec of exposure.

2.2.**4** Mandelonitrile lyase enzyme assay

Triton X-100 detergent was used to disrupt ER bodies in the P1 fraction, releasing HTH-GFP. Protein in the P1 fraction was tested for MDL activity using a spectrophotometric assay. This assay monitored the activity of MDLs by measuring the release of benzaldehyde and HCN following mandelonitrile cleavage (EC 4.1.2.10; Sigma Aldrich). This reaction took place at 25°C, at a pH of 5.4, in a plastic cuvette with a path length of 1 cm. Absorbance readings were taken continuously at an absorbance wavelength of 275 nm on a Cary 100 UV-Vis spectrometer (Agilent Technologies). The final reaction consisted of 97.8 mM sodium acetate buffer, 2.672 mM mandelonitrile, 1.6% (v/v) ethanol, 0.05 U/µl MDL from almonds (M6782; Sigma Aldrich), and 0.003% (w/v) bovine serum albumin. Cuvettes containing a well mixed solution of sodium acetate buffer (pH 5.4) and enzyme (either MDL from almonds (Sigma Aldrich), or P1 aliquots) were loaded into the Cary 100 UV-Vis spectrometer (Agilent Technologies). The solution was

monitored in the spectrophotometer until readings stabilized, at that time, the substrate - mandelonitrile (116025; Sigma Aldrich) was added, mixed quickly by pipetting, and the reaction continuously monitored over a 10-15 min period. Enzyme activity (nmol/mg protein/min) was determined by using the extinction coefficient of benzaldehyde and the slope of the absorbance curve.

2.2.**5** Expression of *HTH_{pro}:HTH-GFP* in *nai1-1* ER body mutant plants

Reciprocal crosses were carried out between *HTH_{pro}:HTH-GFP* transgenic plants and *nai1-1* mutant plants. Progeny were screened for glufosinate resistance (0.0036 g/L; Total WipeOut; Wilson) and tested for the presence of the *HTH_{pro}:HTH-GFP* construct using PCR analysis. To detect for the presence of the *nai1-1* mutation in these crosses, derived cleaved amplified polymorphic sequence (dCAPS) primers were designed which introduced a bp change in the wild-type gene. This base change resulted in the generation of a restriction enzyme site in any wild-type *NAI1* allele. PCR analysis using dCAPS primers followed by *Sal*I restriction enzyme digestion (R0138; NEB), was used to confirm the presence or absence of the single nucleotide *nai1-1* mutation.

2.3 Results

The subcellular localization of HTH has previously been investigated in transgenic plants expressing the translational fusion construct, *HTH$_{pro}$:HTH-EYFP* (Chang, 2016). Colocalization studies showed that HTH-EYFP was localized to ER-derived, spindle-shaped bodies ranging in length from 5-10 μm (Chang, 2016). These large bodies show characteristics of ER-derived bodies that have previously been described in the literature and are known as ER bodies (Gunning, 1998; Hara-Nishimura et al., 1998; Hara-Nishimura and Matsushima, 2003; Hawes et al., 2001; Hayashi et al., 2001; Köhler 1998). In this study, stress induced by exposure of juvenile plants to NaCl, biochemical assays, and genetic crosses were conducted to further investigate HTH localization to ER bodies.

2.3.**1** ER body HOTHEAD localization is induced by salt shock

Salt shock was used in this study as this is the condition under which the fusion of ER bodies was observed in a previous study (Hayashi et al., 2001). Wild-type Ws and transgenic *HTH$_{pro}$:HTH-GFP* 11-day-old plants were salt shocked to investigate whether *HTH* transcript levels increase in response to salt shock and whether HTH-GFP containing iER bodies were induced in rosette leaves following these treatments.

Untreated and NaCl-treated Ws plants were evaluated following 6-, 12-, and 24-hours of exposure to media containing 100 mM NaCl. qRT-PCR was used to quantify changes in transcript levels at each time point. A two-way anova analysis on the qRT-PCR data indicated significant differences within and between time points and treatments (p value < 0.00001). **Within time points:** There was a significant increase in *HTH* transcript levels between untreated

significant difference in *HTH* transcript levels between untreated and NaCl-treated plants at the 6-hour time point (Figure 2.2 A). **Between time points:** There was a significant increase in *HTH* transcript levels at all three time points between NaCl-treated plants (Figure 2.2 A). There was no difference in *HTH* transcript levels between untreated plants at any time point (Figure 2.2 A).

All housekeeping genes used for the normalization of *HTH* expression had acceptable coefficients of variance (CV) and M values. Acceptable CVs are under 0.5, and acceptable M values are under 1 (Ling and Salvaterra, 2011; Strube et al., 2008; Taylor et al., 2015). *ACTIN 7* (*ACT7*; AT5G09810) had a CV of 0.0108 and an M value of 0.127; *GLYCERALDEHYDE-3-PHOSPHATE DEHYDROGENASE C-2* (*GAPC2*; AT1G13440) had a CV of 0.0102 and an M value of 0.202.

Eleven-day old transgenic HTH_{pro}*:HTH-GFP* plants were used to examine HTH-GFP localization following salt shock. Untreated and NaCl-treated transgenic HTH_{pro}*:HTH-GFP* plants were viewed using an epifluorescence microscope 6-, 12-, and 24-hours after treatment. No iER bodies were observed in rosette leaf midrib cells of untreated plants at any time point, although some fluorescence was observed localizing to a reticular network (Figure 2.2 B) (Appendix C). iER bodies were observed in rosette leaf midrib cells of NaCl-treated plants at the 24-hour time point (Figure 2.2 C) but not the 6- or 12-hour time points (Appendix C); some fluorescence was observed in a reticular network similar to that seen in untreated plants.

2.3.**2** Subcellular fractionation and cER body isolation

Differential centrifugation of total cell extracts was used to separate cER bodies, obtained from 11-day-old transgenic HTH_{pro}*:HTH-GFP* roots, from other cellular components. Fractions were subsequently examined using fluorescence microscopy and immunoblot analysis. Using

subcellular fractionation, cER bodies were obtained from root tissue homogenate of transgenic *HTH$_{pro}$:HTH-GFP* plants (Figure 2.3 A). As ER bodies are quite large (~5-10 µm in length and ~1 µm in diameter), they are expected to separate out following centrifugation at low g force and therefore to be enriched in the pellet under such conditions (Figure 2.1). To validate this, fractions obtained following each centrifugation step were viewed under an epifluorescence microscope to check for the presence of fluorescence and cER bodies (Figure 2.3 A). The total homogenate sample contained a few fluorescent spindle-shaped bodies of various sizes as well as some small fluorescent punctate structures (Figure 2.3 A). In contrast, the first pellet fraction (P1) contained many large (~5-10 µm in length and ~1 µm in diameter) fluorescent spindle-shaped bodies as well as some fluorescent punctate structures (Figure 2.3 A). The second pellet fraction (P8) looked very similar to the total fraction with some smaller fluorescent spindle-shaped bodies (~3-5 µm in length and ~1 µm in diameter) as well as small fluorescent punctate structures (Figure 2.3 A). No fluorescent spindle-shaped bodies were detected in the third and fourth fractions (P17 and S17), although some small fluorescent punctate structures were evident (Figure 2.3 A).

The protein loading for the immunoblot analysis was assessed through a Ponceau stain (Figure 2.3 B). Under immunoblot analysis, all fractions were probed with anti-GFP antibodies to identify which contained HTH-GFP protein. The HTH-GFP protein is glycosylated (Chang, 2016) and has a molecular weight of approximately 105 kDa. A band of this size was detected in all fractions; however, the majority was found in the P1 fraction (Figure 2.3 C). To verify for the presence of cER bodies in the HTH-GFP enriched P1 fraction, PYK10, a protein found in concentrated amounts in cER bodies (Matsushima et al., 2003), was probed for using anti-PYK10 antibodies (Figure 2.3 D). The PYK10 protein has a molecular weight of 60 kDa. An

~60 kDa protein that was cross-reactive with the PYK10 antibody was found in all fractions, however, it was most abundant in the P1 fraction, as expected (Matsushima et al., 2003) (Figure 2.3 D). This was likely PYK10 (Matsushima et al., 2003).

2.3.**3** Mandelonitrile lyase activity assays

Bioinformatic analysis had suggested that HTH may function as an MDL (Chang, 2016). To investigate this possibility, HTH-GFP from *HTH$_{pro}$:HTH-GFP* plants was isolated through subcellular fractionation (Figure 2.1) and the P1 pellet fraction used in an MDL assay. The MDL assay monitored the cleavage of mandelonitrile - substrate for MDL - into benzaldehyde. Commercial MDL enzyme from almonds was used as a positive control for this reaction; the addition of this enzyme resulted in an increasing amount of benzaldehyde production over a 10 min period (Figure 2.4 A). Negative controls were also used in this study. An absence of mandelonitrile substrate did not produce benzaldehyde, however, an absence of MDL enzyme did produce benzaldehyde (Figure 2.4 B). This slight increase in benzaldehyde production indicated that the substrate was broken down without the aid of an enzyme under the conditions of the assay (Figure 2.4 C). The sample of HTH-GFP resulted in a slight increase in benzaldehyde production mirroring the trend seen in the negative control (Figure 2.4 D). This indicated that the HTH-GFP protein in P1 fractions did not have MDL activity under the conditions of the assay. Heterologous HTH protein obtained by the expression of recombinant constructs in *E. coli* generated by Le Dreff-Kerwin (2019) was also tested and showed no MDL activity under these conditions (Appendix D).

2.3.**3** HOTHEAD localization in a *nai1-1* mutant background

To further investigate HTH localization to cER bodies, *nai1-1* mutant and transgenic

HTH_{pro}:HTH-GFP plants were crossed to generate plant lines deficient in cER bodies in which HTH-GFP expression could be assessed. Seedlings homozygous for *nai1-1* and expressing the *HTH_{pro}:HTH-GFP* transgene were viewed under an epifluorescence microscope to determine whether the expression pattern of HTH-GFP differed from the pattern seen in *HTH_{pro}:HTH-GFP* transgenic seedlings with the *NAI1* wild-type allele.

The same HTH-GFP tissue level expression profile that was observed in 5-day-old *HTH_{pro}:HTH-GFP* transgenic seedlings (see Section 1.3.3 for a list of the tissues that HTH-GFP localizes to in *HTH_{pro}:HTH-GFP* transgenic seedlings) (see Figures 3.5 to 3.13 for images of HTH-EYFP localized to these tissues) was found in 5-day-old *HTH_{pro}:HTH-GFP* seedlings in a *nai1-1* mutant background (Figure 2.5). Within cells of 5-day-old *HTH_{pro}:HTH-GFP* transgenic seedlings, HTH-GFP was found to localize to the reticular network and ER bodies (Chang, 2016). Within the cells of 5-day-old *HTH_{pro}:HTH-GFP* seedlings in a *nai1-1* mutant background, HTH-GFP localized to a reticular network, however, no large (~5-10 μm in length, ~1 μm in diameter) fluorescent spindle-shaped bodies corresponding to ER bodies were observed these seedlings (Figure 2.6).

Table 2.1. Primers used for quantitative real time polymerase chain reaction. The forward and reverse primers for *HOTHEAD* (*HTH*; AT1G72970), *ACTIN 7* (*ACT7*; AT5G09810), *GLYCERALDEHYDE-3-PHOSPHATE DEHYDROGENASE C-2* (*GAPC2*; AT1G13440) are outlined. These primer pairs were used to amplify the cDNA of *HTH* and housekeeping genes (*ACT7* and *GAPC2*) in salt shocked and untreated 11-day-old Ws plants. The efficiencies and coefficients of determination for these primer pairs was determined through a qRT-PCR assay on a pooled cDNA dilution series.

	Forward Primer	Reverse Primer	Primer Pair Efficiency	Primer Pair Coefficient of Determination
HTH	5′ – GAGAGGTGGCGTTCCGTTTA – 3′	5′ – TTCACGAACGCAGCATCGG – 3′	100.5%	0.992
ACT7	5′ – TGGAACTGGAATGGTGAAGG – 3′	5′ – GACTGAGCTTCATCACCAACG – 3′	104%	0.996
GAPC2	5′ – GGTGACAACAGGTCAAGCATT – 3′	5′ – CAACCACACACAAACTCTCGC – 3′	110.2%	0.998

Figure 2.1. The isolation of subcellular components through fractionation of root homogenate. Total homogenate was centrifuged using increasing centrifugal force to separate out cellular components based on size. As ER bodies are quite large organelles (~5-10 µm in length, (~1 µm in diameter) and should pellet under conditions of low centrifugal force and be found enriched in the first pellet fraction (P1). “P” denotes Pellet; “S" denotes Supernatant; “xg” denotes centrifugal force; numbers 1, 8, and 17 following P or S denote the centrifugal force used to acquire that fraction.

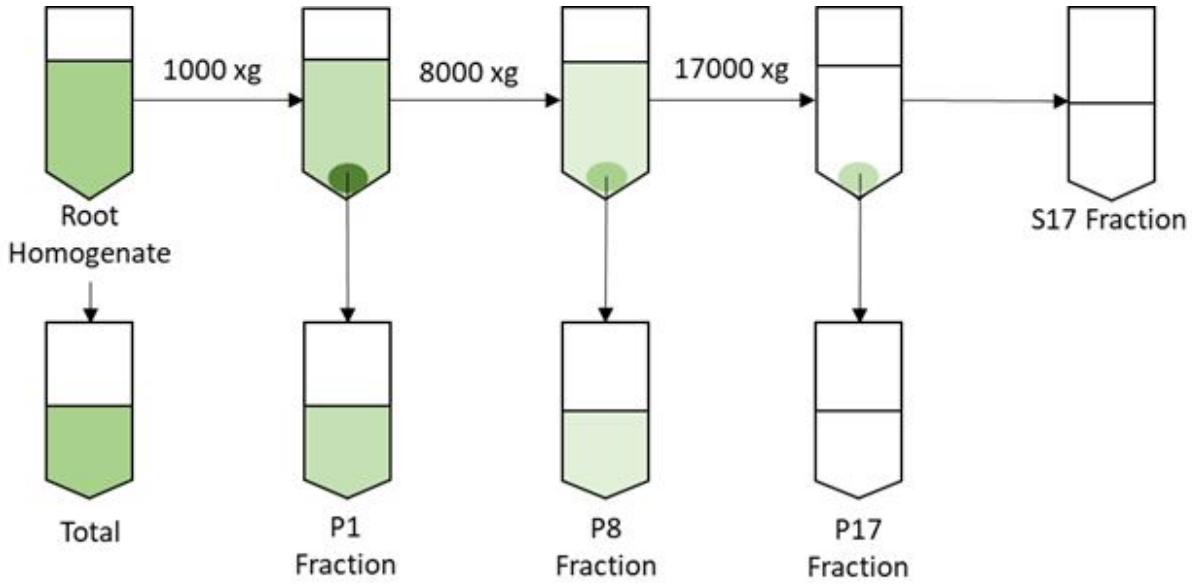
1000 xg
8000 xg
17000 xg
Root
Homogenate
S17 Fraction
Total
P1
Fraction
P8
Fraction
P17
Fraction

Figure 2.2. *HOTHEAD* expression in response to salt shock.

A. *HTH* transcript levels in 11-day-old Ws plants transferred from an MS plate to either a control MS plate or an MS plate supplemented with 100 mM NaCl and then returned to the growth chamber for 6-, 12-, or 24-hours. *HTH* transcript levels were normalized to *ACT7* and *GAPC2* transcript levels by the $2^{-\Delta\Delta CT}$ method. Error bars were generated by taking the standard deviation of two technical replicates. *HTH* expression data were derived from the averages of three biological replicates. Lower case letters indicate significance between samples (significant p values < 0.01). Significance was determined through a two-way anova and a Tukey's HSD test.

B. Midrib cells in rosette leaves of an 11-day-old HTH_{pro}*:HTH-GFP* plant transferred from an MS plate to either a control MS plate or an MS plate supplemented with 100 mM NaCl and then returned to the growth chamber for 24-hours. White outlined arrows indicate fluorescence punctates and the white arrowhead indicates the reticular network. C. Midrib cells in rosette leaves of a HTH_{pro}*:HTH-GFP* plant transferred to MS plates supplemented with 100 mM NaCl for 24-hours. White arrows indicate ER bodies and the white arrowhead indicates the reticular network. HTH-GFP fluorescence is shown in green. Scale bar is 20 µm.

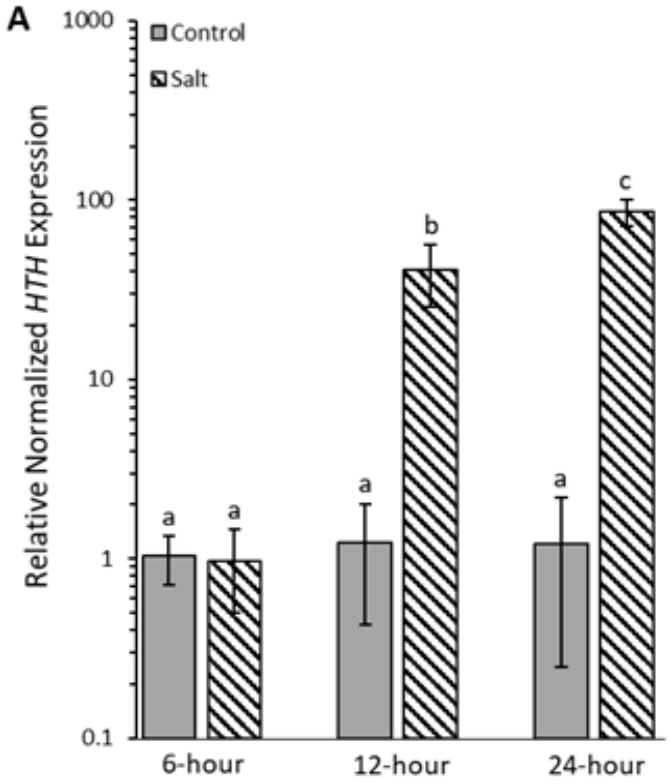
A
1000
100
10
1
0.1
Control
Salt
Relative Normalized HTH Expression
a
a
a
b
a
c
6-hour
12-hour
24-hour

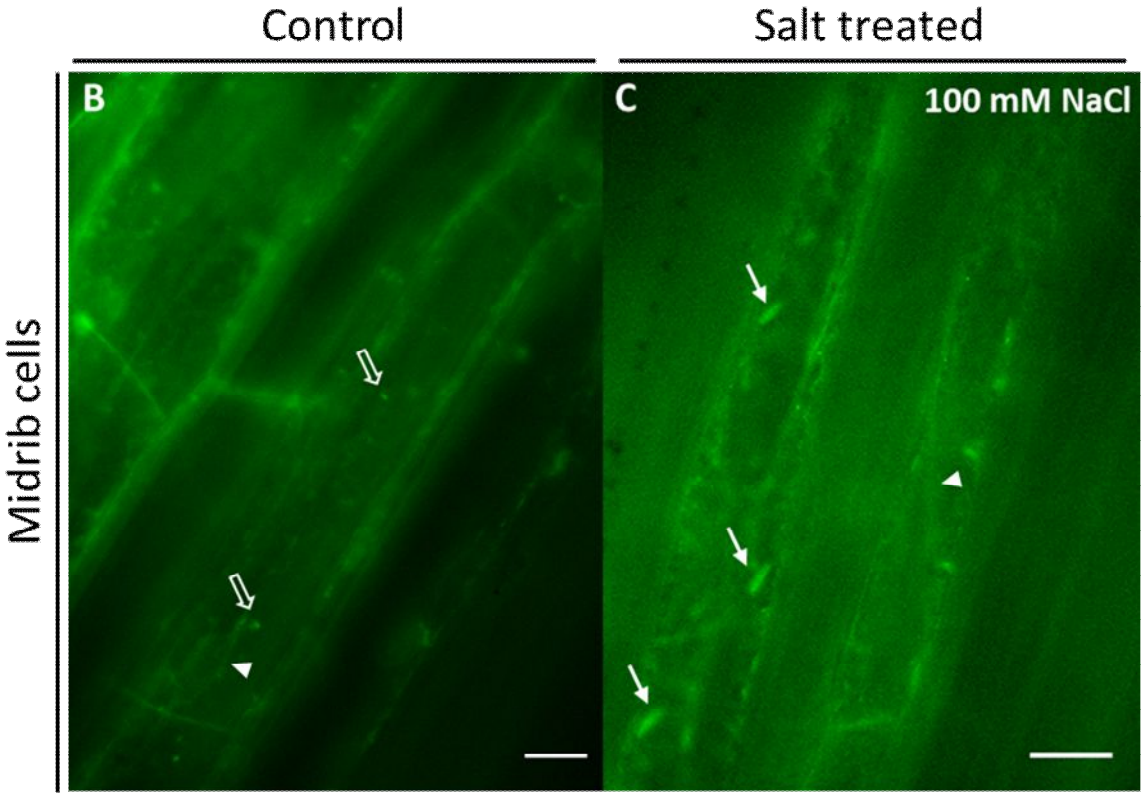
Control
Salt treated
Midrib cells
B
C
100 mM NaCl

Figure 2.3. Visualization of HTH-GFP in cell fractions isolated from 11-day-old *HTH_{pro}:HTH-GFP* plants.

A. Micrographs from left to right: total fraction, P1 fraction, P8 fraction, P17 fraction, S17 fraction. The total fraction shows a low number of fluorescent bodies; the P1 fraction shows a high number of fluorescent bodies; the P8 fraction shows a low number of fluorescent bodies; the P17 fraction shows punctate fluorescent structures; the S17 fraction shows no fluorescent bodies. P(#) indicates the pellet from the respective (#)000 xg spin and S17 indicates supernatant from the 17000 xg spin. White arrows indicate putative ER bodies containing HTH-GFP. HTH-GFP fluorescence is shown in green. Scale bar is 20 μm.

B-D. Protein (20 mg/ml) from each fraction was loaded onto a 10% SDS-polyacrylamide gel and transferred to PVDF membranes. Protein transfer was confirmed through Ponceau staining. B. Ponceau stains of two blots run at the same time, under the same conditions. C. Immunoblot analysis of all five samples with an anti-GFP antibody. Protein bands appear around 100 kDa. D. Immunoblot analysis of all five samples with an anti-PYK10 antibody. Protein bands appear around 60 kDa. Marker (M) is in kDa. Lines underneath the protein standard kDa values in the M lane indicate where that protein band migrated on the blot.

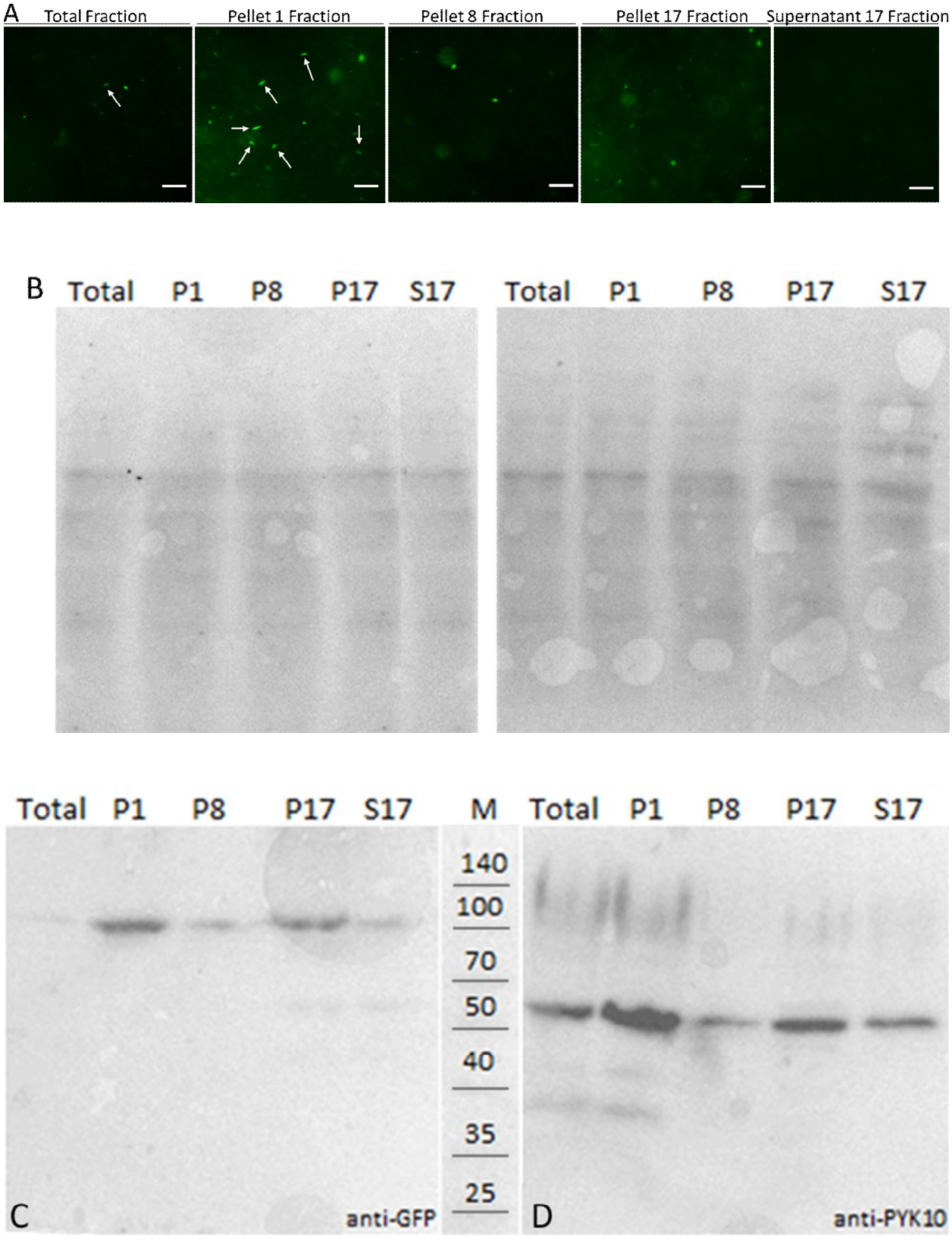
A
Total Fraction
Pellet 1 Fraction
Pellet 8 Fraction
Pellet 17 Fraction
Supernatant 17 Fraction
B
Total
P1
P8
P17
S17
Total
P1
P8
P17
S17
Total
P1
P8
P17
S17
M
140
100
70
50
40
35
25
C
anti-GFP
Total
P1
P8
P17
S17
D
anti-PYK10

Figure 2.4. Mandelonitrile lyase activity in HTH-GFP rich fractions. A. The positive control assay with almond MDL as the enzyme source. B. The no substrate control with almond MDL as the enzyme source. C. The no enzyme control. D. P1 fraction sample tested for MDL activity with mandelonitrile substrate. This P1 fraction contains a large amount of disrupted cER bodies that contained HTH-GFP. The y-axis displays the absorbance (Abs) of benzaldehyde product resulting from the cleavage of mandelonitrile by MDL.

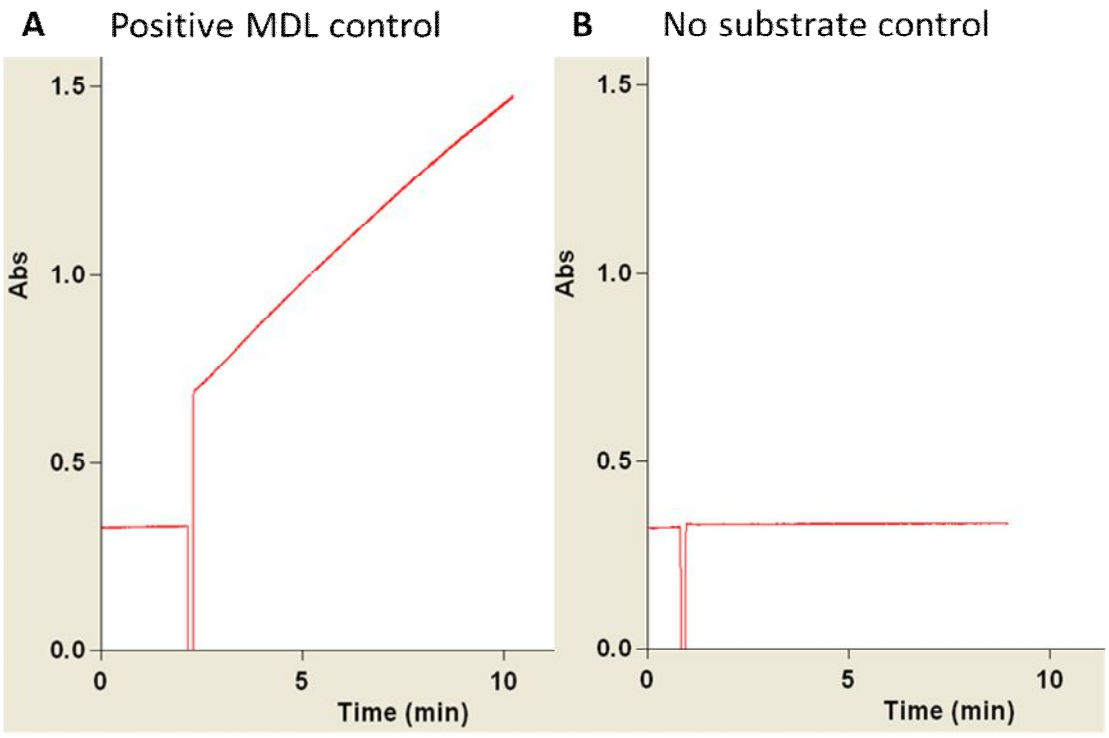
A
Positive MDL control
B
No substrate control
Abs
1.5
1.0
0.5
0.0
0
5
10
Time (min)

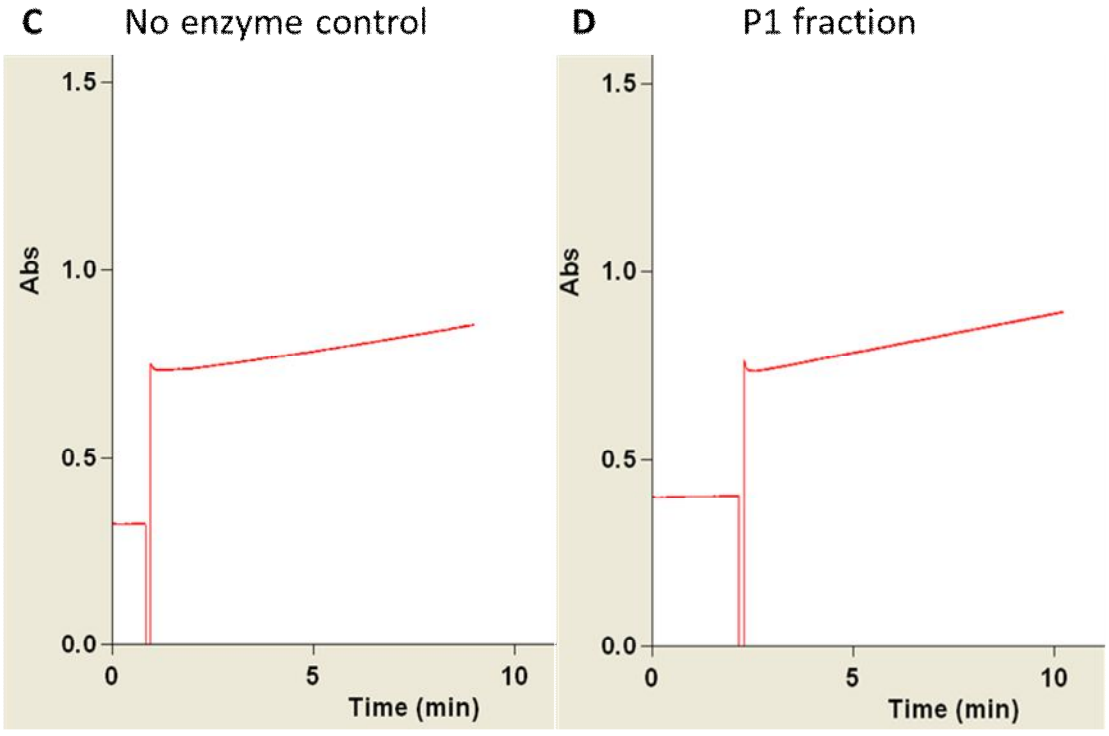
C
No enzyme control
D
P1 fraction
Abs
1.5
1.0
0.5
0.0
0
5
10
Time (min)

Figure 2.5. Micrographs showing tissue expression profiles in the shoot and hypocotyl of HTH-GFP seedlings in the *nai1-1* mutant background. HTH-GFP is expressed in cotyledons (A-C), petioles (D-F), the emerging true leaf (G-I), and the hypocotyl (J-L). The white outline arrows indicate trichomes in panels J-L. M. A higher magnification of the area outlined by the white box in panel A. The white arrows indicate the ER reticular network in panels A-C and M. HTH-GFP fluorescence is shown in green, autofluorescence in red, the other images shown here are merged fluorescence with autofluorescence. Images of HTH-GFP expression in shoot tissues is found in Chapter 3. Scale bar is 50 µm.

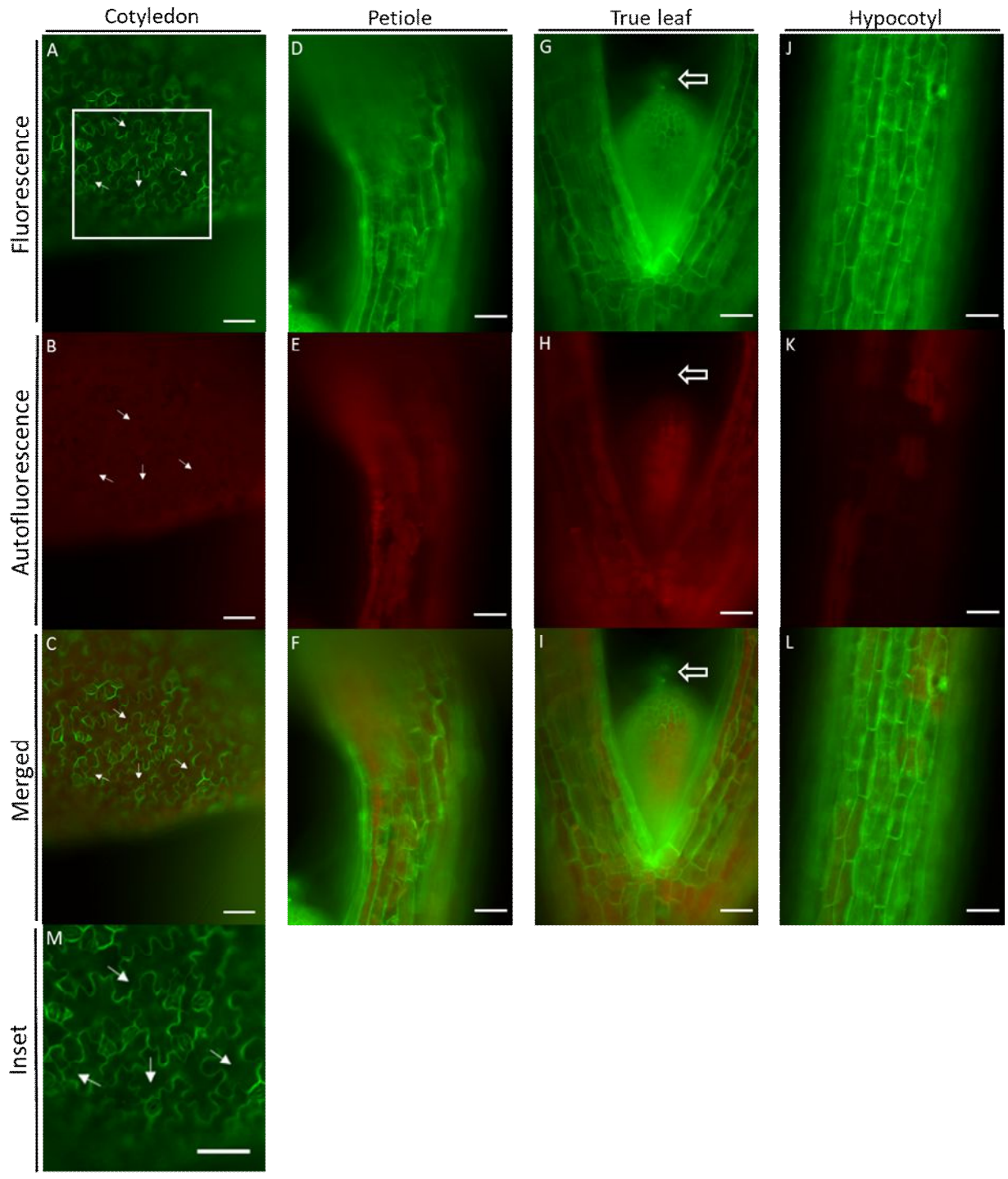
Cotyledon
Petiole
True leaf
Hypocotyl
Fluorescence
Autofluorescence
Merged
Inset
A
B
C
D
E
F
G
H
I
J
K
L
M

Figure 2.6. Micrographs showing tissue expression profiles of HTH-GFP in the *nai1-1* mutant seedling roots. HTH-GFP is expressed in the root-shoot junction (A-C), the primary root elongation zone (D-F), the lateral roots (G-I), and the primary root tip (J-L). HTH-GFP fluorescence is shown in green, autofluorescence in red, the other images shown here are merged fluorescence with autofluorescence. Images of HTH-GFP expression in root tissues is found in Chapter 3. Scale bar is 50 µm.

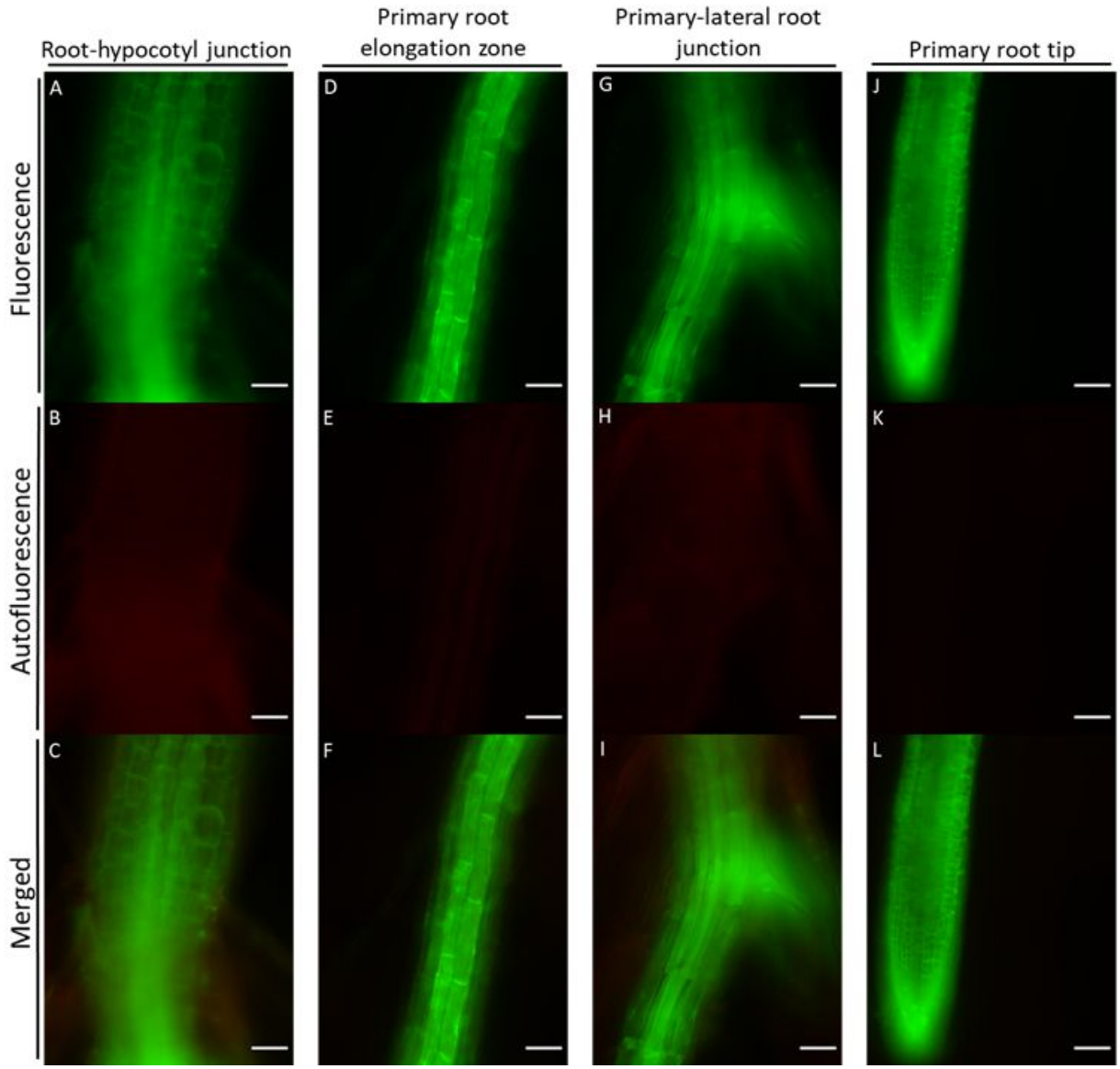
Root-hypocotyl junction
Primary root elongation zone
Primary-lateral root junction
Primary root tip
Fluorescence
Autofluorescence
Merged
A
B
C
D
E
F
G
H
I
J
K
L

2.4 Discussion

2.4.**1** *HOTHEAD* gene expression in response to salt shock

HTH-GFP expression was characterized by Chang (2016) using the HTH_{pro}*:HTH-EYFP* and HTH_{pro}*:HTH-GFP* translational reporter fusion constructs. Using confocal microscopy, Chang (2016) observed the colocalization of HTH-EYFP or HTH-GFP with an ER body fluorescent protein reporter (Chang, 2016; Hayashi et al., 2001). ER bodies are known to be involved in stress pathways in *A. thaliana* (Hayashi et al., 2001; Matsushima et al., 2002; Matsushima et al., 2003b; Nakazaki et al., 2019a; Ogasawara et al., 2009; Takahashi et al., 2011) and are induced in rosette leaves - where they are normally absent - under conditions of wounding or pathogen attack (Matsushima et al., 2003b; Nakazaki et al., 2019a; Ogasawara et al., 2009). The localization of HTH to ER bodies involved in a known stress pathway suggests an additional function for HTH apart from its role in cuticle formation/function.

To further investigate the possible role of HTH in plant stress pathways, Ws *A. thaliana* plants were salt shocked and *HTH* transcript levels monitored over a 24-hour period following treatments. Salt shock was chosen for two reasons. 1. A transcriptional response and subsequent elevated HTH protein expression was demonstrated in response to a molecule that signals biotic stress - MeJA - by Chang (2016). The present study compared Chang's (2016) results to those obtained using an abiotic stressor (salt shock). 2. Salt shock has been shown to trigger an ER body mediated stress response (Hayashi et al., 2001). Upon salt shock, cER bodies were shown to fuse to one another as well as to the vacuole (Hayashi et al., 2001). cER body fusion with the vacuole brings the BGLUs present in cER bodies into contact with their substrate – glucosinolates – within the vacuole; this reaction results in cyanogenesis.

Salt shock is not a common experience for most plants; salt stress is much more common in nature (Shavrukov, 2013). The distinction between salt stress and shock resides in the amount of salt the plant is exposed to over time. Salt shock describes a situation in which a large amount of salt is added to a plant's environment at a single point in time - usually after germination - whereas salt stress is characterized by a slow addition of salt over an extended period of time (Shavrukov, 2013). *A. thaliana* plants are relatively salt sensitive and thus experience salt shock at NaCl concentrations of 100 mM or higher (Shavrukov, 2013). Exposure to salt shock immediately triggers osmotic stress within the plant; under conditions of salt stress, the effects of osmotic stress are minimized (Munns and Tester, 2008; Shavrukov, 2013). Exposure to salt shock also triggers ionic stress; the effect of this stress is not immediate as the concentration of Na within the plant needs to build to toxic levels - this can take days to come into effect (Munns, 2002; Shavrukov, 2013; Roshandel and Flowers, 2009; Verslues et al., 2006).

HTH transcript levels were shown to increase significantly in response to salt shock following 12- and 24-hours of treatment (Figure 2.2 A). The increase in *HTH* transcript levels was very similar to the increase in *HTH* transcript levels shown in response to MeJA exposure (Chang, 2016) (Figure 2.2 A). The comparison of qRT-PCR results from these two studies confirms that *HTH* transcription is induced by stress.

In response to salt shock, *HTH* transcript levels began to increase significantly between 6- and 12-hours of treatment (Figure 2.2 A). Between 12- and 24-hours of treatment, *HTH* transcript levels continue to rise in salt shocked plants (Figure 2.2 A). It is unknown how long this increase in *HTH* transcript level persisted past the 24-hour timepoint. An in-depth time series, over a longer period of time with multiple sample collection timepoints, should be conducted to fully analyze the *HTH* expression profile under salt shock and MeJA exposure.

It is unknown whether the increase in *HTH* transcript seen during salt shock is due to plasmolysis, osmotic stress, or ionic stress. Characterizing the trends in *HTH* expression under salt shock over a longer period could help map out what specific stress *HTH* is responsive to. Most genes responsive to the plasmolysis and osmotic stress aspect of salt shock treatment are upregulated within minutes to hours of exposure (Munns and Tester, 2008); whereas most genes responsive to the ionic stress aspect of salt shock are upregulated days after exposure (Munns, 2002; Roshandel and Flowers, 2009; Verslues et al., 2006). If *HTH* expression follows one of those patterns, this may identify which stressor *HTH* is responsive to. It may also be useful to compare *HTH* responses to salt shock and salt stress over time to pinpoint the signals responsible for the increase in *HTH* transcript expression (Shavrukov, 2013).

2.4.**2** HOTHEAD protein expression in response to salt shock

In response to salt shock, ER bodies containing HTH-GFP were observed in the midrib cells of rosette leaves in NaCl-treated plants after 24-hours of treatment (Figure 2.2 C). These ER bodies were likely iER bodies as they were observed in the rosette leaves of NaCl-treated plants and not in untreated plants (Figure 2.2 B, C). However, it is possible that those ER bodies were not iER bodies and were either cER bodies or L-ER bodies instead. It is unlikely that these were cER bodies as cER bodies are root-specific (Hayashi et al., 2001). However, they may have been L-ER bodies which are a recently described leaf-specific category of ER bodies that, like cER bodies, are constitutively expressed (Hayashi et al., 2001; Nakazaki et al., 2019a). L-ER bodies have been reportedly found constitutively in three types of epidermal cells in rosette leaves; marginal cells, epidermal cells surrounding the midrib, and giant pavement cells (Nakazaki et al., 2019a). As the images showing ER bodies in the midrib cells of NaCl-treated plants were captured using an epifluorescence microscope, it is difficult to determine whether these ER

bodies are in the midrib cells or in the epidermal cells covering the midrib cells (Figure 2.2 C). Although L-ER bodies are not induced by stress (Nakazaki et al., 2019b), they are known to be involved in plant defence (Nakazaki et al., 2019a), thus the localization of HTH to these structures would still be of interest. However, it seems likely that these are iER bodies as they were observed in rosette leaves following salt shock treatment.

HTH-GFP was not observed in iER bodies until 24-hours following salt shock exposure; as there is a lag between transcription and translation, the HTH-GFP seen in these iER bodies may have been transcribed around the 12-hour timepoint. This assumption is supported by the increase in *HTH* transcript observed at the 12-hour timepoint (Figure 2.2). It was not determined whether the increases observed in *HTH* transcript levels translated into increases in HTH protein levels, or how much of that newly translated HTH protein localized to iER bodies, or whether inactive HTH protein residing in the ER was activated by the removal of post-translational conjugates under salt shock.

It is also unknown whether HTH is localized exclusively to iER bodies or to cER bodies (including L-ER bodies) under salt shock. It may be that the majority of HTH is localizing to iER bodies as these are the only ER bodies responsive to stress (Nakazaki et al., 2019b). This would be an interesting area to investigate moving forward as iER bodies have been found to differ in their protein content and mode of formation as compared to cER bodies and L-ER bodies (Hayashi et al., 2001; Kinoshita et al., 1999; Matsushima et al., 2002; Nakazaki et al., 2019a,b; Ogasawara et al., 2009). The localization of HTH to one of these three types of ER bodies could provide insight into HTH's role as a potential MDL involved in cyanogenesis under conditions of salt shock.

To determine what type of ER body HTH localizes to during salt shock, HTH-GFP expression could be examined in a plant line expressing PYK10-RED FLOURESCENT PROTEIN (RFP) or BGLU18-RFP. If HTH-GFP colocalizes with PYK10-RFP in root and shoot ER bodies this would indicate that HTH localizes to cER bodies and L-ER bodies, respectively during salt shock (Matsushima et al., 2004; Nakazaki et al., 2019a). If HTH-GFP colocalizes with BGLU-RFP in pavement cell or giant pavement cell ER bodies this would indicate that HTH localizes to iER bodies or L-ER bodies, respectively during salt shock (Ogasawara et al., 2009; Nakazaki et al., 2019a).

Another way to determine which ER body HTH localizes to under salt shock would be to isolate ER bodies from the roots and leaf tissues separately from salt shocked 11-day-old plants. The homogenate from the two tissue types would be subjected to subcellular fractionation by differential centrifugation (Figure 2.1). Each fraction from those two tissue types would undergo immunoblot analysis which would probe for HTH-GFP, in the same fraction as PYK10 or BGLU18. In the root samples, if HTH-GFP were found in the same fraction as PYK10 this would confirm that HTH localizes to cER bodies even under salt shock. If HTH-GFP were found in the same fraction as BGLU18, this would indicate that iER bodies are expressed under salt shock and that HTH localizes to them. In the leaf samples, if HTH-GFP were found in the same fraction as PYK10 or PYK10 and BGLU18 it would indicate that HTH localizes to L-ER bodies under salt shock. If HTH-GFP were found in the same fraction as BGLU18 but not PYK10 it would indicate that HTH localizes to iER bodies induced in the leaves under salt shock but not to L-ER bodies. The localization of HTH to all three types of ER bodies could indicate that HTH, like ER bodies, may serve different roles that may be tissue dependent and vary under normal and stressed growth conditions.

2.4.**3** HOTHEAD protein in constitutively expressed ER bodies

HTH is known to play a role in cuticle formation/function based on the mutant phenotypes (Chang, 2016; Krolikowski et al., 2003) but uncovering its role in stress responses required further experimental investigation. Chang (2016) utilized microscopy to investigate HTH localization; the current study utilized subcellular fractionation and genetic analysis to investigate HTH-GFP localization to cER bodies.

The isolation of cER bodies has been achieved using relatively simple subcellular fractionation techniques (Hayashi et al., 2001; Matsushima et al., 2003; Yamada et al., 2008). In this study, these methods were used to isolate cER bodies from *HTH_{pro}:HTH-GFP* transgenic roots (Figure 2.1). When viewed using a fluorescence microscope, the Total, P1, and P8 fractions showed evidence that HTH-GFP was localized to cER bodies (Figure 2.3 A). cER bodies are clearly enriched in the P1 fraction as compared to the Total and P8 samples (Figure 2.3 A). Some smaller cER bodies (~ 4-5 μm in length, ~ 1 μm in diameter) were isolated in the P8 fractions, but the majority were found in the P1 fraction (Figure 2.3 A). It is unknown whether the smaller sized ER bodies differ in function or composition from full sized ER bodies. They may simply have been too small to pellet in the P1 fraction and were thus carried over to pellet in the P8 fraction. The punctate structures shown in Figure 2.3 A are likely HTH-GFP aggregates; these may have formed from ruptured cER bodies, the ER, or they may have been derived from other regions within the cell that HTH-GFP has thus far not been found to localize.

Immunoblot analyses of the subcellular fractions are consistent with the results shown in Figure 2.3 A and the findings of Chang (2016); HTH-GFP is found in the P1 fraction (Figure 2.3 C) - which is enriched for cER bodies (Matsushima et al., 2003b) - as well as in the P17 fraction

(Figure 2.3 C) - which may be enriched for the fluorescent punctates observed in Figure 2.3 A. A large proportion of PYK10 - a protein that is relatively abundant in cER bodies - was also found in the P1 fraction (Figure 2.3 D). These experimental findings support the hypothesis that HTH-GFP localizes to cER bodies which were successfully isolated in the P1 fraction. PYK10 was present in each fraction as expected except for the S17 fraction which also contained PYK10 whereas previous studies failed to detect it (Matsushima et al., 2003b) (Figure 2.3 D). This may be due to the methodology used in the present study wherein samples were centrifuged at 17,000 xg instead of 100,000 xg. This may have allowed PYK10 protein to remain in the supernatant as opposed to being isolated in the P17 pellet. Although it is likely that partitioning of PYK10 to supernatant instead of the P17 pellet can be explained by changes in methodology, this discrepancy would need to be addressed going forward.

Upon repeating cellular fractionations, it would be beneficial to include an ER marker such as BiP as an additional control. Previous studies on ER body isolates derived by subcellular fractionation of 7-day-old *A. thaliana* seedlings indicate that BiP levels should remain constant between the first and final pellet fractions (Yamada et al., 2008). Additionally, this should be repeated with salt shocked or MeJA treated plants to further investigate the localization of HTH to iER bodies. The *nai1-1* mutant plants expressing the HTH_{pro}*:HTH-GFP* transgene that were generated in this study should be used as neither cER bodies nor L-ER bodies are produced in this background (Matsushima et al., 2004; Nakazaki et al., 2019a) (Figure 2.5 and 2.6). The expectation is that, under stress conditions, only iER bodies would be present in the *nai1-1* mutant background, thus with an immunoblot analysis, HTH-GFP should be present in the same fraction as BGLU18 but not PYK10 (Ogasawara et al., 2009). This would confirm the localization of HTH to iER bodies under salt stress and MeJA exposure.

The only phenotype of *nai1-1* mutants is the absence of cER bodies (Matsushima et al., 2004). In this mutant background, HTH-GFP was found to be expressed within a reticular network and was not found in ER body-like structures. In other words, no large (~5-10 μm in length), mobile (0.5-1 μm/sec), spindle-shaped structures were observed indicating that in *HTH_{pro}:HTH-GFP* transgenic seedlings HTH-GFP is generally localizing to cER bodies (Figure 2.5 and 2.6). These results should be validated through subcellular fractionation and immunoblot analysis of HTH-GFP in the *nai1-1* background. If the above findings hold true, the majority of the HTH-GFP should be found in the P17 fraction instead of in the P1 fraction (Williamson et al., 2015). If a relatively large amount of HTH-GFP was found in the P1 fraction, that could indicate that HTH-GFP is localizing to iER bodies.

If HTH localization to ER bodies was required for maintaining normal cuticle function, perturbing cER body formation should compromise cuticle properties and potentially result in an organ fusion phenotype. To my knowledge, the *nai1-1* mutant lacks an organ fusion phenotype, however, other aspects of the cuticle phenotype have not been investigated such as treating tissues (floral and rosette leaf) with toluidine blue O (TBO) stains, doing chlorophyll extractions, or pollen germination assays. However, if there are no disruptions to the cuticle of *nai1-1* mutants this would indicate that cER bodies are not required for proper cuticle formation/function (Matsushima et al., 2004). As HTH-GFP has been confirmed to localize to cER bodies, this suggests that proper cuticle formation/function is not dependent on HTH localization to cER bodies. This would need to be explored in-depth; however, it may indicate that HTH plays a distinct role in the ER network that differs from its role within cER bodies.

2.4.4 HOTHEAD enzymatic activity

Bioinformatic analyses of the HTH protein sequence suggest that HTH may function as either an ADH or an MDL (Chang, 2016; Krolikowski et al., 2003; Kurdyukov et al., 2006). To test HTH enzymatic function, affinity purified fractions of HTH expressed in *E. coli* were used in an MDL and an ADH assay, but this proved uninformative (Chang, 2016; Le Dreff-Kerwin, 2019) (Figure 2.4). Isolation of active protein using heterologous approaches present challenges especially when employing prokaryotic systems to express eukaryotic proteins. Preliminary data show that HTH is a glycosylated protein (Chang 2016). In *E. coli* post-translational modification such a glycosylation does not occur thus the HTH protein produced in *E. coli* may not have been functional (Khow and Suntrarachun, 2012). In this study, fractions obtained from HTH_{pro}*:HTH-GFP* transgenic plants enriched for HTH-containing cER bodies were used for the MDL assay. Although no activity was detected in these experiments, these results do not exclude the possibility that HTH functions as an MDL.

Immunoblot analyses suggest that the HTH-GFP protein degrades rapidly once extracted from plants. Samples derived from crude protein plant extracts or subcellular fractionations left at 4°C in extraction buffer for longer than an hour resulted in an immunoblot displaying multiple protein bands of varying sizes. This speed of degradation may explain the lack of activity seen in cell fractionation experiments. One way to check for protein integrity in this fraction would be to test for the enzymatic activity of another cER body resident protein such as PYK10. If PYK10 does not show any enzymatic activity it could indicate that the enzymes in this fraction have degraded or are in unfavourable conditions. One thing that may be contributing to potentially unfavourable conditions within this cER body enriched fraction could be the lack of other cellular proteins. PYK10 has been found to increase in enzymatic activity when complexed with other proteins (Nagano et al., 2005, 2008). A similar situation may be true for HTH, thus without

the presence of proteins that may complex with HTH, the enzymatic activity of the protein may be too low to detect. Another factor that may contribute to unfavourable enzyme conditions may be the buffer (CB) that this fraction is suspended in. Experiments conducted with commercial almond MDL suspended in CB were found to attenuate commercial almond MDL enzymatic activity (Appendix D).

The HTH protein may be tightly regulated and not produced in large amount under no-stress conditions. This may be supported by the presence of multiple uORFs within the 5' upstream region of the *HTH* gene discussed above which may act to inhibit translation. This may result in the translation of few HTH proteins which would make it difficult to perform enzymatic assays on a low amount of protein. There are many aspects of this assay that could be improved; the use of quartz instead of plastic cuvettes, further concentrating protein in the P1 fraction, and using dialysis to change the P1 fraction buffer. The most likely avenue for success in deducing HTH enzyme function is to assay HTH recombinant protein that has been expressed in a eukaryotic system.

2.5 Conclusion

In this study I provide three lines of evidence that confirm the localization of HTH to ER bodies. First, I subjected transgenic seedlings to salt shock and showed HTH localization to iER bodies. Second, I confirmed the presence of HTH-GFP in cell fractions enriched for cER bodies, and thirdly, I confirmed that HTH-GFP-containing ER bodies were absent in *nai1-1* mutant plants.

The salt shock treatment demonstrated that *HTH* is responsive to salt shock, as transcript levels increased 12-hours after NaCl treatment, and HTH-GFP was found to localize to ER bodies that were induced by the NaCl treatment. The isolation of cER bodies allowed for the investigation into what proteins were present in these structures. Using immunoblot analysis against HTH-GFP and PYK10, it was shown that HTH-GFP was in the same fraction as PYK10 which indicated that HTH-GFP is localized to cER bodies (the main protein in cER bodies is PYK10). These HTH-GFP enriched fractions derived from the isolation of cER bodies provided the material used for the MDL assay – this was uninformative – although hopefully this method of obtaining HTH rich fractions may be used in future enzymatic assays. Finally, HTH-GFP did not localize to any large spindle-shaped ER body structures in the *nai1-1* mutant background. As *nai1-1* mutants do not produce cER bodies this indicates that in a wildtype background, HTH-GFP would normally localize to cER bodies. When cER bodies are absent, HTH-GFP remains localized to a reticular network.

Chapter 3 HOTHEAD isoform localization and function

3.1 Introduction

The cuticle is a heterogeneous structure made up of waxes, cutin polymers, and polysaccharides. It is found external to the cell walls of shoot epidermal cells of most plants (Bessire et al., 2007; Hegebarth and Jetter, 2017; Li-Beisson et al., 2009; Xue et al., 2014). The cuticle is the plant's first line of defence against pathogen attack and herbivory. The cuticle also plays a principal role in maintaining organ separation during plant development (Lolle et al., 1992). Mutations that affect cuticle composition or structure often give rise to plants with ectopic organ fusions illustrating the importance of the cuticle in limiting these types of interactions (Bird et al., 2007; Ingram and Nawrath, 2017; Lolle et al., 1992; Sieber et al., 2000; Wellesen et al., 2001).

Altering the permeability of the seed coat has been shown to alter germination which can be detrimental to the plant's survival (Beeckman et al., 2000). The seed coat is maternally derived and composed of five cell layers; oi1, oi2, ii1, ii1', and ii2 (Beeckman et al., 2000; Raviv et al., 2017; Robinson-Beers et al., 1992) (Figure 1.2). At the one-cell stage of embryo development, an electron-dense layer is found to border cells of the ii1 layer internal to the seed coat, bordering the developing embryo (Figure 1.2). This electron-dense layer is thought to be a cuticle layer and is present throughout embryo development (Beeckman et al., 2000). At the torpedo-stage, the oi1 layer cells thicken with an electron-dense substance which will become "wall 3" (Beeckman et al., 2000) (Figure 1.2). The oi1 layer cells respond to mechanical stress of the growing embryo pushing on the seed coat by depositing cutin-like monomers into wall 3 (Creff et al., 2015; Luo et al., 2005). Thickening of wall 3 due to cutin-like monomer deposition has been shown to regulate seed size (Creff et al., 2015; Luo et al., 2005).

The oi2 layer cells are also electron-dense, however, this layer is mainly composed of suberin-like rather than cutin-like materials (Beisson et al., 2007; Molina et al., 2008). Upon contact with water, the oi2 layer ruptures, releasing mucilage (Dean et al., 2007), however, it is unknown whether the oi2 layer is responsible for seed coat permeability or whether one of the two, or both, cutin layers within the seed coat regulate permeability. Seed coat permeability can be tested using a tetrazolium red stain (Wharton, 1955). This stain forms red formazans upon contact with the embryo, thus a population of seed that has a higher percentage of red stained seeds indicates a plant line with a highly permeable seed coat (Wharton, 1955).

The *HTH* gene is encoded by 2834 bp's in Col and consists of six exons that are predicted to translate into a 65.3 kDa HTH protein (AT1G72970.1) (Figure 1.4). The splice variant of the *HTH* gene is translated into a 62.2 kDa HTH isoform that is missing a 27 aa peptide sequence from the middle of the fifth exon (Figure 1.4). The AT1G72970.1 protein model (full-length HTH) predicts a putative N-terminal signal peptide, five putative N-glycosylation sites, and four putative PKC phosphorylation sites (Chang, 2016) (Figure 1.4). The AT1G72970.2 protein model (splice variant HTH) predicts a putative N-terminal signal peptide, four instead of five putative N-glycosylation sites, and three instead of four putative PKC phosphorylation sites (Chang, 2016) (Figure 1.4).

The deletion of an N-glycosylation and a PKC phosphorylation site could greatly impact protein folding, function, or localization in the splice variant. The 27 aa deletion in the splice variant isoform occurs upstream of the three putative HTH catalytic residues and does not disrupt any of the key functional aa, however, it does occur within the proposed GMC oxidoreductase C-terminal domain (Chang, 2016) (Figure 1.4). The C-terminal domain of GMC oxidoreductase family proteins is proposed act as the substrate binding domain; thus, a deletion in this region

could result in the two HTH isoforms binding to different substrates.

The localization pattern of the HTH splice variant isoform was examined through the native *HTH* promoter driven expression of the HTH splice variant isoform tagged with EYFP (*HTH_{pro}:HTH-EYFP*). This expression pattern was compared to the full-length HTH protein expression pattern to gain insight into the putative function of the splice variant isoform. Protein expression studies using *HTH_{pro}:HTH-EYFP* identified HTH expression in floral buds, sepals, petals, stamens and ovaries (Chang, 2016). Expression of HTH was found in the vasculature of primary and lateral roots, the hypocotyl, and cotyledons, as well as in the epidermal cells of emerging true leaves, the hypocotyl and cotyledons (Chang, 2016). Expression of HTH was also found in the SAM, trichomes, and guard cells (Chang, 2016). Within the cells, HTH was expressed in a reticular network as well as in cER bodies.

The *HTH_{pro}:SV-EYFP* construct was transformed into a wild-type Ws background and a mutant *hth-9* background. The presence of the *HTH_{pro}:SV-EYFP* construct in a *hth* mutant background allowed for the determination of *hth* mutant phenotype rescue by the *HTH_{pro}:SV-EYFP* construct. Additionally, as the *hth-9* mutant background is not expected to express HTH or SV, the introduction of the *HTH_{pro}:SV-EYFP* construct should not result in SV overexpression.

3.2 Materials and Methods

3.2.**1** Growth conditions

A. thaliana lines used in this study include wild-type Ws, *hth-9* mutant, and transgenic *HTH_{pro}:HTH-EYFP*. Seeds were germinated and seedlings grown under the conditions outlined in Materials and Methods 2.2.**1** above. Sterilized seeds were plated on half-strength MS media (Sigma-Aldrich) at a density of 10-15 seeds/plate for microscopy studies. Conditions for sterile growth are outlined in Materials and Methods 2.2.**1** above.

3.2.**2** Generation of the HOTHEAD splice variant construct and transgenic plants

A 1.8 kilobase (kb) *HTH* genomic fragment was synthesized by Genscript Biotech and subcloned into *HTH_{pro}:HTH-EYFP* (Chang, 2016), using *Xho*I (R0146; NEB) and *Sac*I (R0156; NEB) restriction enzymes (Appendix E). The resulting transgene was designated *HTH_{pro}:HTHSplice Variant-EYFP (HTH_{pro}:SV-EYFP).* This construct introduced an 81-bp deletion within the 5th exon of *HTH* resulting in a 27 aa deletion in HTH resulting in a known splice variant isoform of HTH (AT1G72970.2) (Appendix F). The plasmid was verified through PCR and sanger PCR sequencing (The Centre for Applied Genomics; SickKids).

The *HTH_{pro}:SV-EYFP* construct was transformed into chemically competent DH5-α *Escherichia coli* (*E. coli*) bacterial cells. Transformants containing the construct were selected on spectinomycin containing (100 µg/ml) Luria broth plates and the plasmid was verified through PCR and sanger plasmid sequencing (The Centre for Applied Genomics; SickKids). Verified plasmids isolated from spectinomycin-resistant *E. coli* were subsequently transformed into GV3101 *Agrobacterium tumefaciens* (*A. tumefaciens*) via a freeze-thaw method (Höfgen and

Willmitzer, 1988). Transformants containing the construct were selected on spectinomycin (100 µg/ml), Gentamicin (30 µg/ml), Rifampicin (10 µg/ml) containing Luria broth plates and the plasmid sequence verified through PCR and sanger plasmid sequencing (The Centre for Applied Genomics; SickKids). Spectinomycin resistant *A. tumefaciens* were used to generate transgenic plants in the Ws and the homozygous *hth-9* mutant background using the floral dip method (Clough and Bent, 1998). Four transgenic lines, determined to be homozygous using segregation analysis for glufosinate resistance (0.0036 g/L; Total WipeOut; Wilson), were used for subsequent phenotypic characterization and microscopy experiments.

3.2.**3** Chlorophyll permeability assay

One cauline leaf was taken from three, 4- to 6-week-old *hth-9* and Ws T3 homozygous HTH_{pro}*:SV-EYFP* plants. These leaves were weighed and placed in tubes containing 2 ml of 80% ethanol. The tubes were agitated gently while covered in aluminum foil to protect the samples from light. Three hundred µl was removed for spectrophotometric analysis (MultiSkan Spectrum; Thermo Lab Systems) and replaced 20 min, 40 min, 60 min, 90 min, and 24 hours after the immersion of the leaf in ethanol. The amount of chlorophyll in each sample was determined using the following equation: Total µmol chlorophyll = 7.93 (A_{664}) + 19.53 (A_{647}) (Lolle et al., 1997). Each sample was normalized to the 24-hour time point, to adjust for total chlorophyll content. The chlorophyll diffusion rates were plotted against time and the standard deviation for each data point was assessed. This assay consisted of three technical replicates and used tissue obtained from two independently transformed HTH_{pro}*:SV-EYFP* transgenic lines in the Ws and *hth-9* background. This assay was performed once.

3.2.**4** Analysis of seed phenotype

The morphology of seeds derived from homozygous *HTH$_{pro}$:SV-EYFP* transgenic plants in the Ws and homozygous *hth-9* mutant background was examined under a Nikon SMZ 1500 (Nikon Corp) dissecting microscope. Images were captured using a Nikon CoolPIX 990 (Nikon Corp) camera mounted on the dissecting microscope. The weight of ~ 660 seeds from each transgenic line were determined using an analytical balance. Approximately 660 seeds were used as this was the maximum number of seeds that were derived from one of the four independently transformed T3 homozygous SV-EYFP transgenic lines. Approximately 660 seeds were manually counted out from each line and weighed in bulk as a single *A. thaliana* seed could not be weighed as it was too small. The weights of the transgenic seeds were compared to the weights of Ws and *hth-9* seeds using ~660 seeds from these lines. Data were analyzed using a one-way anova and significant interactors were determined using a post hoc test - Tukey's HSD.

Seeds obtained from homozygous *HTH$_{pro}$:SV-EYFP* transgenic plants in the Ws and homozygous *hth-9* mutant background were stained using tetrazolium red to determine relative seed coat permeability. One hundred seeds from each line were incubated in a solution of 1% tetrazolium red in the dark at 30°C for 48 hours. Following incubation, seeds were viewed under a Nikon SMZ 1500 (Nikon Corp) dissecting microscope and images captured with the Nikon CoolPIX 990 (Nikon Corp) camera. The number of seeds that stained red were compared to the Ws and *hth-9* transgenic lines. This assay was replicated three times; each batch of 100 seeds used in these replicates was derived from one homozygous T2 plant. Two independently transformed *HTH$_{pro}$:SV-EYFP* transgenic lines in each background were tested.

3.2.**5** Microscopy

Seedlings and floral tissue from the *HTH$_{pro}$:HTH-EYFP* and *HTH$_{pro}$:SV-EYFP* lines were mounted

on glass microscope slides in milliQ water and examined under an epifluorescence microscope (Zeiss Axio Imager D1; Carl Zeiss Inc.). Two wavelengths were used (ex/em); EYFP - 500/515 nm and autofluorescence - 550/570 nm. Twenty independent T2 lines were surveyed for expression patterns. It was unknown whether these lines were homozygous or not; while waiting for glufosinate resistance (0.0036 g/L; Total WipeOut; Wilson) screens to identify homozygous T3 plants, the expression profile in the T2 plants was examined. Half of the lines were examined by Erica Cushnie (an undergraduate thesis student) and the results from all twenty pooled. Four homozygous T3 lines were identified and screened by Erica Cushnie (an undergraduate thesis student) and the author, Therese Francom. Images of seedling and floral tissue from the homozygous T3 lines were captured with the Zeiss AxioCam MRm camera (Carl Zeiss Inc.) using the AxioVision software.

3.3 Results

The *HTH$_{pro}$:SV-EYFP* construct was generated using the *HTH$_{pro}$:HTH-EYFP* construct (Chang, 2016) by introducing an 81 bp deletion in the fifth exon. Both constructs were transcriptionally controlled by the native *HTH* promoter region (Appendix E). In this study, the *HTH$_{pro}$:SV-EYFP* construct was expressed in Ws wild-type and *hth-9* mutant plants. Transgenic plant phenotypes were assessed visually, using chlorophyll permeability assays, and by determining relative seed weights.

3.3.**1** Phenotypes of *HTH$_{pro}$:SV-EYFP* transgenic plants

The *HTHpro:HTH:EYFP* transgene had been shown to fully rescue the mutant phenotype when expressed in the *hth-9* mutant background (Chang, 2016). These transgenic plants showed no evidence of floral organ fusions, did not support pollen germination on vegetative tissues, showed normal levels of permeability to chlorophyll when tissue samples were immersed in 80% alcohol and restored seed size and morphology to wild-type.

To examine whether the SV-EYFP protein rescued the *hth-9* floral organ fusion phenotype, *HTH$_{pro}$:SV-EYFP* transgenic plants were examined for evidence of floral fusions. Wild-type Ws floral buds emerge in a spiral phyllotaxy where floral buds remain physically separated from one another. As flowers matured, sepals opened, allowing petals and reproductive organs to emerge and undergo expansion growth (Figure 3.1 A). Mature mutant *hth-9* flowers remained unopened, with floral organs adhering to one another, constraining expansive growth; some floral buds however, opened allowing petals to emerge slightly (Figure 3.1 A). The *HTH$_{pro}$:SV-EYFP* transgene when expressed in a Ws background resulted in plants with a wild-type floral phenotype (Figure 3.1 A). In a *hth-9* mutant background, however, *HTH$_{pro}$:SV-EYFP* transgenic

plants showed a *hth* mutant floral phenotype (Figure 3.1 A) suggesting failure to complement this aspect of the mutant phenotype.

The rate of chlorophyll extraction from the cauline leaves of Ws, Ws transgenic, *hth-9*, and *hth-9* transgenic plants was monitored over a 24-hour period. The lowest rate of chlorophyll extraction (RCE) was shown from cauline leaves of Ws (Figure 3.2). The RCE from one of the Ws independently transformed transgenic lines (ITL) fell between the RCE for Ws and *hth-9* (Figure 3.2). The RCE from the second Ws ITL was similar to the RCE from *hth-9* and the RCE from the two *hth-9* ITLs were greater than the RCE from *hth-9* (Figure 3.2). These experimental results suggest a failure to complement the mutant phenotype as the RCE in transgenic leaves is greater than the RCE of their respective backgrounds (Figure 3.2).

To assess the rescue of seed phenotypes, seed size, morphology, and coat permeability were examined. Wild-type Ws seeds were small, oval-shaped, and relatively uniform in size. Seed-to-seed adhesion was not observed (Figure 3.3 A). Mutant *hth-9* seeds were visibly larger than Ws seed, although they varied in size and shape, and in some instances were found to adhere to one another (Figure 3.3 A). Seeds obtained from HTH_{pro}*:SV-EYFP* transgenic WS plants were found to resemble Ws seed (Figure 3.3 A). Seeds obtained from HTH_{pro}*:SV-EYFP hth-9* transgenic plants were found to resemble mutant *hth-9* seed suggesting that the HTH_{pro}*:SV-EYFP* transgene did not rescue the mutant seed phenotype (Figure 3.3 A).

The weights of ~660 seeds from each plant line were determined (Figure 3.3 B). A one-way anova analysis indicated a significant difference between some but not all plant lines based on seed weights (p value < 0.000001). Seed weights did not differ between one of the Ws transformed lines and wild-type Ws, however, seed weights from the second Ws transformed

line differed from the wild-type Ws (Figure 3.3 B). This pattern was mirrored in *hth-9* background lines (Figure 3.3 B). Finally, any seeds in the *hth-9* background weighed significantly more than any seeds in the Ws background (Figure 3.3 B).

Ws, *hth-9*, and transgenic HTH_{pro}*:SV-EYFP* seeds were assessed for changes in coat permeability using the tetrazolium red staining assay (Figure 3.4 A). Wild-type Ws seeds were found to stain around 8% of the time while Ws transgenic seeds were found to stain approximately 80% of the time (Figure 3.4 B). Mutant *hth-9* seeds stained around 58% of the time, and *hth-9* SV-EYFP transgenic seeds stained approximately 55% of the time (Figure 3.4 B). The values stated here represent the average staining of two independently transformed transgenic lines in each background.

3.3.**2** Splice variant isoform protein localization in seedlings

The protein localization of SV-EYFP in HTH_{pro}*:SV-EYFP* plants was compared to the localization of HTH-EYFP in HTH_{pro}*:HTH-EYFP* plants. As the SV protein is expected to be translated in HTH_{pro}*:HTH-EYFP* plants, the expression pattern of HTH-EYFP characterized by Chang (2016) should be a summation of the SV-EYFP and HTH-EYFP expression patterns (Appendix J). The expression pattern of SV-EYFP was characterized in HTH_{pro}*:SV-EYFP* plants to distinguish the expression pattern of HTH from SV.

Expression of the SV-EYFP protein was localized to primary and lateral root tips (Figure 3.5, 3.6). Micrographs of HTH_{pro}*:SV-EYFP* roots indicate SV-EYFP was not expressed in the root cap (~0-50 µm from the tip of the root (Romanchuk, 2010)) or root apical meristem (RAM) (~50-150 µm from the tip of the root (Romanchuk, 2010)) (Figure 3.5). SV-EYFP was mainly expressed in the transition zone - also known as the distal elongation zone or basal meristem region (Barrada

et al., 2015; De Smet et al., 2015; Péret et al., 2009; Romanchuk, 2010) (Figure 3.5). This region spanned approximately 150-350 µm from the tip of the root (Figure 3.5). SV-EYFP expression was confined to specific files/columns of cells in this region (Figure 3.5). SV-EYFP may be localizing to alternating files of cells in this region (Figure 3.5). In other words, SV-EYFP may localize to one file but not the files on either side of that first file of cells (Figure 3.5). This would need to be confirmed through the examination of a root tip cross section. In comparison, HTH-EYFP expression was found in the root cap, RAM, and transition zone of the developed primary and lateral roots (Figure 3.5).

In emerging lateral roots, SV-EYFP was initially expressed in the tip of the root; as the emerging lateral root developed, SV-EYFP expression was confined to the transition zone region (Figure 3.6). In comparison, HTH-EYFP expression was faintly expressed all throughout the lateral root during emergence (Figure 3.6).

Absence of SV-EYFP expression in the vasculature was consistent throughout all tissues in *HTH_{pro}:SV-EYFP* transgenic seedlings (Figure 3.5 to 3.15). In Figures 3.5 and 3.6 SV-EYFP expression was seen in cell files that may be of stelar, cortical, or epidermal origin. Across all images of the root tip surveyed (data not included), fluorescence was consistently observed in epidermal cell files and not subepidermal. To resolve this, a higher resolution image would be required.

In *HTH_{pro}:SV-EYFP* seedlings, SV-EYFP was expressed in the epidermal cells of cotyledons, petioles, emerging true leaves, trichomes, and hypocotyl (Figure 3.8 to 3.13), however, SV-EYFP expression here was less intense compared to HTH-EYFP expression in *HTH_{pro}:HTH-EYFP* seedlings. Most notably, SV-EYFP expression was barely detected in the basal end of the

hypocotyl (near the shoot-root junction), however, the fluorescent signal increased as one moved to the apical region of the hypocotyl (apex, near the SAM) (Figure 3.11 to 3.13). Additionally, SV-EYFP expression was observed in guard cells but was absent in the SAM (Figure 3.8 and 3.11). The expression pattern of SV-EYFP changed in 8-day-old seedlings. This differs from HTH- EYFP expression which remained unchanged in the tissues outlined above in 5- to 11-day-old seedlings. At 8-days, there was no SV-EYFP expression in the petioles or cotyledons. Expression of SV-EYFP was observed in developing trichomes (Appendix G).

3.3.**3** Subcellular localization of the splice variant isoform

Within the epidermal cells, HTH-GFP has been shown to localize to the reticular network, ER bodies, and small punctate structures in the roots, hypocotyl, and cotyledons (Chang, 2016). SV-EYFP was found to localize to the reticular network in developing trichomes as well as in the epidermis of hypocotyls, emerging true leaves, petioles, and cotyledons (Figure 3.8 and 3.12). SV-EYFP was found infrequently in ER bodies in the apical region of the hypocotyl as well as in the petioles of 5-day old HTH_{pro}*:SV-EYFP* seedlings.

3.3.**4** Splice variant isoform protein localization in floral organs

Chang (2016) found HTH-EYFP expression in floral buds, the ovary wall of the pistil and in the vasculature and epidermal cells of the sepals, petals, and anthers. SV-EYFP was not found in any floral tissue (Figure 3.14 and 3.15).

Figure 3.1. Floral phenotypes of Ws, *hth-9*, and *HTH_{pro}:SV-EYFP* transgenic plants. A. Wild-type Ws flowers. B. A magnification of Ws wild-type immature floral buds. C. Mutant *hth-9* flowers show a fused floral organ phenotype. D. A magnification of mutant *hth-9* immature floral buds show a fused floral organ phenotype with undulating silique morphology. E. Flowers of Ws *HTH_{pro}:SV-EYFP* transgenic plants show a wild-type phenotype. F. A magnification of Ws *HTH_{pro}:SV-EYFP* transgenic immature floral buds show a wild-type phenotype. G. Flowers of *hth-9 HTH_{pro}:SV-EYFP* transgenic plants show an organ fusion phenotype. H. A magnification of *hth-9 HTH_{pro}:SV-EYFP* transgenic immature floral buds show a fused floral organ phenotype with undulating silique morphology. Scale bar is 0.5 mm.

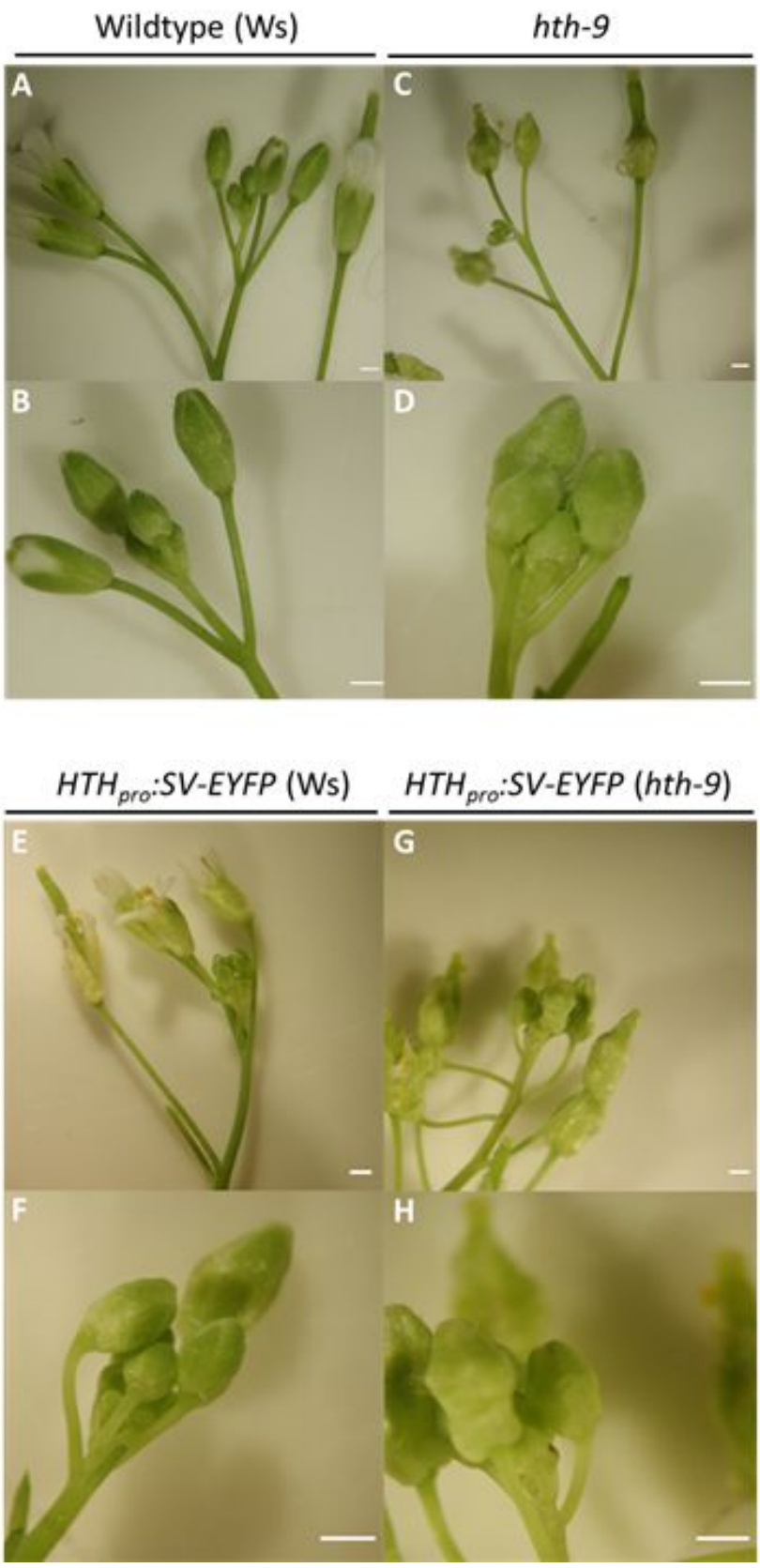
Wildtype (Ws)
hth-9
A
C
B
D
HTH$_{pro}$:SV-EYFP (Ws)
HTH$_{pro}$:SV-EYFP (hth-9)
E
G
F
H

Figure 3.2. Chlorophyll extraction rates from cauline leaves of Ws, *hth-9* mutant, and HTH_{pro}*:SV-EYFP* transgenic plants. The concentration of chlorophyll extracted from cauline leaves in 80% ethanol was monitored over a 90-minute period. The maximum concentration of chlorophyll after 24 hours was set to 100%. Two independently transformed HTH_{pro}*:SV-EYFP* lines (ITL1 and ITL2) in each background were examined. The controls used were the Ws and *hth-9* lines. Standard deviations were derived from three technical replicates.

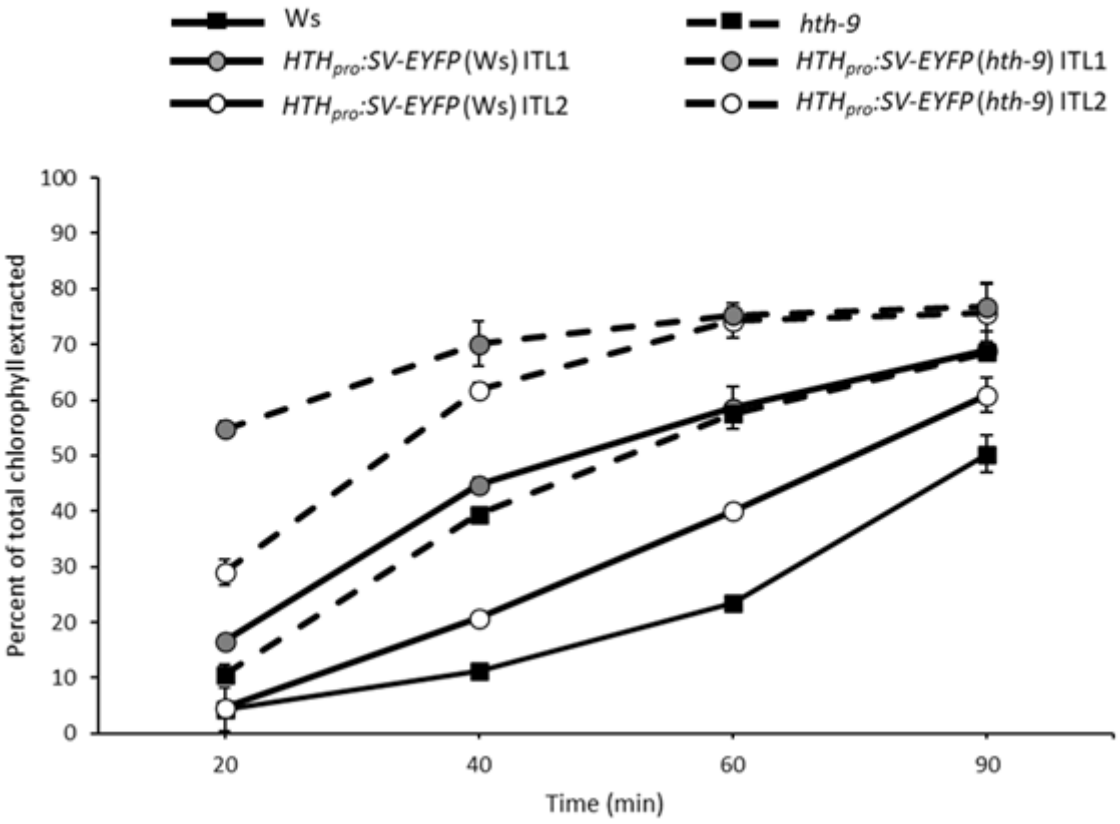
Ws
HTH_pro:SV-EYFP (Ws) ITL1
HTH_pro:SV-EYFP (Ws) ITL2
hth-9
HTH_pro:SV-EYFP (hth-9) ITL1
HTH_pro:SV-EYFP (hth-9) ITL2
Percent of total chlorophyll extracted
100
90
80
70
60
50
40
30
20
10
0
20
40
60
90
Time (min)

Figure 3.3. Seed morphology and weights of Ws, *hth-9*, and *HTH_{pro}:SV-EYFP* transgenic plants.

A. From left to right: wild-type Ws seeds, mutant *hth-9* seeds of differing size and morphology, seeds from Ws plants transformed with the *HTH_{pro}:SV-EYFP* construct, seed from *hth-9* plants transformed with the *HTH_{pro}:SV-EYFP* construct show an altered morphology. White arrows indicate seeds with an altered morphology, the black arrowheads indicate two seeds that are attached.

B. Bar graph showing relative seed weights for wild-type Ws, *hth-9* mutant, and *HTH_{pro}:SV-EYFP* transgenic lines. Two independently transformed transgenic lines in each background were examined. The weights of *hth-9* and the transgenic seeds were normalized to the Ws weights to give a percent increase in seed weight. Lower case letters indicate significance between samples (significant p values < 0.01). Scale bar is 0.5 mm.

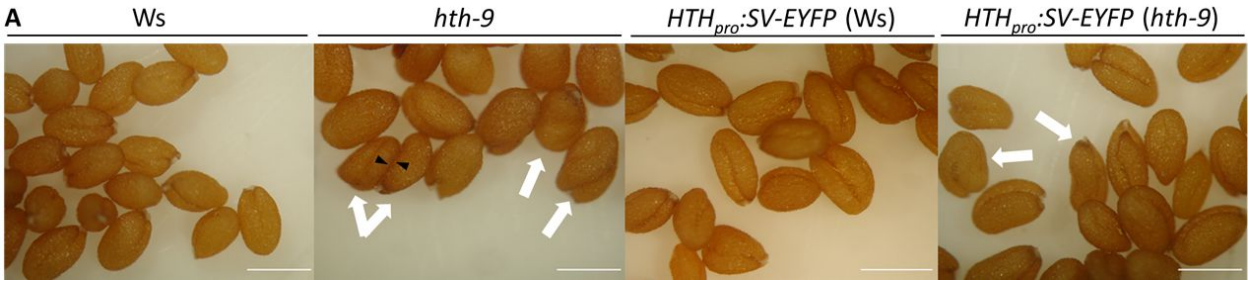
A
Ws
hth-9
HTH_pro:SV-EYFP (Ws)
HTH_pro:SV-EYFP (hth-9)

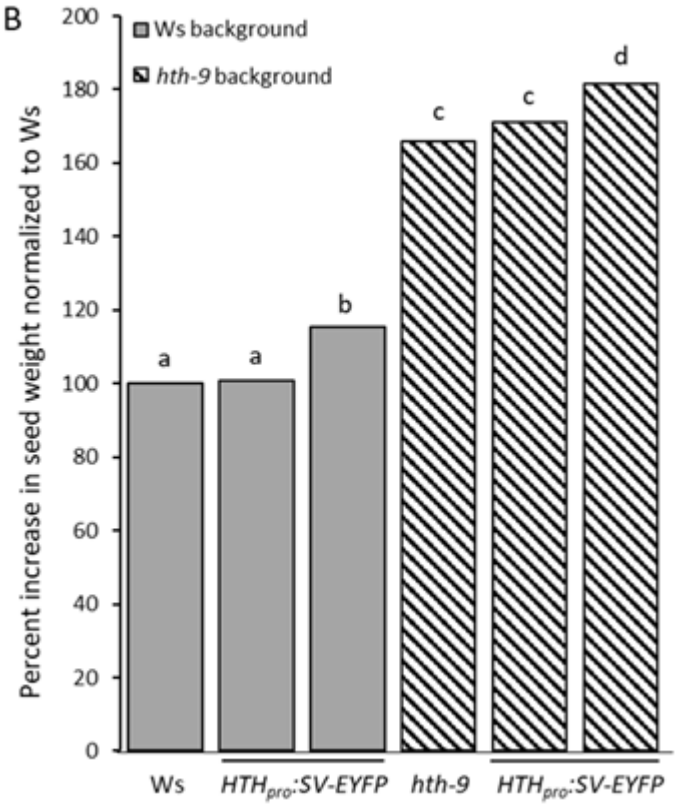
B
Ws background
hth-9 background
Percent increase in seed weight normalized to Ws
0
20
40
60
80
100
120
140
160
180
200
a
a
b
c
c
d
Ws
HTH_pro:SV-EYFP
hth-9
HTH_pro:SV-EYFP

Figure 3.4. Seed coat permeability of Ws, *hth-9* mutant, and HTH_{pro}*:SV-EYFP* transgenic seeds.

A. From left to right: tetrazolium red stained Ws wild-type seeds, *hth-9* mutant seeds, HTH_{pro}*:SV-EYFP* transgenic seeds in a Ws background, HTH_{pro}*:SV-EYFP* transgenic seeds in a *hth-9* mutant background. Yellow to red color gradient - the black line indicates the threshold used to determine whether an embryo was stained red or not.

B. Table showing the number of tetrazolium red stained embryos for each seed line out of 100 seeds tested. Standard deviations were calculated from three replicates. Two independently transformed transgenic lines in each background were examined. Scale bar is 0.5 mm.

A

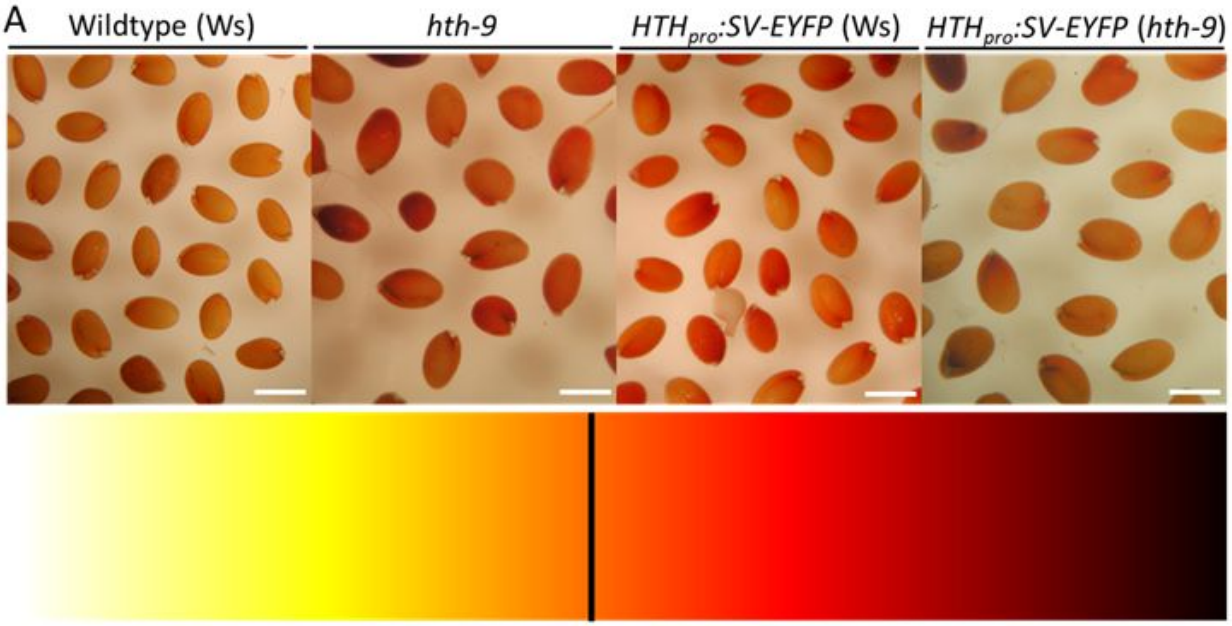

B	**Number of tetrazolium red stained embryos (of 100 seeds)**
Ws	8 ± 5
HTH$_{pro}$:SV-EYFP (Ws)	86 ± 15
HTH$_{pro}$:SV-EYFP (Ws)	74 ± 5
hth-9	58 ± 11
HTH$_{pro}$:SV-EYFP (*hth-9*)	52 ± 11
HTH$_{pro}$:SV-EYFP (*hth-9*)	59 ± 4

Figure 3.5. Micrographs showing HTH-EYFP and SV-EYFP expression in the primary root tip of 5-day-old *HTH_{pro}:HTH-EYFP* and *HTH_{pro}:SV-EYFP* transgenic seedlings. HTH-EYFP is expressed throughout the root tip including the root cap and SV-EYFP expression is seen only in distinct files of cells within the putative transition zone (150-350 µm from the root tip). Fluorescence of HTH-EYFP and SV-EYFP are shown in yellow (A and B). Autofluorescence of HTH-EYFP and SV-EYFP are shown in red (C and D). E and F. Merged micrographs - fluorescence and autofluorescence. The white arrow indicates the root cap. Scale bar is 50 µm.

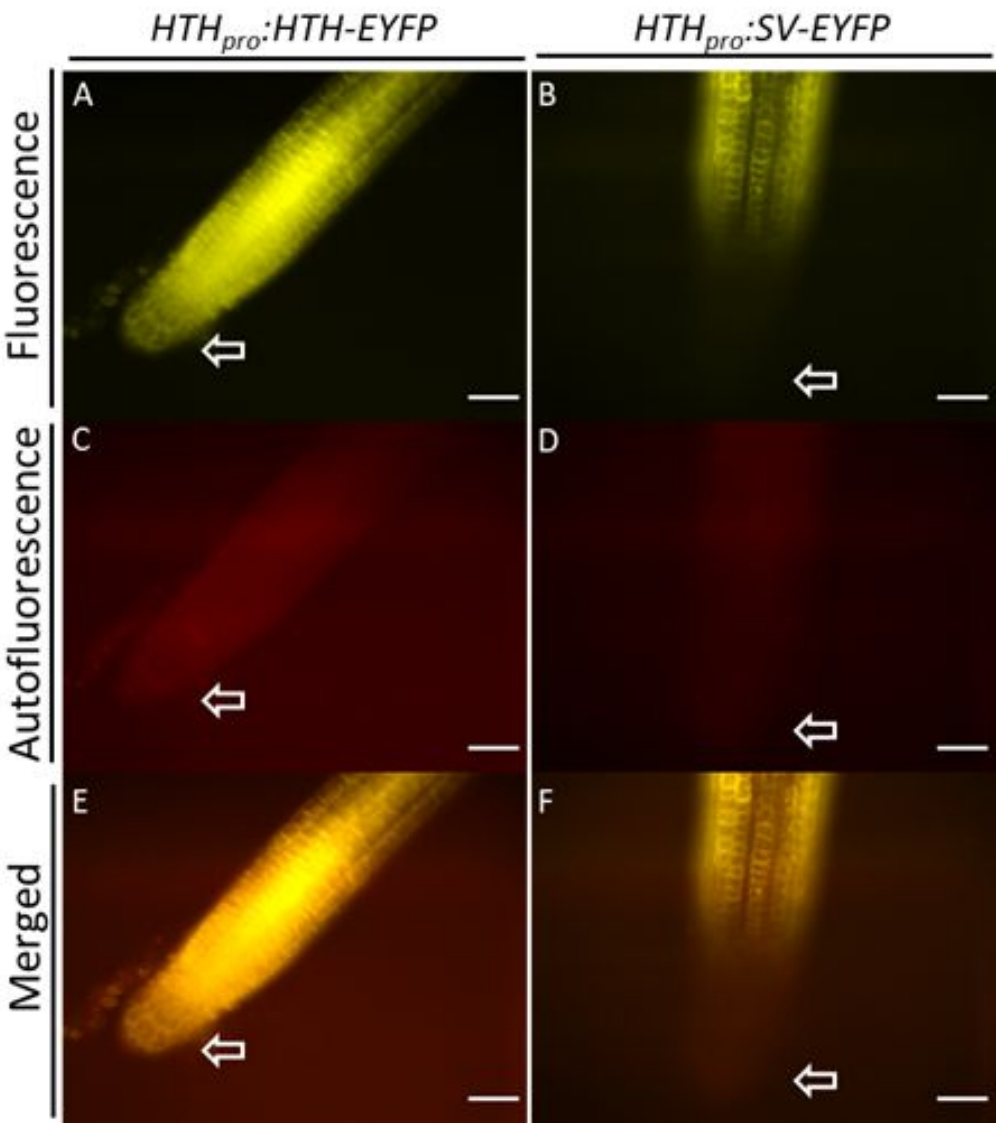
HTH_pro:HTH-EYFP
HTH_pro:SV-EYFP
Fluorescence
Autofluorescence
Merged
A
B
C
D
E
F

Figure 3.6. Micrographs showing HTH-EYFP and SV-EYFP expression in lateral roots emerging from the primary root of 5-day-old *HTH_{pro}:HTH-EYFP* and *HTH_{pro}:SV-EYFP* transgenic seedlings. A. HTH-EYFP is expressed uniformly throughout the developing lateral root and SV-EYFP is expressed at the tip in the emerging lateral root. B. HTH-EYFP is expressed uniformly throughout the developing lateral root and SV-EYFP is expressed along the circumference of the emerging lateral root. C. HTH-EYFP is expressed uniformly throughout the developing lateral root and SV-EYFP is putatively expressed within the epidermal cells of the emerging lateral root. D. HTH-EYFP is expressed uniformly throughout the developing lateral root and SV-EYFP is expressed in the putative transition zone of developed lateral roots. Fluorescence of HTH-EYFP and SV-EYFP are shown in yellow. Autofluorescence of HTH-EYFP and SV-EYFP are shown in red. Merged micrographs - fluorescence and autofluorescence. The white arrows track SV-EYFP expression. Scale bar is 50 μm.

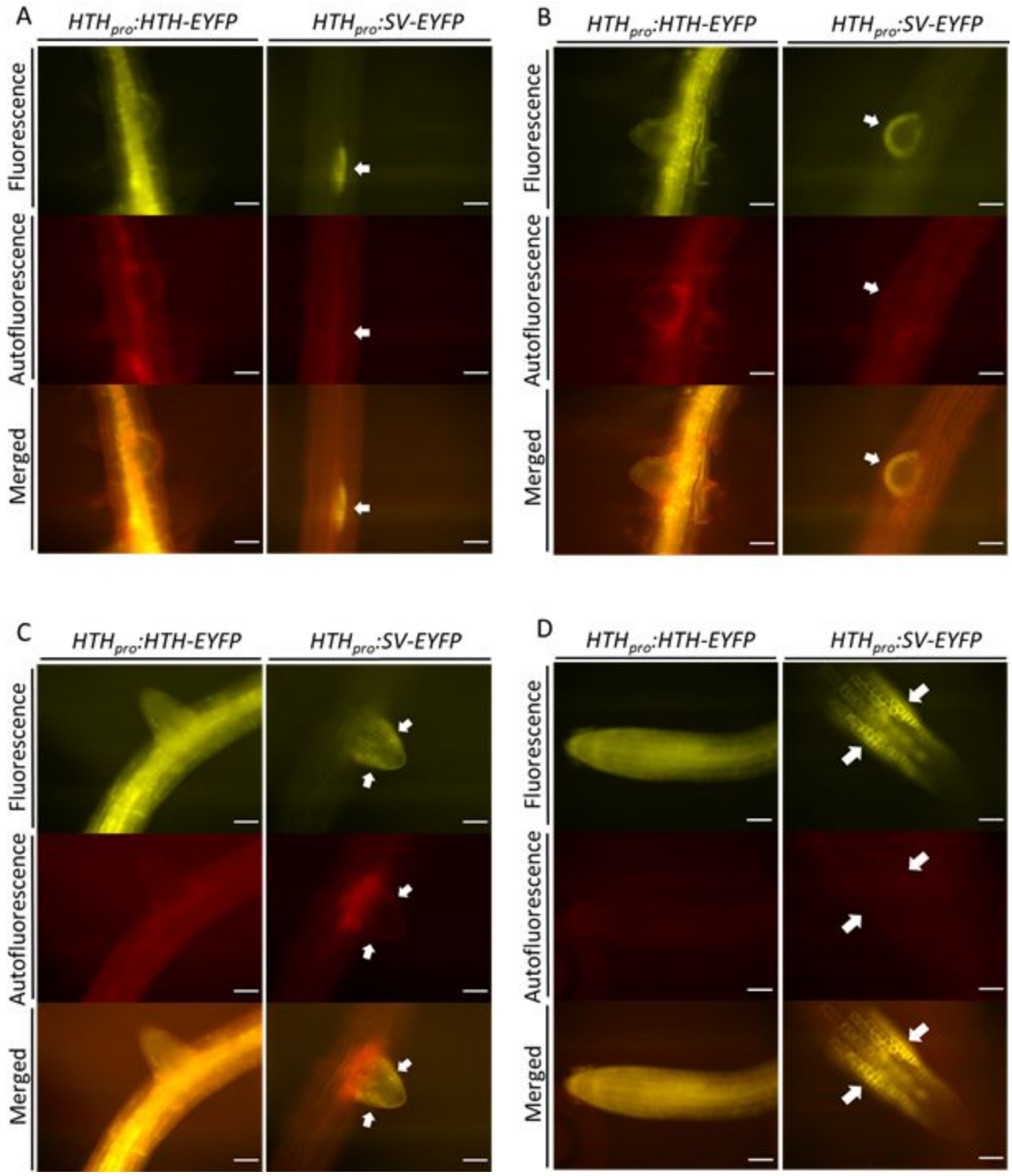
A
HTH_pro:HTH-EYFP
HTH_pro:SV-EYFP
Fluorescence
Autofluorescence
Merged
B
HTH_pro:HTH-EYFP
HTH_pro:SV-EYFP
Fluorescence
Autofluorescence
Merged
C
HTH_pro:HTH-EYFP
HTH_pro:SV-EYFP
Fluorescence
Autofluorescence
Merged
D
HTH_pro:HTH-EYFP
HTH_pro:SV-EYFP
Fluorescence
Autofluorescence
Merged

Figure 3.7. Micrographs showing HTH-EYFP and SV-EYFP expression in the elongation zone of the primary root of 5-day-old *HTH_{pro}:HTH-EYFP* and *HTH_{pro}:SV-EYFP* transgenic seedlings. HTH-EYFP is strongly expressed in the vascular cylinder in this region of the root and SV-EYFP shows no detectable expression. Fluorescence of HTH-EYFP and SV-EYFP are shown in yellow (A and B). Autofluorescence of HTH-EYFP and SV-EYFP are shown in red (C and D). E and F. Merged micrographs - fluorescence and autofluorescence. Scale bar is 50 µm.

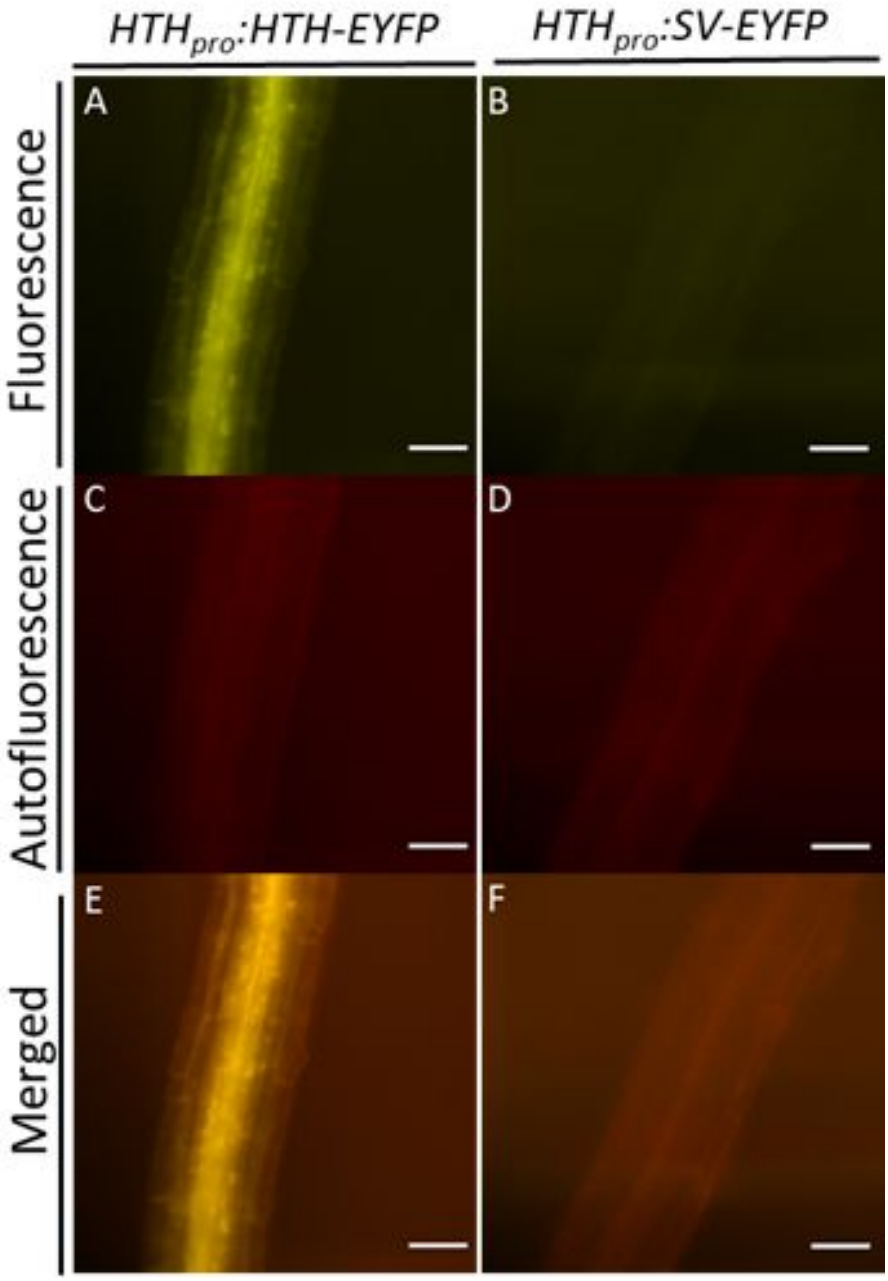
HTH$_{pro}$:HTH-EYFP
HTH$_{pro}$:SV-EYFP
Fluorescence
Autofluorescence
Merged
A
B
C
D
E
F

Figure 3.8. Micrographs showing HTH-EYFP and SV-EYFP expression in the cotyledons of 5-day-old *HTH_{pro}:HTH-EYFP* and *HTH_{pro}:SV-EYFP* transgenic seedlings. Both HTH-EYFP and SV-EYFP are expressed in cotyledons showing overlapping expression patterns. Fluorescence of HTH-EYFP and SV-EYFP are shown in yellow (A and B). Autofluorescence of HTH-EYFP and SV-EYFP are shown in red (C and D). E and F. Merged micrographs - fluorescence and autofluorescence. White arrowheads indicate ER bodies; blue arrowheads indicate the ER reticular network. The white boxes in E and F are shown at higher magnification in panels G and H. Scale bar is 50 μm.

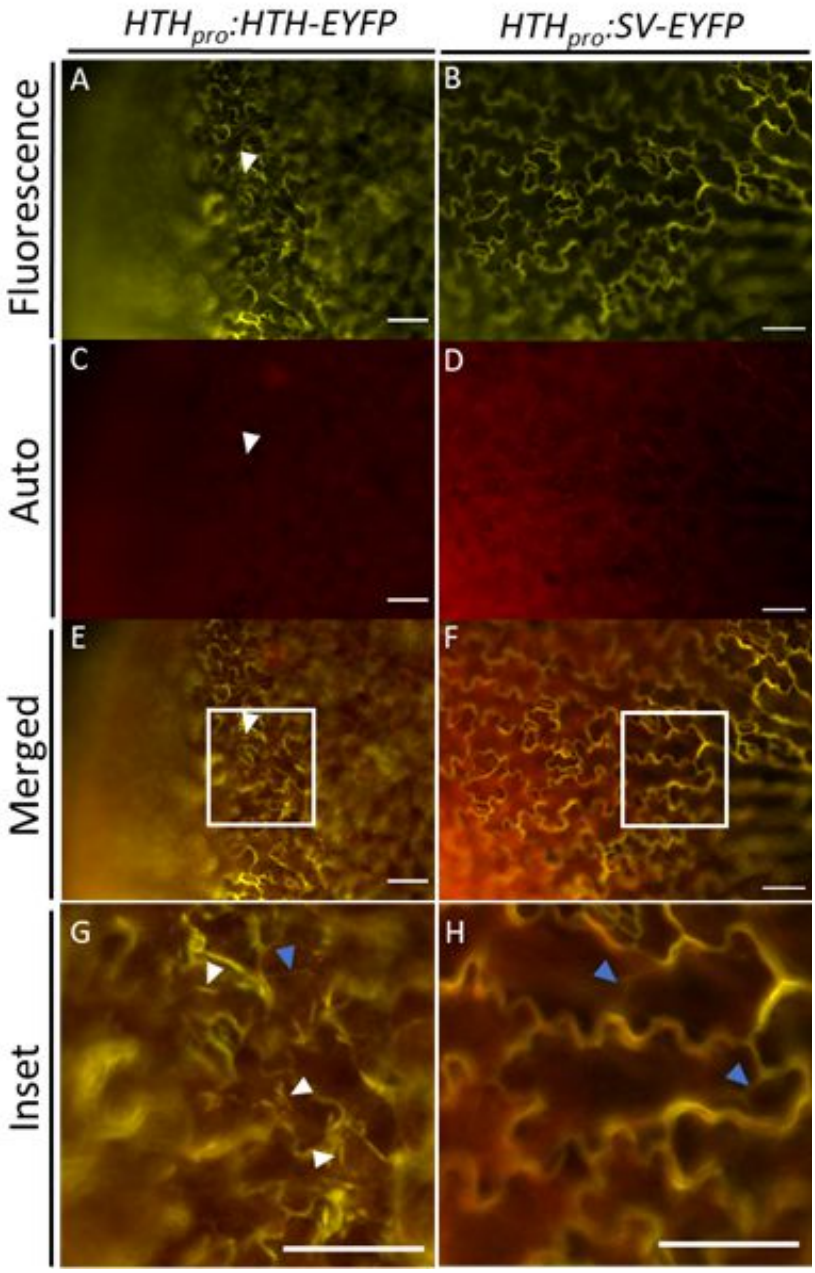
HTH_pro:HTH-EYFP
HTH_pro:SV-EYFP
Fluorescence
Auto
Merged
Inset
A
B
C
D
E
F
G
H

Figure 3.9. Micrographs showing HTH-EYFP and SV-EYFP expression in the petioles of 5-day-old *HTH_{pro}:HTH-EYFP* and *HTH_{pro}:SV-EYFP* transgenic seedlings. Both HTH-EYFP and SV-EYFP show similar patterns of expression in petioles. Fluorescence of HTH-EYFP and SV-EYFP are shown in yellow (A and B). Autofluorescence of HTH-EYFP and SV-EYFP are shown in red (C and D). E and F. Merged micrographs - fluorescence and autofluorescence. Scale bar is 50 µm.

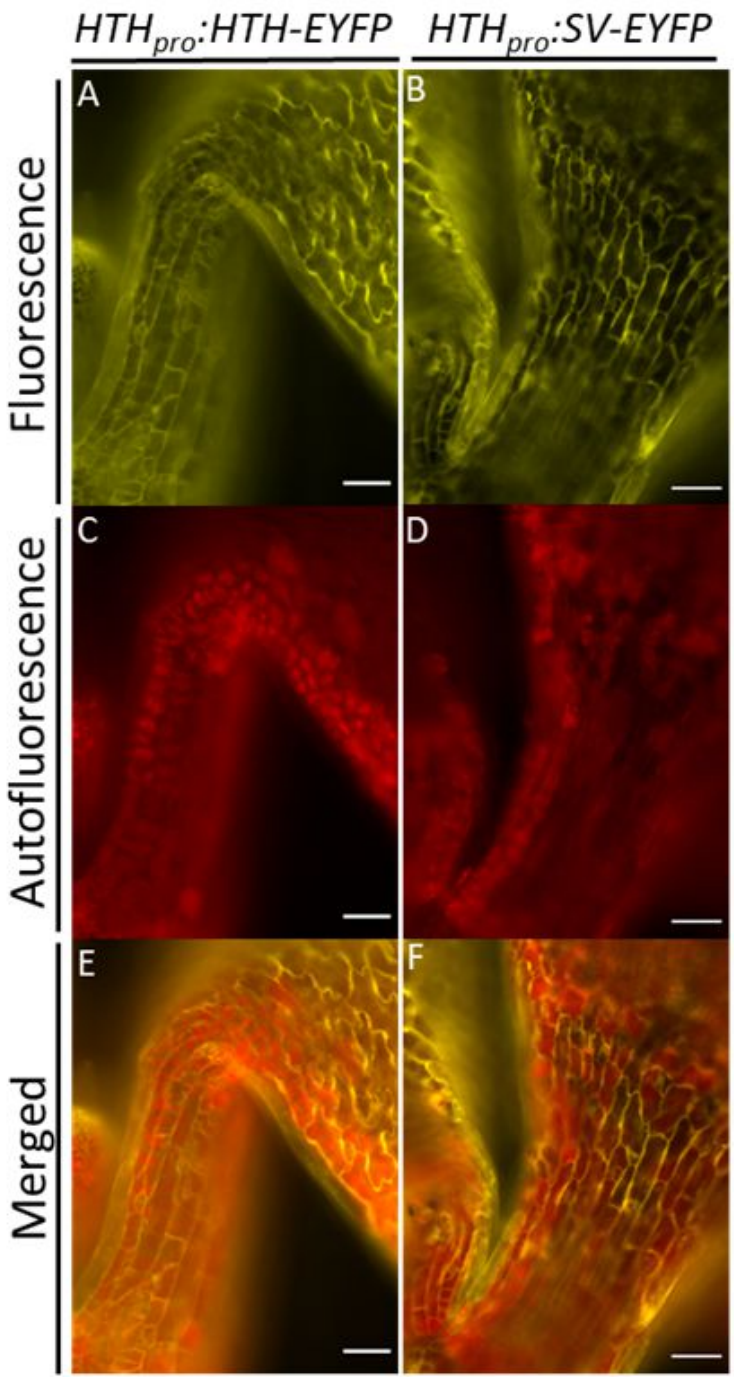
HTH_pro:HTH-EYFP
HTH_pro:SV-EYFP
Fluorescence
Autofluorescence
Merged
A
B
C
D
E
F

Figure 3.10. Micrographs showing HTH-EYFP and SV-EYFP expression in the emerging true leaves of 5-day-old *HTH_{pro}:HTH-EYFP* and *HTH_{pro}:SV-EYFP* transgenic seedlings. Both HTH-EYFP and SV-EYFP are expressed in emerging true leaves. Fluorescence of HTH-EYFP and SV-EYFP are shown in yellow (A and B). Autofluorescence of HTH-EYFP and SV-EYFP are shown in red (C and D). E and F. Merged micrographs - fluorescence and autofluorescence. The white arrow indicates the trichome in each image. Scale bar is 50 µm.

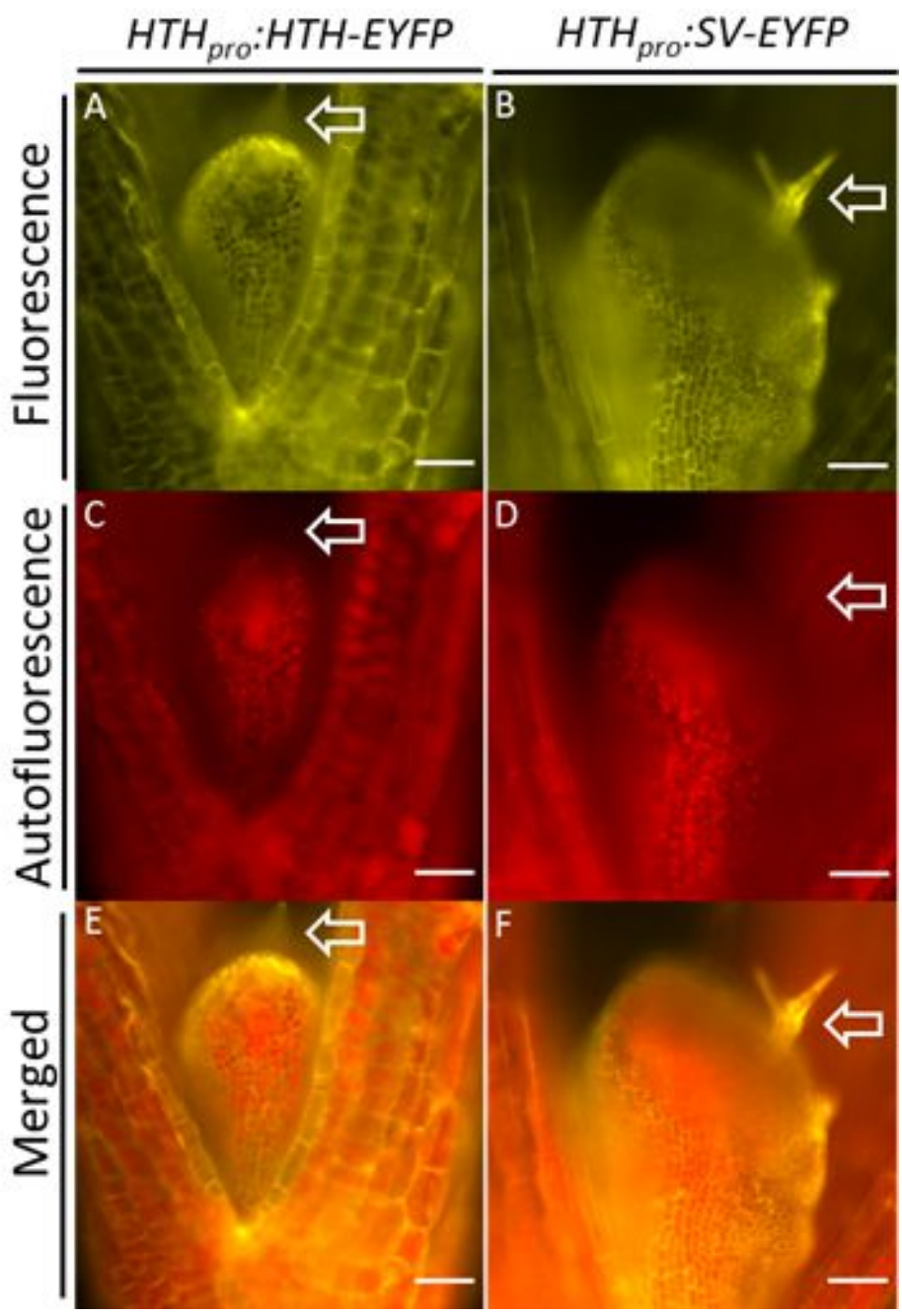
HTH_pro:HTH-EYFP
HTH_pro:SV-EYFP
Fluorescence
Autofluorescence
Merged
A
B
C
D
E
F

Figure 3.11. Micrographs showing HTH-EYFP and SV-EYFP expression in the hypocotyl apex of 5-day-old *HTH_{pro}:HTH-EYFP* and *HTH_{pro}:SV-EYFP* transgenic seedlings. Both HTH-EYFP and SV-EYFP are expressed in cells at the apex of the hypocotyl, between cotyledon petioles. Fluorescence of HTH-EYFP and SV-EYFP are shown in yellow (A and B). Autofluorescence of HTH-EYFP and SV-EYFP are shown in red (C and D). E and F. Merged micrographs - fluorescence and autofluorescence. The white arrow indicates the SAM in each micrograph. Scale bar is 50 µm.

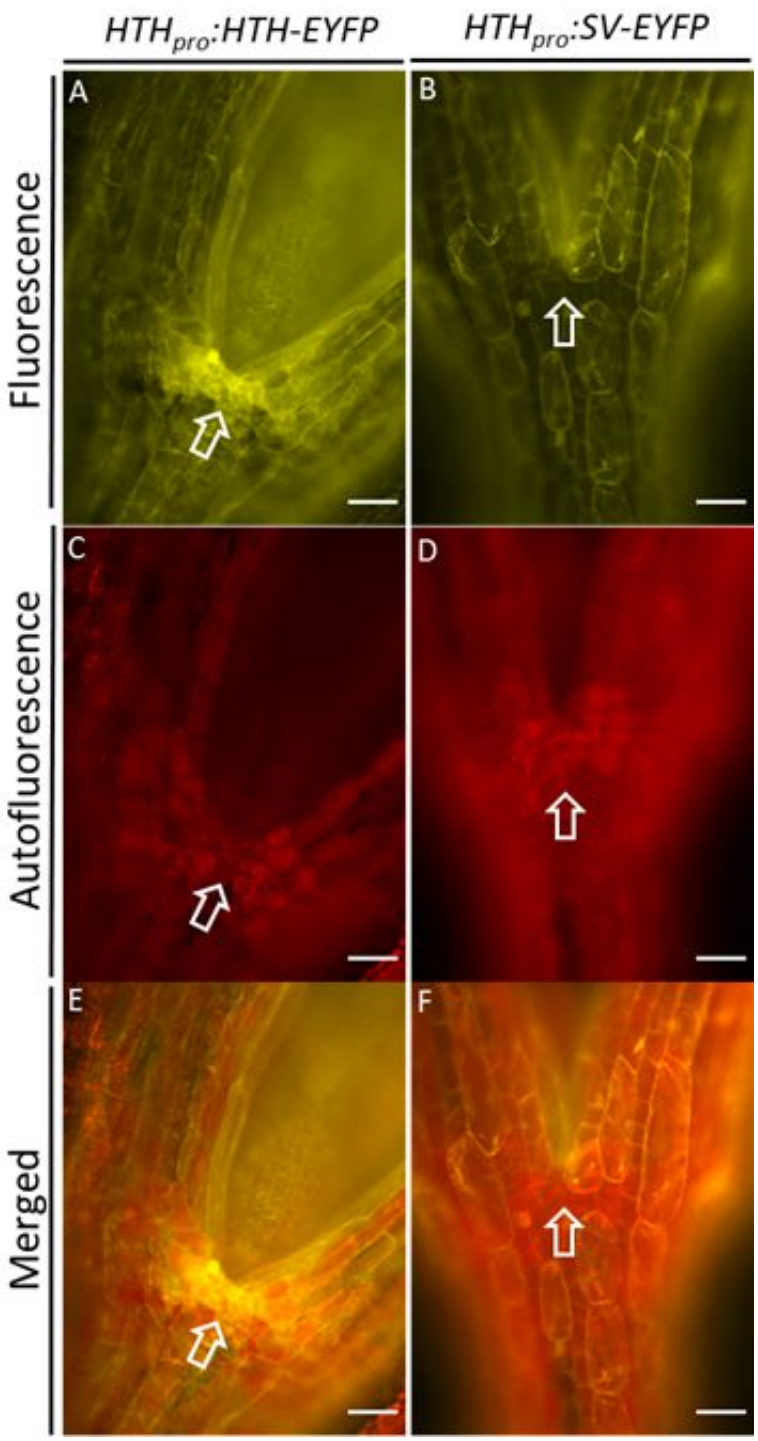
HTH$_{pro}$:HTH-EYFP
HTH$_{pro}$:SV-EYFP
Fluorescence
Autofluorescence
Merged
A
B
C
D
E
F

Figure 3.12. Micrographs showing HTH-EYFP and SV-EYFP expression in the hypocotyl of 5-day-old *HTH_{pro}:HTH-EYFP* and *HTH_{pro}:SV-EYFP* transgenic seedlings. Both HTH-EYFP and SV-EYFP are expressed in the hypocotyl. Fluorescence of HTH-EYFP and SV-EYFP are shown in yellow (A and B). Autofluorescence of HTH-EYFP and SV-EYFP are shown in red (C and D). E and F. Merged micrographs - fluorescence and autofluorescence. The white arrowheads indicate ER bodies; the black arrowheads indicate the ER reticular network. The areas included in white boxes in E and F are shown at a higher magnification in panels G and H. Scale bar is 50 µm.

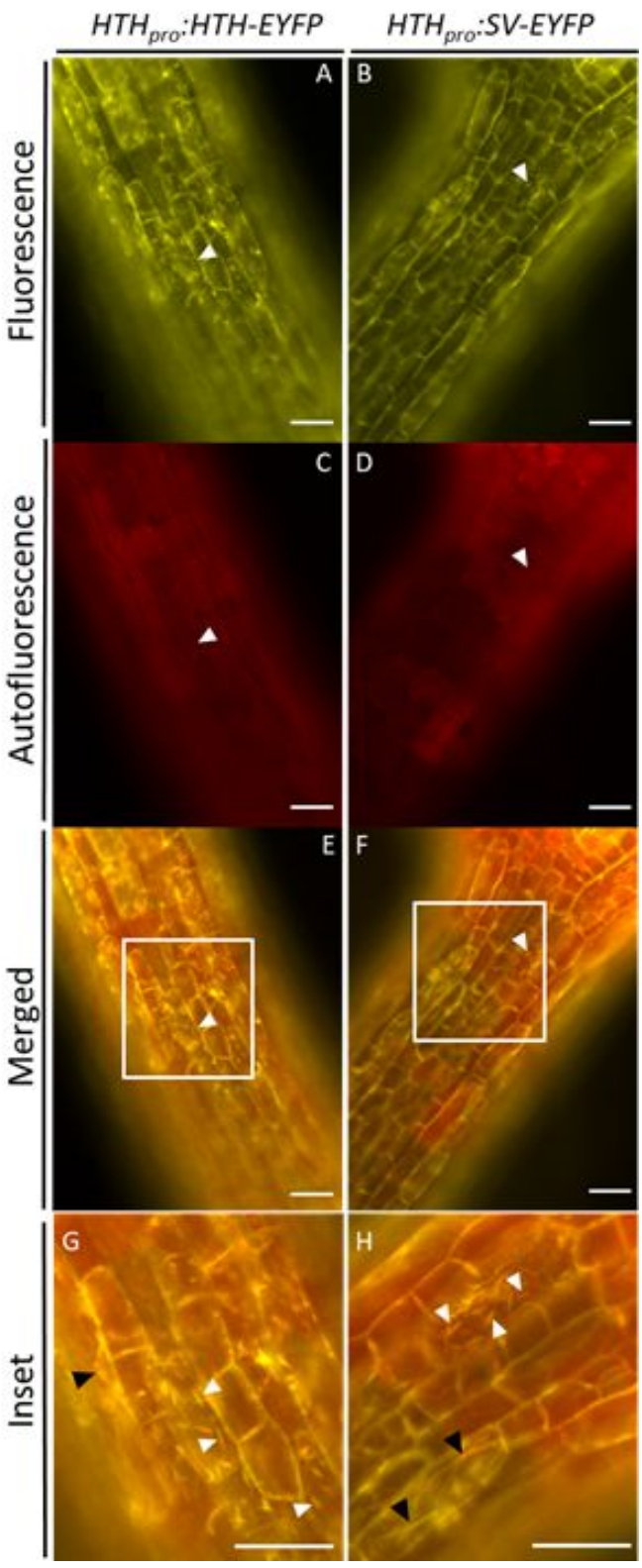
HTH_pro:HTH-EYFP
HTH_pro:SV-EYFP
Fluorescence
Autofluorescence
Merged
Inset
A
B
C
D
E
F
G
H

Figure 3.13. Micrographs of HTH-EYFP and SV-EYFP expression in the root-shoot junction of 5-day-old *HTH_{pro}:HTH-EYFP* and *HTH_{pro}:SV-EYFP* transgenic seedlings. HTH-EYFP is expressed in the root-shoot junction, SV-EYFP is not. Fluorescence of HTH-EYFP and SV-EYFP are shown in yellow (A and B). Autofluorescence of HTH-EYFP and SV-EYFP are shown in red (C and D). E and F. Merged micrographs - fluorescence and autofluorescence. Scale bar is 50 µm.

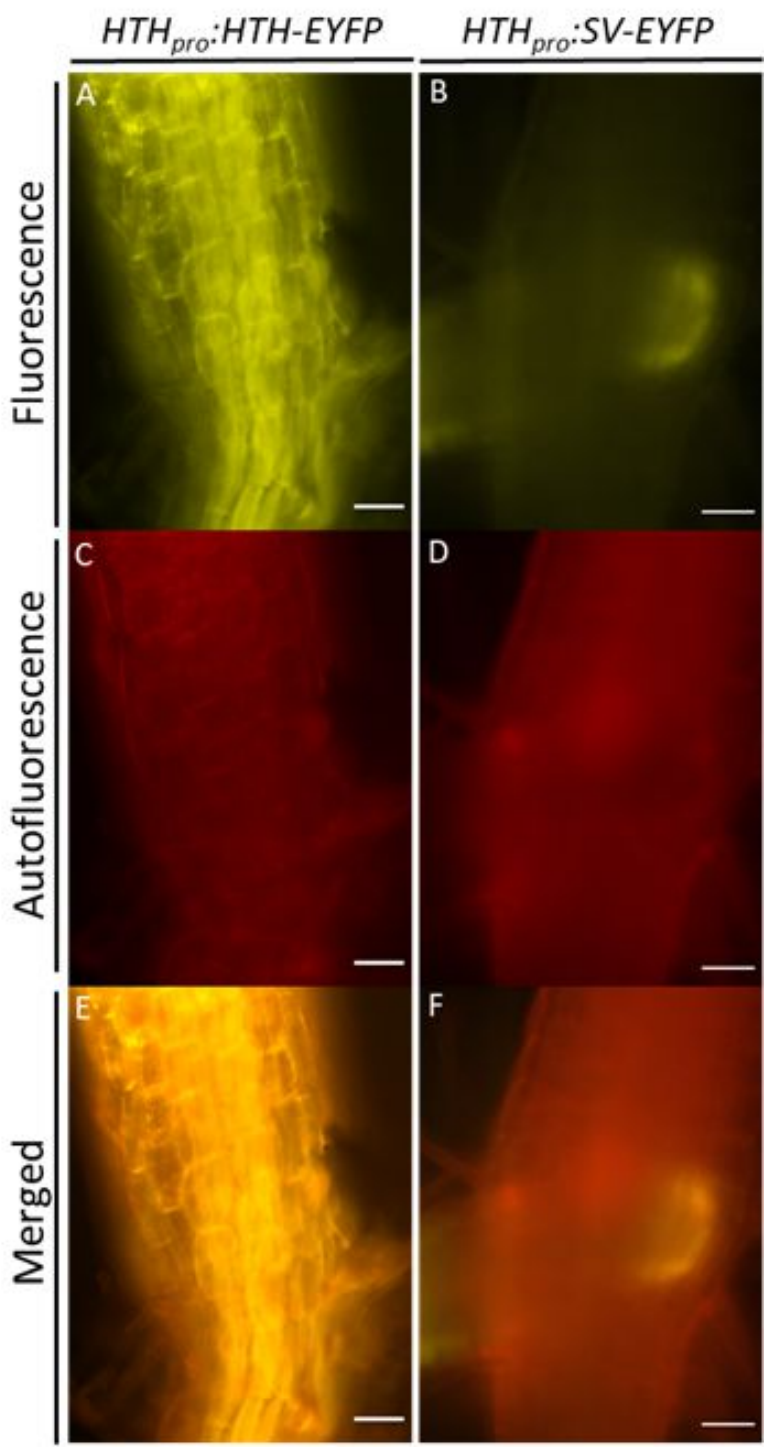
HTH$_{pro}$:HTH-EYFP
HTH$_{pro}$:SV-EYFP
Fluorescence
Autofluorescence
Merged
A
B
C
D
E
F

Figure 3.14. Micrographs showing HTH-EYFP and SV-EYFP expression in floral buds, sepals, and petals of *HTH_{pro}:HTH-EYFP* and *HTH_{pro}:SV-EYFP* transgenic plants. A. HTH-EYFP but not SV-EYFP expression is seen in the floral buds. B. HTH-EYFP expression is seen in the sepals while some SV-EYFP expression may be found. C. HTH-EYFP but not SV-EYFP expression is seen in the petals. Fluorescence of HTH-EYFP and SV-EYFP are shown in yellow. Autofluorescence of HTH-EYFP and SV-EYFP are shown in red. Merged micrographs consist of both fluorescence and autofluorescence. Scale bar is 50 μm.

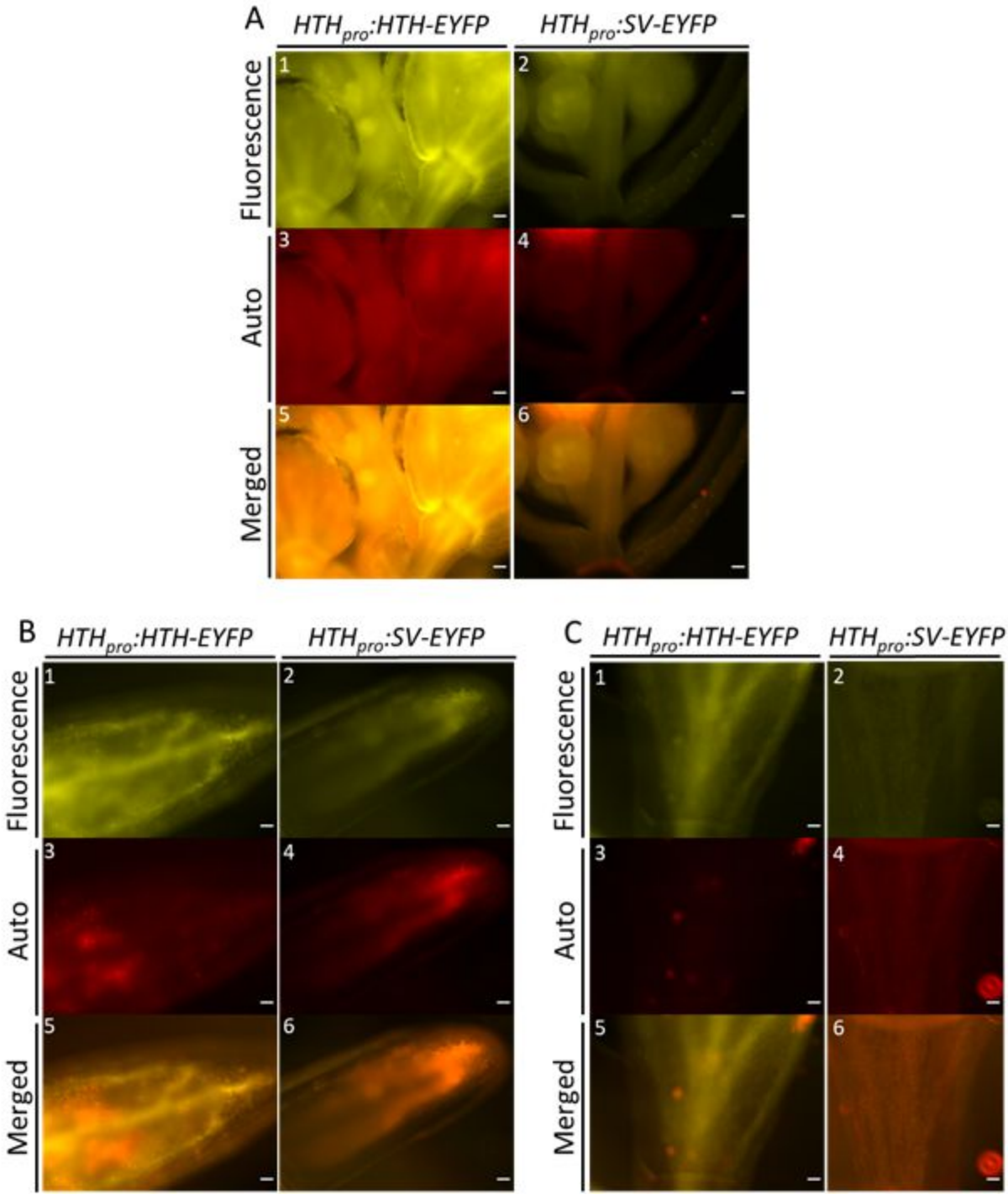
A
HTH$_{pro}$:HTH-EYFP
HTH$_{pro}$:SV-EYFP
Fluorescence
Auto
Merged
1
2
3
4
5
6
B
HTH$_{pro}$:HTH-EYFP
HTH$_{pro}$:SV-EYFP
Fluorescence
Auto
Merged
1
2
3
4
5
6
C
HTH$_{pro}$:HTH-EYFP
HTH$_{pro}$:SV-EYFP
Fluorescence
Auto
Merged
1
2
3
4
5
6

Figure 3.15. Micrographs showing HTH-EYFP and SV-EYFP expression in pistils and anthers of *HTH_{pro}:HTH-EYFP* and *HTH_{pro}:SV-EYFP* transgenic plants. A. Pistils. B. Anthers. Fluorescence of HTH-EYFP and SV-EYFP are shown in yellow. Autofluorescence of HTH-EYFP and SV-EYFP are shown in red. Merged micrographs consist of both fluorescence and autofluorescence. Scale bar is 50 μm.

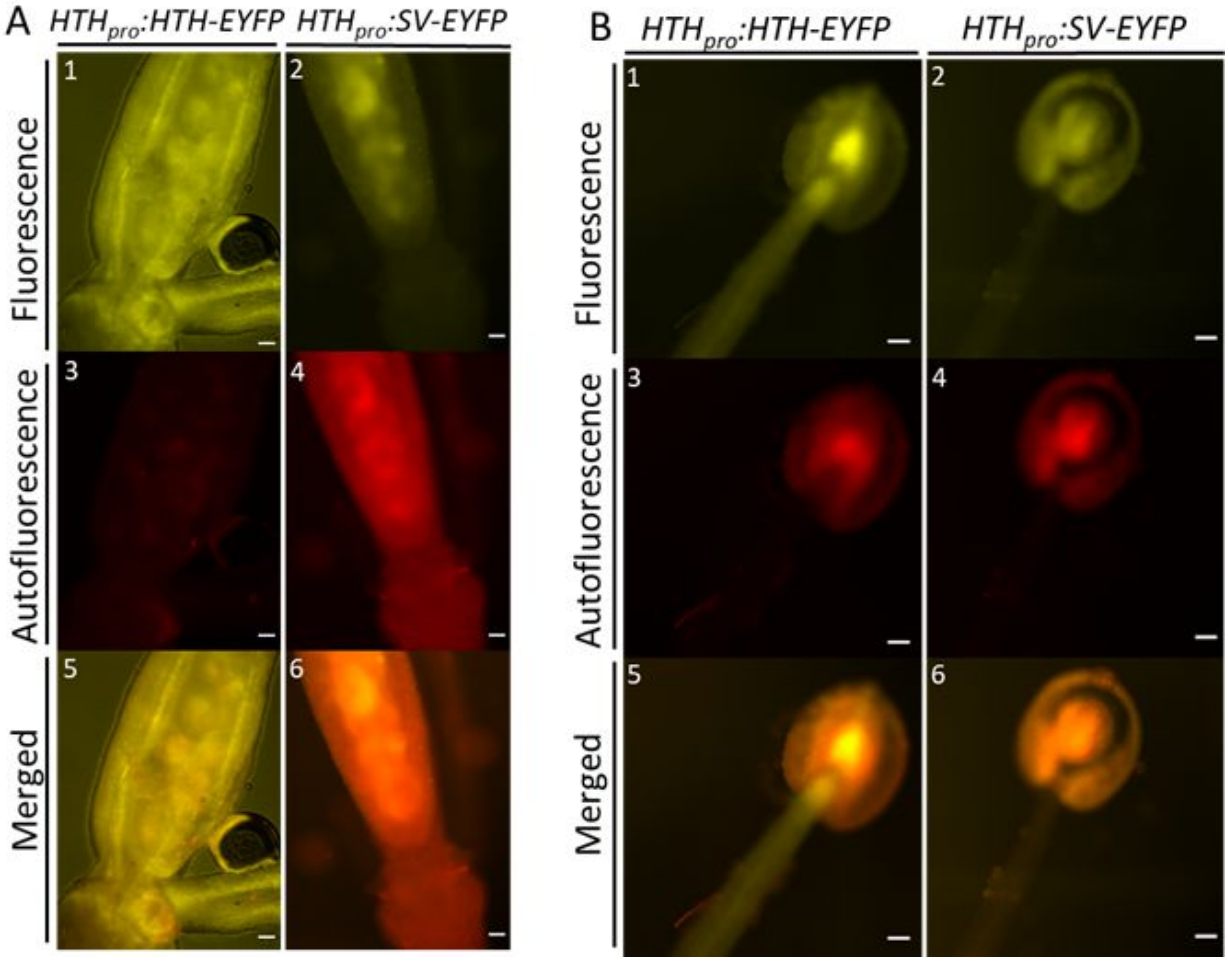
A
HTH_pro:HTH-EYFP
HTH_pro:SV-EYFP
Fluorescence
Autofluorescence
Merged
1
2
3
4
5
6
B
HTH_pro:HTH-EYFP
HTH_pro:SV-EYFP
Fluorescence
Autofluorescence
Merged
1
2
3
4
5
6

3.4 Discussion

3.4.**1** The splice variant isoform of HOTHEAD

A splice variant of the *HTH* gene (AT1G72970.2) was identified through transcript analysis (Theologis et al., 2000). The splice variant is characterized by an 81 bp deletion in the fifth exon of *HTH* which results in a 27 aa deletion just upstream of the three predicted catalytic active sites of HTH (Figure 1.4) (Chang, 2016). The effect of this deletion on HTH protein folding and function has not been determined.

Splicing is a strategy commonly used by organisms to make multiple proteins from a single stretch of genetic code (Filichkin et al., 2010). Splicing can be used to remove unnecessary sequences or place exons together in different ways to yield proteins with different functions (Filichkin et al., 2010). An isoform of the stress responsive *HTH* gene may indicate that while HTH is involved in cuticle formation/function, the splice variant isoform protein may be involved in stress response or the other way around. It is also possible that the splice variant is involved in female gametophyte development – a process in which HTH is thought to play a role (Chang, 2016; Pagnussat et al., 2005).

As the protein structure of HTH and SV are unknown it is difficult to draw conclusions about their enzymatic functions. Work is currently in progress to express the full-length HTH protein in yeast; this can then be transferred over to express the splice variant isoform of HTH (SV) in yeast. With the isolation of HTH and SV proteins, the crystal structures may be investigated for differences in protein folding, enzymatic function, and predicted binding partners.

To shed light on HTH and SV function without the aid of the crystal structures, Chang (2016)

generated a theoretical tertiary structure of HTH and the SV proteins modeled onto (R)-mandelonitrile lyase 2 of *Prunus dulcis* (PdMDL2) and pyranose dehydrogenase of *Agaricus meleagris* (AmPDH). Modeling was repeated in this study (Appendix H). PdMDL2 (UniProt: Q945K2) and AmPDH (UniProt: Q3L245) were chosen as models because they have the enzymatic activities that HTH is proposed to possess based on bioinformatic analysis. These two model proteins had been characterized in the past and share the most sequence similarity with HTH - PdMDL2 has 39% sequence identity with 88% sequence coverage and AmPDH has 25% sequence identity with 93% sequence coverage (Chang, 2016). Through this modeling, Chang (2016) found that the deleted 27 aa peptide putatively folds as an alpha helix and is predicted to be situated on the surface of the full-length HTH protein (Appendix H).

In this study, the SV protein model (AT1G72970.2) was threaded onto the PdMDL2 and AmPDH protein models using Phyre2 (Appendix H). These models of SV were compared to models of HTH threaded onto the same two proteins (PdMDL2 and AmPDH) (Appendix H). HTH threaded onto AmPDH had an 85% coverage and 22% identity while SV on AmPDH had an 87% coverage and 22% identity. HTH threaded onto PdMDL2 had an 83% coverage and 40% identity while SV on PdMDL2 had an 83% coverage and 42% identity. This increase in identity between HTH and SV on PdMDL2 is interesting and may provide preliminary evidence to suggest that SV may function as an MDL.

When examining the SV protein modeled onto PdMDL2 and/or AmPDH, it is worth noting that an alpha helix exists in the same position that it does in the HTH models even though the peptide that corresponds to this alpha helix in HTH is absent in SV (Appendix H). The random coils that followed the 27 aa peptide in the full-length protein putatively fold into an alpha helix in SV models (Appendix H). If this modeling is correct, this conservation of tertiary structure could

indicate that this alpha helix is crucial to a potential quaternary structure, enzymatic function, or recognition/binding to other proteins (Chen et al., 2007; Ihalainen et al., 2008). The alpha helix in both the HTH and SV protein is easily accessible to binding partners or ligands as in both the HTH and SV, it is situated on the protein's surface; any interaction here could alter the activity, function, or configuration of HTH (Kristiansen, 2004).

3.4.**2** *HTH_{pro}:SV-EYFP* plant phenotypes and implications for cuticle permeability

The effect of SV in *A. thaliana* was examined in a wildtype Ws and *hth-9* mutant background. The *HTH_{pro}:SV-EYFP* construct had no discernible effect on floral organ development in the Ws or *hth-9* background; in other words, expression of the *HTH_{pro}:SV-EYFP* construct in a *hth-9* background did not rescue the *hth-9* floral organ fusion phenotype (Figure 3.1 A). No SV-EYFP expression was observed in the floral organs of SV-EYFP transgenic plants irrespective of the genetic background (Figure 3.14 and 3.15). This expression profile was investigated through immunoblot analysis of transgenic floral buds (Appendix I). This immunoblot did not provide any conclusions about SV-EYFP expression as the extracted proteins appeared to be degraded. SV-EYFP expression was not detected on the immunoblot, however, the expression of SV-EYFP may be so low in comparison to HTH-EYFP that a different chemiluminescent detection solution may be required to view SV-EYFP protein bands (Appendix I). This immunoblot should be repeated multiple times (this analysis was performed once due to the laboratory shutdown during covid-19) using additional homozygous transgenic lines from each background (two in each background were used in this immunoblot - four total).

The failure to rescue the floral organ fusion phenotype suggests that SV protein does not directly function in floral cuticle formation/function but, may have some indirect role or may serve a

completely unrelated function in *A. thaliana*. The involvement of SV in cuticle formation/function should be explored further through cuticle permeability assays of cauline leaves and seed coats (Bessire et al., 2007; Chang, 2016; Lolle et al., 1997; Wharton, 1955).

The rate of chlorophyll extraction from transgenic cauline leaves showed that the presence of the SV-EYFP construct in either background resulted in an increase in cuticle permeability compared to the respective background line (Figure 3.2). This suggests that the presence of SV-EYFP may influence the cuticle permeability of leaves but not floral organs. This is interesting as the composition of the cuticle differs between the leaves and floral tissues in *A. thaliana* (Bonaventure et al., 2004; Pollard et al., 2008; Li-Beisson et al., 2009). This difference between the leaves and floral tissue is observed within the *BODYGUARD* (*bdg*) mutant - fusions of the leaves occur, however the flowers of *bdg* mutants remain unaffected (Ingram and Nawrath, 2017; Kurdyukov et al., 2006a). This indicates that SV may have a role to play in certain pathways involved in cuticle formation/function. To confirm this phenotype, this experiment should be repeated with additional independent transgenic lines as only two from each background were used in this study. Additionally, as the stem shares a similar cuticle composition with the leaves in *A. thaliana*, the rate of chlorophyll extraction from stems should also be examined (Bonaventure et al., 2004; Pollard et al., 2008). Finally, a TBO stain should be used to examine the cuticle permeability of floral organs, stems, and leaves (Chang, 2016).

3.4.**3** A role for the splice variant isoform in seed coat development

Mutations in genes involved in cuticle formation/function have been shown to influence seed size and/or permeability (Chang, 2016; De Giorgi et al., 2015; Panikashvili et al., 2009). Weighing a group of seeds was used to determine seed size (Chang, 2016; Debeaujon et al.,

2000). The weights of transgenic seeds were similar to those collected in the respective background line. In other words, Ws transgenic seeds closely resembled the weights of Ws seed, and *hth-9* transgenic seeds closely resembled the weights of *hth-9* seed (Figure 3.3 B). These results support the idea that SV does not have a seed-specific effect in cuticle formation/ function.

There were some differences between the seed weights of independently transformed lines within each background (Figure 3.3 B). Due to a limited supply of transgenic seeds, only 660 seeds could be obtained and weighed from each line, and there were only two lines from each background used in this study. This is not a robust data set for the application of statistical analyses and thus errors in interpretation may arise (Öztuna et al., 2006). Previous studies on seed weights of *hth-9* mutants used 2000 seeds which is a much larger sample pool (Chang, 2016). The data in the present study serves as preliminary and the experiment will need to be repeated, preferably with the inclusion of more homozygous transgenic lines.

The results of the tetrazolium assay to determine seed coat permeability are also preliminary as the same issue of limited seed was faced here. Previous studies used 50 mg of seeds for this assay which is a much larger sample pool than the 100 seeds used in the present study (Chang, 2016; Debeaujon et al., 2000) (100 seeds roughly equate to 0.003 mg).

Upon contact with NADPH-dependent reductases in the ER, formazans are produced from the tetrazolium salts which stain the embryo red (Berridge et al., 1996). In Ws seed this occurs rarely, whereas in *hth-9* seed, over half of the seeds stained red indicating that perturbing HTH function alters seed coat permeability (Chang, 2016) (Figure 3.4). In Ws transgenic seed, tetrazolium stained most of the seeds, whereas in *hth-9* SV-EYFP transgenic seed, tetrazolium

stained a little over half of the seeds indicating that introducing the SV-EYFP transgene into wild-type seed alters seed coat permeability (Figure 3.4). The results of the preliminary tetrazolium assay indicate that SV may be playing a yet unclear role in seed coat permeability (Figure 3.4 A).

Going forward the tetrazolium red staining pattern on embryos should be examined as the staining pattern can provide insight into the composition of the seed coat (Molina et al., 2008). The *gpat5* mutant embryo begins to stain at the radicle and cotyledon tips of the embryo next to the chalazal end (Beisson et al., 2007; Molina et al., 2008), whereas the *fatb* and *ap2-7* mutant embryos stain uniformly (Molina et al., 2008). The *gpat5* mutant is deficient in C20-C26 suberin monomers which is a large portion of the suberin monomers within a seed coat (Beisson et al., 2007; Molina et al., 2008). The *fatb* plant has a mutation within a protein involved in cutin biosynthesis; FATB provides precursors for cutin biosynthesis, in the *fatb* mutant levels of C16 cutin monomers are diminished (Molina et al., 2008). The *ap2-7* mutant was found to have a reduction in C22 and C24 suberin monomers (Molina et al., 2008). The examination of the embryo staining pattern would also allow for the observation of faint staining that may have been overlooked when examining seed coat coloration changes.

HTH may be a multimeric protein and SV-EYFP may interfere with the quaternary structure of HTH in the Ws transgenic plants. This disturbance in structure could alter the function of HTH or render it inactive. This could lead to the altered seed coat permeability phenotype of the Ws transgenic seeds discussed above. Bioinformatic analysis on the quaternary structure of the AT1G72970.1 and .2 HTH protein model was performed using QuatIdent and QuaBingo. These analyses reported that HTH is likely a monomer. In addition to this, the quaternary structures of proteins that share sequence similarity to HTH were all found to be monomers again suggesting

that HTH may be a monomer.

If SV-EYFP does not disrupt quaternary structure, it might compete with HTH for ligands or binding partners. As the SV portion of the SV-EYFP protein is slightly smaller than HTH, ligands may preferentially bind to SV-EYFP over HTH based on reduced steric hindrance (Childers et al., 2016). Alternatively, as more SV may be present in Ws transgenic seeds compared to wild-type Ws seeds, SV may outcompete HTH for binding partners or ligands as there is theoretically more SV than HTH expressed in these seeds (Appendix J). In future, work needs to be done to examine whether HTH and SV form multimeric structures consisting of two or more subunits of HTH, SV or a combination of both HTH and SV proteins. This can be tested by determining the crystal structure, using affinity column assays, yeast two hybrid screens, or by examining migration patterns of HTH-EYFP or SV-EYFP on native gels.

The increase in Ws transgenic seed coat permeability may also be due to the overexpression of SV-EYFP (Appendix J). Expression of the SV-EYFP protein may enhance seed coat permeability when expressed in conjunction with the normal titer of HTH protein. In the Ws background, SV is naturally expressed to some unknown degree in conjunction with HTH and the level of SV protein is increased by the addition of the transgene - of which there are at least two copies. In the *hth-9* SV-EYFP transgenic plants, the *hth-9* mutant allele is not transcribed and therefore neither the native HTH nor SV proteins are present (Appendix J). Thus, the increased titer in SV would manifest itself only in the Ws transgenic lines (Appendix J). This increase in SV may lead to phenotypic artifacts and may explain the tetrazolium staining result seen in Ws transgenic seeds (Figure 3.4). This could likely be the case as in *hth-9* transgenic seeds, where theoretically no HTH or SV protein is expressed, the permeability phenotype is like *hth-9* (Figure 3.4) – there is no effect from SV overexpression.

HTH-EYFP was found to localize to the oi1 and oi2 cell layers of developing *HTH$_{pro}$:HTH-EYFP* transgenic seed coats (Chang, 2016). It was thought that, in the oi1 layer, HTH was involved in the biosynthesis of suberin-like and cutin-like materials that would be deposited in the oi2 and wall 3 layers, modulating seed coat permeability as well as seed size, respectively (Beeckmann et al., 2000; Beisson et al., 2007; Chang, 2016; Creff et al., 2015; Luo et al., 2005; Molina et al., 2008). Ws seed coat permeability is affected by the presence of the SV-EYFP construct, however, seed size is not (Figure 3.3 and 3.4). Studies have shown that a change in the composition of the oi2 layer commonly leads to an increase in tetrazolium staining (Beisson et al., 2007; Debeaujon et al., 2000), however, it has also been theorized that the cutin monomers in the ii layers of the seed coat provide partial protection against tetrazolium staining (Molina et al., 2008). This suggests that SV may play a role in seed coat permeability through the deposition of suberin-like monomers in the oi2 layer of the seed coat. This could also indicate that HTH may play a role in this process and has been interrupted by the increase in SV protein titer in Ws transgenic seeds (discussed above). As mentioned above, seed size is regulated by the deposition of cutin-like monomers into wall 3 by oi1. Thus, as seed size is unaffected in Ws transgenic seeds, this suggests that SV-EYFP does not have a role to play in wall 3 deposition of cutin monomers. Additionally, this may suggest that SV-EYFP does not disrupt the role that HTH plays in wall 3 deposition of cutin monomers.

The localization pattern of SV-EYFP in the seed coat needs to be determined as this may provide insight into the role of SV-EFP in seed coat development and function. To investigate the localization of SV-EYFP to the seed coat, siliques from transgenic plants were collected for immunoblot analysis (Appendix I). The preliminary results were inconclusive as the blot revealed protein degradation (Appendix I). The experiment could not be repeated due to the

covid-19 laboratory shutdown in March 2020. Additionally, the siliques used in this analysis were a mix of siliques in developmental stages ranging from of immature siliques collected 1 day after flowering (DAF) to mature siliques collected 15 DAF. If SV-EYFP is expressed at a specific stage of seed coat development, this immunoblot analysis might fail to detect it (Appendix I). To rectify this, *HTH$_{pro}$:SV-EYFP* transgenic siliques 1 DAF to 20 DAF should be collected at individual time points for SV-EYFP immunoblot analysis (Kleindt et al., 2010; Louvet et al., 2006). Additionally, due to the limited amount of seed there was a limited amount of tissue that could be harvested for this experiment. This study should be repeated multiple times (this analysis was performed once due to covid-19 shutdowns), with various amount of starting tissue and using additional homozygous transgenic lines in each background (two in each background were used in this study for a total of four transgenic lines).

3.4.**4** Splice variant isoform expression

The introduction and expression of the SV-EYFP transgene into the *hth-9* mutant plants did not rescue any of the mutant phenotypes tested. This lowers the confidence in any conclusions that may be drawn in relation to the expression profile and function of the SV protein.

In examining SV-EYFP expression, there were many differences between the HTH-EYFP and SV-EYFP proteins in transgenic seedlings. The SV-EYFP protein was not localized to the vasculature of cotyledons (including the hydathode), petioles, or hypocotyl of 5-day-old Ws or *hth-9* transgenic seedlings (Figures 3.8 to 3.13). Results suggest that no SV-EYFP protein was expressed in the stele of the primary or lateral roots or in the RAM or root cap of 5-day-old Ws or *hth-9* transgenic seedlings, however, further studies of root tip cross sections would need to be performed to confirm this (Figures 3.5 to 3.7). Finally, no SV-EYFP expression was found in the

SAM or in fully developed trichomes of 5-day-old Ws or *hth-9* transgenic seedlings (Figure 3.11) (Appendix G). The differences in expression patterns indicate that some regulation of the *SV* transcript or protein is occurring that differs from the regulation of the full-length *HTH* transcript or protein.

Using *HTH* promoter driven GUS expression, Kurdyukov et al. (2006) observed GUS expression in the vasculature of young leaves, the SAM, and the lateral roots of four-leaf stage *A. thaliana* plants. As GUS expression was regulated by the same promoter as HTH and SV transgenes used here, the expression pattern of GUS in the above study could shed some insight into the expression pattern of HTH and SV. However, any translational or post-translational modifications which could alter protein expression patterns would not be revealed using these GUS expression lines (Tokmakov et al., 2012). As SV-EYFP contains a 27 aa deletion, it may not be surprising that SV-EYFP does not localize to the same regions that *HTH* promoter driven GUS and HTH-EYFP do. Further analysis on the regulation of the SV and HTH protein would be useful in determining the function of HTH and SV. Identifying the conditions under which the SV isoform is transcribed and translated may indicate what pathways this protein is involved in. Additionally, any post-translational modification of the SV isoform that differs from the post-translational modifications of HTH could shed light on the functional significance of the 27 aa peptide in this HTH protein isoform.

As both HTH and SV are expected to be expressed in the wild-type plant, both HTH-EYFP and SV-EYFP are expected to be expressed in the HTH_{pro}*:HTH-EYFP* transgenic plant as well (Appendix J). Thus the HTH-EYFP expression profile seen in HTH_{pro}*:HTH-EYFP* transgenic plants is due in part to SV-EYFP (Appendix J). To tease apart these protein expression patterns, SV-EYFP expression was characterized in HTH_{pro}*:SV-EYFP* transgenic plants. Any similarities in

the expression profiles of HTH_{pro}:*HTH-EYFP* and HTH_{pro}:*SV-EYFP* transgenic plants may be attributed to SV-EYFP expression: any differences may represent the true localization pattern of HTH-EYFP. However, the possibility of expression artifacts within HTH_{pro}:*SV-EYFP* transgenic plants must be considered due to potential elevated protein titres of SV in Ws transgenic plants (Appendix J). One way to assess this is by comparing the expression pattern of SV-EYFP in *hth-9* transgenic plants to Ws transgenic plants.

Chang (2016) discovered the first evidence of HTH localization to trichomes in HTH_{pro}:*HTH-EYFP* transgenic seedlings. SV-EYFP was also found to localize to trichomes (Figure 3.10), however, SV-EYFP localization occurred predominantly within developing trichomes and not within those that were fully developed (Appendix G). This suggests that SV plays a role distinct from HTH in trichome developments.

Studies have determined that the trichome cuticle layer of *A. thaliana* has a different composition as compared to neighbouring pavement cells; the trichome cuticle layer contains a higher amount of VLCFA derivatives and expresses unique wax biosynthesis genes (Hegebarth et al., 2016; Hegebarth and Jetter, 2017). Transcript profiling studies have also found low expression, if not a downregulation, of genes involved in cuticle biosynthesis within mature trichomes (Jakoby et al., 2008). This could suggest that HTH's role in cuticle formation/function may be attenuated in these cells; perhaps SV in wild-type plants acts to block interactions that HTH would normally have in cuticle formation/function. Putative evidence for SV acting to block HTH function is seen in the seed coat permeability assay discussed above. The transcript study mentioned above, along with others, found that genes involved in stress response were upregulated in developing and mature trichomes (Jakoby et al., 2008; Kryvych et al., 2008). This could indicate that SV and HTH play roles responding to stress in trichomes. The specificity of the SV and HTH roles may

differ as the cellular environment of the developing trichome differs from the environment of the developed trichome (Hegebarth et al., 2016; Hegebarth and Jetter, 2017; Hülskamp, 2000).

The patterning of trichome cell fate is controlled by a set of transcription factors; GLABRA (GL)1, GL3, and TRANSPARENT TESTA GLABRA1 (TTG1) (Galway et al., 1994; Pattanaik et al., 2014; Schellmann et al., 2002). Similar transcription factors also regulate root hair cell fate and act through a common mechanism (Schellmann et al., 2002). There are two types of cells in root hairs - atrichoblasts and trichoblasts - these cell types are arranged in an alternating epidermal cell files in the root (Berger et al., 1998). Upon signaling from subjacent cortical cells, atrichoblasts express GL2 (Lee and Schiefelbein, 2002). The expression of GL2 in root hairs results in the suppression of growth, thus trichoblasts, which do not express GL2, initiate growth and become root hairs (Masucci et al., 1996; Schellmann et al., 2002). This phenomenon is reversed in trichome development; the atrichoblast cells correspond to trichome cells (Schellmann et al., 2002). This is interesting as the present study has shown SV-EYP localization in specific, alternating files of cells in the transition zone of transgenic roots which could correspond to atrichoblasts and trichoblasts cell files (Figure 3.5 and 3.6). This may indicate a role for SV in root and shoot epidermal cell fate determination.

The expression profile of SV-EYFP was characterized using an epifluorescence microscope, this does not allow for an in-depth examination of cell type expression patterns. Thus, it cannot be said for certain whether SV-EYFP localizes to the atrichoblasts or trichoblasts of the root. This could be clarified by examining SCRI Renaissance 2200- or TBO- stained transgenic root cross sections (Dolan et al., 1993). Within these stained cross sections, trichoblasts and atrichoblasts can be identified by their positional location in reference to cortical cells. Trichoblasts are positioned over the cleft of two underlying cortical cells while atrichoblasts are in contact with

one cortical cell (Schellmann et al., 2002). Trichoblasts can also be identified by differential TBO staining as trichoblasts are heavily stained with TBO compared to other root cells (Dolan et al., 1993). The localization of SV-EYFP to the root transition zone is also called into question as this area was not defined using the fluorescence microscope. Studies that involve the use of a confocal microscope will need to be conducted to confirm SV-EYFP putative localization to atrichoblasts or trichoblasts within the transition zone of the root.

The putative localization of SV-EYFP to the transition zone of the primary and lateral root is interesting as this zone is known to be involved in growth and development and has been proposed to be a zone for the integration of environmental stimuli (Kong et al., 2018). The transition zone is located distal the RAM and proximal to the root zone of elongation (Baluska et al., 1996; Verbelen et al., 2006). In this zone, cells transition from rapid division to rapid cell elongation and move into the elongation zone (Di Mambro et al., 2017). These cells are perceptive to plant hormones such as auxin and cytokinin which regulate root growth (Dello Ioio et al., 2007; Muller and Sheen, 2008). These cells are also responsive to environmental stresses such as aluminum and low phosphate stress (Kong et al., 2018). This could indicate a role for SV in responding to stress.

SV-EYFP was also found to localize to the emerging lateral roots (Figure 3.6). Expression of SV-EYFP during lateral root development is likely confined to the epidermal cells, however, without confocal microscopy, this assumption cannot be verified. SV-EYFP appears to remain in the root apex from the point of emergence to fully developed lateral roots (Figure 3.6). A recent study by Berhin et al (2019) found that the first layer of root cap cells produce cutin which serves to protect the developing primary root tip until the seedling reaches the 5- to 6-day stage; this layer is also observed in developing lateral roots (Berhin et al., 2019). This is quite interesting,

and as SV-EYFP is found to localize to the tip of the lateral root during emergence (Figure 3.6 A), SV-EYFP could play a role in the biosynthesis of this newly identified cuticle layer.

As mentioned above, the leaf and stem cuticle layer in *A. thaliana* differs in composition to the cuticle covering the floral tissues (Bonaventure et al., 2004; Pollard et al., 2008; Li-Beisson et al., 2009). As SV-EYFP localizes to the shoot tissue in seedlings but does not appear to localize to the floral tissue, this may indicate that SV-EYFP is involved in a particular pathway in the biosynthesis of the cuticle. As HTH-EYFP localizes to both the shoot and the floral tissues, this may indicate that HTH plays a more general role in cuticle formation/function compared to SV. However, this expression of HTH-EYFP in the shoot tissue of seedlings may have been SV-EYFP expression. If this were true, it would indicate that HTH plays a role in floral tissue cuticle formation/function while SV plays a role in seedling shoot cuticle formation/function.

Both HTH-EYFP and SV-EYFP have been found to localize to cER bodies and the ER network (Figure 3.8 and 3.12), suggesting that SV, but not HTH, localizes to cER bodies. As the expression profile of HTH-EYFP in HTH_{pro}*:HTH-EYFP* transgenic plants is theoretically the summation of the HTH-EYFP and SV-EYFP expression profiles (Appendix J) this could indicate that the HTH-EYFP signal seen within cER bodies of HTH_{pro}*:HTH-EYFP* transgenic plants may have been SV-EYFP. Thus, perhaps SV is the only HTH isoform to localize to cER bodies. Alternatively, perhaps both HTH isoforms localize to cER bodies.

One way to investigate SV-EYFP localization to the ER network and ER bodies would be to colocalize SV-EYFP with an ER marker in an ER marker plant line as was done by Chang (2016). Another way to investigate this possibility would be to design an antibody against the 27 aa peptide that is absent in SV. This antibody would be able to detect the full length HTH or

HTH-EYFP protein but not the SV-EYFP protein. cER bodies from the roots of *HTH_{pro}:HTH-EYFP* transgenic plants would be isolated and examined through immunoblot analysis with the newly designed antibody and anti-PYK10.

Additionally, it would be interesting to see whether SV-EYFP localizes exclusively to cER bodies or whether it also localizes to iER bodies. This could be done by analyzing an immunoblot of an ER body enriched fraction from stressed *HTH_{pro}:SV-EYFP* transgenic plants in a *hth-9 nai1-1* mutant background.

3.4 Conclusion

The HTH splice variant isoform, which contains a 27 aa deletion in the fifth exon of HTH, does not rescue any of the *hth-9* mutant phenotypes tested in this study. In fact, the presence of SV-EYFP increases the severity of the leaf cuticle permeability and seed coat permeability *hth* mutant phenotypes. As the transgene does not complement any of the mutant phenotypes surveyed, any interpretation of these data is preliminary.

The presence of the SV-EYFP protein does not seem to impact the floral phenotypes of either Ws or *hth-9* plants. However, the presence of the SV-EYFP protein was shown to increase cauline leaf cuticle permeability in both Ws and *hth-9* lines. Additionally, the seed coat permeability of Ws transgenic seeds was significantly increased compared to the *hth-9* transgenic, Ws, and *hth-9* seeds. This indicates that SV-EYFP may have some role to play in cuticle formation/function. This role likely deals with the synthesis of α-ω-dicarboxylic acids as this is the main component in the leaf cuticle layer (Bonaventure et al., 2004) – an area that is affected by the presence of the SV transgene (Figure 3.2). It is also found in low concentrations in the floral cuticle (Li-Beisson et al., 2009) – an area the SV does not affect (Figure 3.1). Finally, high α-ω-dicarboxylic acid content is usually indicative of suberin (Bonaventure et al., 2004) – the polymer that contributes to seed coat permeability (Molina et al., 2008) which is affected by the presence of the SV-EYFP transgene in Ws transgenic plants (Figure 3.4).

SV-EYFP localization to cER bodies may suggest that either both HTH isoforms are identified in cER bodies or that cER bodies contain SV and not full-length HTH protein. Although the expression profile of the HTH full-length protein suggest that it is localized to cER bodies, this expression profile represented a summation of the HTH full length and SV expression profiles.

SV localization to cER bodies may indicate a role for SV as an MDL; if full-length HTH does not localize to cER bodies it may indicate a role for HTH as an ADH involved in cuticle formation/function.

Finally, the tissue level expression pattern of the SV-EYFP protein differed from the expression pattern of the HTH-EYFP protein; SV-EYFP was not localized to the vasculature of cotyledons, petioles, hypocotyl or the stele of the primary or lateral roots. SV-EYFP was also absent in the SAM, mature trichomes, the RAM, and root cap of 5-day-old transgenic seedlings. The expression of SV-EYFP in the root tip and developing trichomes may indicate a role of the SV protein in developmental regulation or cell fate determination. A role for the SV protein in development links back to work done by Chang (2016). Chang (2016) observed HTH-EYFP expression in the chalazal end of the developing embryo sac. In this study, SV-EYFP localization studies were not conducted on developing female gametophytes and remain areas for further investigation. If SV-EYFP was found to localize to the chalazal embryo sac region, it could strengthen the hypothesis that SV is involved in development. This could implicate SV as a moonlighting protein with roles in plant development/cell fate determination, stress response, and potentially cuticle formation/function.

Chapter 4 Summary

Based on genetic studies, HTH is known to be involved in cuticle formation/function, however, it has subsequently been shown to be associated with stress responses in *A. thaliana*. Under conditions of wounding or salt shock, the ER induces the formation of ER bodies which house BGLUs that possess the ability to catalyze vacuolar glucosinolates to produce toxic compounds (Halkier and Gershenzon, 2006; Hayashi et al. 2001). The *HTH* gene is responsive to MeJA exposure and salt shock and the protein has been found to localize to cER bodies and likely iER bodies as well (Chang, 2016; Figures 2.2, 2.3). The HTH protein is proposed to either function as an ADH or MDL (Chang, 2016; Krolikowski et al., 2003; Kurdyukov et al. 2006b). MDLs have been known to be involved in the conversion of glucosinolates to toxic compounds, a process known as cyanogenesis (Halkier and Gershenzon, 2006). This localization to ER bodies containing BGLUs indicates that HTH may be involved in stress responses through cyanogenesis. Cyanogenesis is a process that results in the production of HCN. HCN deters herbivory and may act as a signalling molecule (Machingura et al., 2016).

The localization of HTH to cER bodies was confirmed through subcellular fractionations and genetic crosses into an ER body mutant background. cER bodies isolated through subcellular fractionation of root tissue contained HTH-GFP (Figure2.1 and 2.3). HTH-GFP within the *nai1-1* background localized to a reticular network and was not found in any ER body structures. As the *nai1-1* mutant background does not form cER bodies or L-ER bodies, this indicates that since HTH-GFP did not localize to any ER body structures in the roots of seedlings, then HTH does localize to cER bodies and L-ER bodies in wildtype plants. This study could be expanded through the analysis of HTH-GFP localization in other ER body mutant backgrounds such as

nai2-1, *pyk10-1*, or *meb1-1* (Matsushima et al., 2003; Nagano et al., 2008; Yamada et al., 2008; Yamada et al., 2013).

The localization of HTH to other ER bodies should be examined; using the *bglu18* mutant background where no iER bodies are expressed; in a *bglu18*, *nai1-1* double mutant no cER bodies, iER bodies, or L-ER bodies should be expressed (Matsushima et al., 2003; Nakazaki et al., 2019a,b; Ogasawara et al., 2009). If HTH-GFP localizes to ER body structures in a *bglu18*, *nai1-1* double mutant, it would indicate that HTH does not localize to iER bodies.

The splice variant isoform of the HTH protein likely does not play a role in cuticle formation/function as it was not found to rescue the *hth-9* mutant phenotypes. However, as we are unsure of the levels of SV normally found in wild-type plants it is unclear whether this system is inherently aberrant due to an overexpression of SV protein levels. Work in these conditions of over expression may have resulted in artifacts which would not lend much confidence to work in these HTH_{pro}*:SV-EYFP* transgenic lines. The role of the SV protein is unknown; however, it is of interest to investigate the expression pattern of this smaller HTH protein isoform where 27 aa's are eliminated from a region predicted to be on the protein surface and close to the putative catalytic site (Chang, 2016). This region is also predicted to contain two post-translational modification sites and may disrupt the putative substrate binding domain of the HTH protein.

Understanding why the plant goes to the trouble of naturally creating the SV protein could imply that there is some function of the SV protein that was not observed in this study. HTH has been proposed to be involved in cuticle formation/function, stress responses, and female gametophyte development. Perhaps there is a role for the splice variant isoform in stress response or female

gametophyte development. As SV-EYFP was shown to localize to cER bodies, this may suggest that SV could act as an MDL in stress response.

References

Aljbory, Z. and Chen, M. (2016). Indirect plant defense against insect herbivores: a review. Insect Science, 25(1):2-23.

Araki, T., Nakatani, M. and Iwabuchi, M. (1998). ADHESION OF CALYX EDGES, a gene involved in the regulation of postgenital fusion in *Arabidopsis*. Paper presented at the 9th International Conference on Arabidopsis Research.

Baluska, F., Volkmann, D. and Barlow, P.W. (1996). Specialized zones of development in roots: view from the cellular level. Plant Physiology, 112(1):3-4.

Bannwarth, M., Bastian, S., Heckmann-Pohl, D., Giffhorn, F. and Schulz, G.E. (2004). Crystal structure of pyranose 2-oxidase from the white-rot fungus *Peniophora* sp. Biochemistry, 43(37):11683-11690.

Beeckman, T., De Rycke, R., Viane, R. and Inzé, D. (2000). Histological study of seed coat development in *Arabidopsis thaliana*. Journal of Plant Research, 113:139-148.

Beisson, F., Li, Y., Bonaventure, G., Pollard, M. and Ohlrogge, J.B. (2007). The acyltransferase GPAT5 is required for the synthesis of suberin in seed coat and root of *Arabidopsis*. The Plant Cell, 19:351-368.

Berens, M.L., Berry, H.M., Mine, A., Argueso, C.T. and Tsuda, K. (2017). Evolution of hormone signalling networks in plant defense, 55:401-425.

Berger, F., Hung, C.Y., Dolan, L. and Schiefelbein, J. (1998). Control of cell division in the root epidermis of *Arabidopsis thaliana*. Developmental Biology, 194(2):235-245.

Berhin, A., de Bellis, D., Franke, R.B., Buono, R.A., Nowack, M.K. and Nawrath, C. (2019). The root cap cuticle: A cell wall structure for seedling establishment and lateral root formation. Cell, 176; 1367-1378.

Berridge, M.V., Tan, A.S., McCoy, K.D. and Wang, R. (1996). The biochemical and cellular basis of cell proliferation assays that use tetrazolium salts. Biochemica, 4:15–20.

Bessire, M., Borel, S., Fabre, G., Carraça, L., Efremova, N., Yephremov, A., Cao, Y., Jetter, R., Jacquat, A.C., Métraux, J.P. and Nawrath, C. (2011). A member of the PLEIOTROPIC DRUG RESISTANCE family of ATP binding cassette transporters is required for the formation of a functional cuticle in *Arabidopsis*. Plant Cell, 23(5):1958–1970.

Bessire, M., Chassot, C., Jacquat, A.C., Humphry, M., Borel, S., Petétot, J.M., Métraux, J.P. and Nawrath, C. (2007). A permeable cuticle in *Arabidopsis* leads to a strong resistance to *Botrytis cinerea*. EMBO Journal, 26(8):2158–2168.

Bethke, P.C., Gubler, F., Jacobsen, J.V. and Jones, R.L. (2004). Dormancy of *Arabidopsis* seeds and barley grains can be broken by nitric oxide. Planta, 219(5):847–855.

Bird, D., Beisson, F., Brigham, A., Shin, J., Greer, S., Jetter, R., Kunst, L., Wu, X., Yephremov, A. and Samuels, L. (2007). Characterization of *Arabidopsis* ABCG11/WBC11, an ATP binding cassette (ABC) transporter that is required for cuticular lipid secretion. Plant Journal 52(3):485–498.

Bonaventure, G., Beisson, F., Ohlrogge, J. and Pollard, M. (2004). Analysis of the aliphatic monomer composition of polyesters associated with *Arabidopsis* epidermis: occurrence of octadeca-cis-6, cis-9-diene-1,18-dioate as the major component. Plant Journal, 40(6):920-930.

Brabban, A.D. and Edwards, C. (1995). The effects of glucosinolates and their hydrolysis products on microbial growth. Journal of Applied Bacteriology, 79(2):171-177.

Broun, P., Poindexter, P., Osborne, E., Jiang, C.Z. and Riechmann, J.L. (2004). WIN1, a transcriptional activator of epidermal wax accumulation in *Arabidopsis*. Proceedings of the National Academy of Sciences of the United States of America, 101(13):4706-4711.

Chang, P. (2016). Localization and possible functions of Arabidopsis HOTHEAD protein. UWSpace. http://hdl.handle.net/10012/11033.

Chen, Y., Zhou, Y. and Ding, J. (2007). The helix–coil transition revisited. Proteins, 69(1):58-68.

Childers, M.C., Towse, C.L. and Daggett, V. (2016). The effect of chirality and steric hindrance on intrinsic backbone conformational propensities: tools for protein design. Protein Engineering, Design, and Selection, 29(7):271-280.

Chivasa, S. and Carr, J.P. (1998). Cyanide restores N gene-mediated resistance to tobacco mosaic virus in transgenic tobacco expressing salicylic acid hydroxylase. The Plant Cell, 10(9):1489–1498.

Chrispeels, M.J. and Herman, E.M. (2000). Endoplasmic reticulum-derived compartments function in storage and as mediators of vacuolar remodeling via a new type of organelle, precursor protease vesicles. Plant Physiology, 123:1227-1234.

Clough, S.J. and Bent, A.F. (1998). Floral dip: a simplified method for *Agrobacterium*-mediated transformation of *Arabidopsis thaliana*. The plant Journal, 16(6):735-743.

Creff, A., Brocard, L. and Gwyneth, I. (2015). A mechanically sensitive cell layer regulates the physical properties of the *Arabidopsis* seed coat. Nature Communications, 6:6382-6389.

De Giorgi, J., Piskurewicz, U., Loubery, S., Utz-Pugin, A., Bailly, C., Mene-Saffrane, L. and Lopez-Molina, L. (2015). An endosperm-associated cuticle is required for *Arabidopsis* seed viability, dormancy and early control of germination. PLoS Genetics, 11(12):e1005708.

De Smet, S., Cuypers, A., Vangronsveld, J. and Remans, T. (2015). Gene networks involved in hormonal control of root development in *Arabidopsis thaliana*: A framework for studying its disturbance by metal stress. International Journal of Molecular Science, 16:19195-19224.

Dean, G.H., Zheng, H., Tewari, J., Huang, J., Young, D.S., Hwang, Y.T., Western, T.L., Carpita, N.C., McCann, M.C., Mansfield, S.D. and Haughn, G.W. The *Arabidopsis* MUM2 gene encodes a β-galactosidase required for the production of seed coat mucilage with correct hydration properties. The Plant Cell, 19(12):4007-40021.

Debeaujon, I., Leon-Kloosterziel, K.M. and Koornneef, M. (2000). Influence of the testa on seed dormancy, germination, and longevity in *Arabidopsis*. Plant Physiology, 122(2):403-413.

Debono, A., Yeats, T.H., Rose, J.K.C., Bird, D., Jetter, R., Kunst, L. and Samuels, L. (2009). *Arabidopsis* LTPG is a glycosylphosphatidylinositol-anchored lipid transfer protein required for export of lipids to the plant surface. Plant Cell, 21(4):1230–1238.

Dello Ioio, R. Linhares, F.S., Scacchi, E., Casamitjana-Martinez, E., Heidstra, R., Costantino, P. and Sabatini, S. (2007). Cytokinins determine *Arabidopsis* root meristem size by controlling cell differentiation. Current Biology, 17(8):678–682.

Deising, H.B., Werner, S. and Wernitz, M. (2000). The role of fungal appressoria in plant infection. Microbes and Infection, 2(13):1631–1641.

Deng, Y., Humbert, S., Liu, J.X., Srivastava, R., Rothstein, S.J. and Howell, S.H. (2011). Heat induces the splicing by IRE1 of a mRNA encoding a transcription factor involved in the unfolded protein response in *Arabidopsis*. Proceedings of the National Academy of Sciences of the United States of America, 108(17):7247–7252.

Deng, Y., Srivastava, R. and Howell, S.H. (2013). Endoplasmic reticulum (ER) stress response and its physiological roles in plants. International Journal of Molecular Sciences, 14(4):8188-8212.

Di Mambro, R., De Ruvo, M., Pacifici, E., Salvi, E., Sozzani, R., Benfey, P.N., Busch, W., Novak, O., Ljung, K., Di Paola, L., Marée, A.F.M., Costantino, P., Grieneisen, V.A. and Sabatini, S. (2017). Auxin minimum triggers the developmental switch from cell division to cell differentiation in the *Arabidopsis* root. Proceedings of the National Academy of Sciences of the United States of America, 114(36):E7641–E7649.

Doblas, V.G., Geldner, N. and Barberon, M. (2017). The endodermis, a tightly controlled barrier for nutrients. Plant Biology, 39:136–143.

Dolan, L., Janmaat, K., Willemsen, V., Linstead, P., Poethig, S., Roberts, K. and Scheres, B. (1993). Cellular organisation of the *Arabidopsis thaliana* root. Development, 119:71-84.

Domínguez, E., Heredia-Guerrero, J.A. and Heredia, A. (2011). The biophysical design of plant cuticles: an overview. New Physiologist, 189(4):938-949.

Dreveny, I., Gruber, K., Glieder, A., Thompson, A. and Kratky, C. (2001). The hydroxynitrile lyase from almond: a lyase that looks like an oxidoreductase. Structure, 9(9):803-815.

Ellgaard, L. and Helenius, A. (2003). Quality control in the endoplasmic reticulum. Nature Reviews Molecular Cell Biology, 4(3):181–191.

Eigenbrode, S.D. and Jetter, R. (2002). Attachment to plant surface waxes by an insect predator. Integrative and Comparative Biology, 42(6):1091–1099.

Fernández, V., Guzmán-Delgado, P., Graça, J., Santos, S. and Gil, L. (2016). Cuticle structure in relation to chemical composition: re-assessing the prevailing model. Frontiers in Plant Science, 7:427.

Fich, E.A., Segerson, N.A. and Rose, J.K.C. (2016). The plant polyester cutin: biosynthesis, structure, and biological roles. Plant Biology, 67:207-233.

Filichkin, S.A., Priest, H.D., Givan, S.A., Shen, R., Bryant, D.W., Fox, S.E., Wong, W.K. and Mockler, T.C. (2010). Genome-wide mapping of alternative splicing in *Arabidopsis thaliana*. Genome research, 20(1);45-58.

Fontes, E.B., Shank, B.B., Wrobel, R.L., Moose, S.P., Gr, O.B., Wurtzel, E.T. and Boston, R.S. (1991). Characterization of an immunoglobulin binding protein homolog in the maize floury-2 endosperm mutant. Plant Cell, 3(5):483–496.

Gao, H., Brandizzi, F., Benning, C. and Larkin, R.M. (2008). A membrane-tethered transcription factor defines a branch of the heat stress response in *Arabidopsis thaliana*. Proceedings of the National Academy of Sciences of the United States of America, 105(42):16398–16403.

Galway, M.E., Masucci, J.D., Lloyd, A.M., Walbot, V., Davis, R.W. and Schiefelbein, J.W. (1994). The TTG gene is required to specify epidermal cell fate and cell patterning in the *Arabidopsis* root. Developmental Biology, 166(2):740-754.

Geem, K.R., Kim, D.H., Lee, D.W., Kwon, Y., Lee, J., Kim, J.H. and Hwang, I. (2019). Jasmonic acid-inducible TSA1 facilitates ER body formation. Plant Journal, 97(2):267–280.

Gleadow, R.M. and Møller B.L. (2014). Cyanogenic glycosides: synthesis, physiology, and phenotypic plasticity. Annual Review of Plant Biology, 65:155–185.

Gotor, C., Garcia, I., Aroca, A., Laureano-Marin, A.M., Arenas-Alfonseca, L., Jurado-Flores, A., Moreno, I. and Romero, L.C. (2019). Signalling by hydrogen sulfide and cyanide through post-translational modification. Journal of Experimental Biology, 70(16):4251-4265.

Grossmann, K. (1996). A role for cyanide, derived from ethylene biosynthesis, in the development of stress symptoms. Physiology Plant, 97(4):772-775.

Guzman, P., Fernandez, V., Garcia, M.L., Khayet, M., Fernandez, A. and Gil, L. (2014). Localization of polysaccharides in isolated and intact cuticles of eucalypt, poplar and pear leaves by enzyme-gold labelling. Plant Physiology and Biochemistry, 76:1-6.

Hakenjos, J.P., Bejai, S., Ranftl, Q., Behringer, C., Vlot, A.C., Absmanner, B., Hammes, U., Heinzlmeir, U., Kuster, B. and Schwechheimer. (2013). ML3 is a NEDD8- and ubiquitin-modified protein. Plant Physiology, 163(1):135–149.

Halkier, B.A. and Gershenzon, J. (2006). Biology and biochemistry of glucosinolates. Annual Review of Plant Biology, 57:303-333.

Hara-Nishimura, I., Matsushima, R., Shimada, T. and Nishimura, M. (2004). Diversity and formation of endoplasmic reticulum-derived compartments in plants. Are these compartments specific to plant cells? Plant Physiology, 136(3):3435-3439.

Hara-Nishimura, I., Shimada, T., Hatano, K., Takeuchi, Y. and Nishimura, M. (1998). Transport of storage proteins to protein storage vacuoles is mediated by large precursor-accumulating vesicle. Plant Cell, 10(5):825-836.

Haslam, T.M. and Kunst, L. (2013). Extending the story of very-long-chain fatty acid elongation. Plant Science, 210:93-107.

Hayashi, Y., Yamada, K., Shimada, T., Matsushima, R., Nishizawa, N.K., Nishimura, M. and Hara-Nishimura, I. (2001). A proteinase-storing body that prepares for cell death or stresses in the epidermal cells of *Arabidopsis*. Plant Cell Physiology, 42(9):894–899.

Hegebarth, D. and Jetter, R. (2017). Cuticular waxes of *Arabidopsis thaliana* shoots: cell-type-specific composition and biosynthesis. Plants, 6(3):27.

Hegebarth, D., Buschhaus, C., Wu, M., Bird, D. and Jetter, R. (2016). The composition of surface wax on trichomes of *Arabidopsis thaliana* differs from wax on other epidermal cells. Plant Journal, 88(5):762-774.

Heredia, A. and Benavente, J. (1991). A study of membrane potential across isolated fruit cuticles for NaCl and CaCl2 solutions. Biochimica et Biophysica Acta, 1062(2):239-244.

Heredia-Guerrero, J.A., Benitez, J.J., Dominguez, E., Bayer, I.S., Cingolani, R., Athanassiou, A. and Heredia, A. (2014). Infrared and Raman spectroscopic features of plant cuticles: A review. Frontiers in Plant Science, 5:305.

Höfgen, R. and Willmitzer, L. (1988). Storage of competent cells for *Agrobacterium* transformation. Nucleic Acids Research, 16(20);9877.

Howell, S.H. (2013). Endoplasmic reticulum stress responses in plants. Annual Review Plant Biology, 64:477-499.

Ihalainen, J.A., Paoli, B., Muff, S., Backus, E.H.G., Bredenbeck, J., Woolley, G.A., Caflisch, A. and Hamm, P. (2008). α-Helix folding in the presence of structural constraints. Proceedings of the National Academy of Sciences of the United States of America, 105(28):9588-9593.

Ingram, G. and Nawrath, C. (2017). The roles of the cuticle in plant development: organ adhesions and beyond. Journal of Experimental Botany, 68(19):5307-5321.

Jakoby, M.J., Falkenhan, D., Mader, M.T., Brininstool, G., Wischnitzki, E., Platz, N., Hudson, A., Hülskamp, M., Larkin, J. and Schnittger, A. (2008). Transcriptional profiling of mature *Arabidopsis* trichomes reveals that *NOECK* encodes the MIXTA-like transcriptional regulator MYB106. Plant Physiology, 148:1583-1602.

Javelle, M., Vernoud, V., Rogowsky, P.M. and Ingram, G.C. (2011). Epidermis: the formation and functions of a fundamental plant tissue. New Phytologist, 189:17-39.

Journot-Catalino, N., Somssich, I.E., Roby, D. and Kroj, T. (2006). The transcription factors WRKY11 and WRKY17 act as negative regulators of basal resistance in *Arabidopsis thaliana*. Plant Cell,18:3289-3302.

Kauss, H., Fauth, M., Merten, A. and Jeblick, W. (1999) Cucumber hypocotyls respond to cutin monomers via both an inducible and a constitutive H_2O_2-generating system. Plant Physiology, 120(4):1175–1182.

Kavita, P. and Burma, P.K. (2008). A comparative analysis of green fluorescent protein and β-glucuronidase protein-encoding genes as a reporter system for studying the temporal expression profiles of promoters. Journal of Biosciences, 33:337–343.

Kerstiens, G. (1996). Signalling across the divide: a wider perspective of cuticular structure—function relationships. Trends in Plant Science, 1(4):125–129.

Khow, O. and Suntrarachun, S. (2012). Strategies for production of active eukaryotic proteins in bacterial expression system. Asian Pacific Journal of Tropical Biomedicine, 2(2):159-162.

Kinoshita, T., Yamada, K., Hiraiwa, N., Nishimura, M. and Hara-Nishimura, I. (1999). Vacuolar processing enzyme is up-regulated in the lytic vacuoles of vegetative tissues during senescence and under various stressed conditions. Plant Journal, 19:43–53.

Kissen, R. and Bones, A.M. (2009). Nitrile-specifier proteins involved in glucosinolate hydrolysis in *Arabidopsis thaliana*. Journal of Biological Chemistry, 284(18):12057-12070.

Kleindt, C., Stracke, R., Mehrtens, F. and Weisshaar, B. (2010). Expression analysis of flavonoid biosynthesis genes during *Arabidopsis thaliana* silique and seed development with a primary focus on the proanthocyanidin biosynthetic pathway. BioMed Central Research Notes, 3(1):255.

Koizumi, N., Martinez, I.M., Kimata, Y., Kohno, K., Sano, H. and Chrispeels, M.J. (2001). Molecular characterization of two *Arabidopsis* Ire1 homologs, endoplasmic reticulum-located transmembrane protein kinases. Plant Physiology, 172(3):949–962.

Kosma, D.K., Bourdenx, B., Bernard, A., Parsons, E.P., Lü, S., Joubès, J., Jenks, M.A. (2009). The impact of water deficiency on leaf cuticle lipids of *Arabidopsis*. Plant Physiology, 151(4):1918–1929.

Kong, X., Liu, G., Liu, J. and Ding, Z. (2018). The root transition zone: a hot spot for signal crosstalk. Trends in Plant Science, 23(5):403-409.

Kristiansen, K. (2004). Molecular mechanisms of ligand binding, signaling, and regulation within the superfamily of G-protein-coupled receptors: molecular modeling and mutagenesis approaches to receptor structure and function. Pharmacology & Therapeutics, 103(1):21-80.

Krolikowski, K.A., Victor, J.L., Wagler, T.N., Lolle, S.J. and Pruitt, R.E. (2003). Isolation and characterization of the *Arabidopsis* organ fusion gene HOTHEAD. Plant Journal, 35(4):501-511.

Kryvych, S., Nikiforova, V., Herzog, M., Perazza, D. and Fisahn, J. (2008). Gene expression profiling of the different stages of *Arabidopsis thaliana* trichome development on the single cell level. Plant Physiology and Biochemistry, 46:160-173.

Kumpf, R.P. and Nowack, M.K. (2015). The root cap: a short story of life and death. Journal of Experimental Botany, 66(19):5651-5662.

Kurdyukov, S., Faust, A., Nawrath, C., Bär, S., Voisin, D., Franke, R., Schreiber, L., Saedler, H., Métraux, J.P. and Yephremov, A. (2006a). The epidermis-specific extracellular BODYGUARD controls cuticle development and morphogenesis in *Arabidopsis*. Plant Cell, 18:321–339.

Kurdyukov, S., Faust, A., Trenkamp, S., Bar, S., Franke, R., Efremova, N., Tietjen, K., Schreiber, L., Saedler, H. and Yephremov, A. (2006b). Genetic and biochemical evidence for involvement of HOTHEAD in the biosynthesis of long-chain α-,ω-dicarboxylic fatty acids and formation of extracellular matrix. Planta, 224(2):315-329.

Lambrix, V., Reichelt, M., Mitchell-Olds, T., Kliebenstein, D.J. and Gershenzon, J. (2001). The *Arabidopsis* epithiospecifier protein promotes the hydrolysis of glucosinolates to nitriles and influences Trichoplusia ni herbivory. Plant Cell, 18(6):1537.

Le Dreff-Kerwin, E. (2019). The HOTHEAD protein: assessing enzymatic activity using computational and recombinant protein expression approaches. UWSpace, http://hdl.handle.net/10012/14589.

Lee, M.M. and Schiefelbein, J. (2002). Cell pattern in the *Arabidopsis* root epidermis determined by lateral inhibition with feedback. Plant Cell, 14(3):611-618.

Li-Beisson, Y., Pollard, M., Sauveplane, V., Pinot, F., Ohlrogge, J. and Beisson, F. (2009). Nanoridges that characterize the surface morphology of flowers require the synthesis of cutin polyester. Proceedings of the National Academy of Sciences of the United States of America, 106(51):22008–22013.

Liu, J.X. and Howell, S.H. (2010). bZIP28 and NF-Y transcription factors are activated by ER stress and assemble into a transcriptional complex to regulate stress response genes in *Arabidopsis*. Plant Cell, 22(3):782–796.

Liu, J.X. and Howell, S.H. (2016). Managing the protein folding demands in the endoplasmic reticulum of plants. New Phytology, 211(2):418–428.

Liu, J.X., Srivastava, R. and Howell, S. H. (2008). Stress-induced expression of an activated form of AtbZIP17 provides protection from salt stress in *Arabidopsis*. Plant Cell and Environment, 31(12), 1735–1743.

Liu, J.X., Srivastava, R., Che, P. and Howell, S.H. (2007). An endoplasmic reticulum stress response in *Arabidopsis* is mediated by proteolytic processing and nuclear relocation of a membrane-associated transcription factor, bZIP28. Plant Cell, 19(12):4111–19.

Liu, M.J., Wu, S.H., Wu, J.F., Lin, W.D., Wu, Y.C., Tsai, T.Y., Tsai, H.L. and Wu, S.H. (2013). Translational landscape of photomorphogenic Arabidopsis. Plant Cell, 25(10):3699–3710.

Livak, K.J. and Schmittgen, T.D. (2001). Analysis of relative gene expression data using real-time quantitative PCR and the $2^{-\Delta\Delta CT}$ method. Methods, 25(4):402-408.

Llamas, E., Pulido, P. and Rodriguez-Concepcion, M. (2017**).** Interference with plastome gene expression and Clp protease activity in Arabidopsis triggers a chloroplast unfolded protein response to restore protein homeostasis**.** PLOS Genetics, 13(9):e1007022.

Lolle, S.J. and Pruitt, R.E. (1999). Epidermal cell interactions: A case for local talk. Trends in Plant Science, 4(1):14-20.

Lolle, S.J., Berlyn, G.P., Engstrom, E.M., Krolikowski, K.A., Reiter, W.D. and Pruitt, R.E. (1997). Developmental regulation of cell interactions in the *Arabidopsis* fiddlehead-1 mutant: A role for the epidermal cell wall and cuticle. Developmental Biology, 189(2):311-321.

Lolle, S.J., Cheung, A.Y. and Sussex, I.M. (1992). Fiddlehead: An *Arabidopsis* mutant constitutively expressing an organ fusion program that involves interactions between epidermal cells. Developmental Biology, 152(2):383-392.

Lolle, S.J., Hsu, W. and Pruitt, R.E. (1998). Genetic analysis of organ fusion in *Arabidopsis thaliana*. Genetics, 149(2):607-619.

Longhi. S. and Cambillau. C. (1999). Structure-activity of cutinase, a small lipolytic enzyme. Biochimica et Biophysica Acta, 1441(2-3):185–196.

Lopez-Casado, G., Matas, A.J., Dominguez, E., Cuartero, J. and Heredia, A. (2007). Biomechanics of isolated tomato (Solanum lycopersicum L.) fruit cuticles: the role of the cutin matrix and polysaccharides. Journal of Experimental Botany, 58(14):3875-3883.

Louvet, R., Cavel, E., Gutierrez, L., Guénin, S., Roger, D., Gillet, F., Guerineau, F. and Pelloux, J. (2006). Comprehensive expression profiling of the pectin methylesterase gene family during silique development in *Arabidopsis thaliana*. Planta, 224(4):782-791.

Lü, S., Song, T., Kosma, D.K., Parsons, E.P., Rowland, O. and Jenks, M.A. (2009). *Arabidopsis* CER8 encodes LONG-CHAIN ACYL-COA SYNTHETASE 1 (LACS1) that has overlapping functions with LACS2 in plant wax and cutin synthesis. Plant Journal, 59(4):553–564.

Luo, M., Dennis, E.S., Berger, F., Peacock, W.J. and Chaudhury, A. (2005). MINISEED3 (MINI3), a WRKY family gene, and HAIKU2 (IKU2), a leucine-rich repeat (LRR) KINASE gene, are regulators of seed size in *Arabidopsis*. Proceedings of the National Academy of Sciences of the United States of America, 102:17531–17536.

Machingura, M., Salomon, E., Jez, J.M. and Ebbs, S.D. (2016). The β-cyanoalanine synthase pathway: beyond cyanide detoxification. Plant Cell and Environment, 39(10):2329-2341.

Masucci, J.D., Rerie, W.G., Foreman, D.R., Zhang, M., Galway, M.E., Marks, M.D. and Schiefelbein, J.W. (1996). The homeobox gene GLABRA2 is required for position-dependent cell differentiation in the root epidermis of *Arabidopsis thaliana*. Development, 122(4):1253-1260.

Masumura, T., Shigemitsu, T., Morita, S. and Satoh, S. (2015). Identification of the region of rice 13 kDa prolamin essential for the formation of ER-derived protein bodies using a heterologous expression system. Bioscience Biotechnology and Biochemistry, 79(4):566-573.

Matsushima, R., Hayashi, Y., Kondo, M., Shimada, T., Nishimura, M. and Hara-Nishimura, I. (2002). An endoplasmic reticulum-derived structure that is induced under stress conditions in *Arabidopsis*. Plant Physiology, 130:1807-1814.

Matsushima, R., Hayashi, Y., Yamada, K., Shimada, T., Nishimura, M. and Hara-Nishimura, I. (2003). The ER body, a novel endoplasmic reticulum-derived structure in *Arabidopsis*. Plant and Cell Physiology, 44(7):661-666.

Matsushima, R., Kondo, M., Nishimura, M. and Hara-Nishimura, I. (2003b). A novel ER derived compartment, the ER body, selectively accumulates a β-glucosidase with an ER-retention signal in *Arabidopsis*. Plant Journal, 33(3):493-502.

Matsushima, R., Fukao, Y., Nishimura, M. and Hara-Nishimura, I. (2004). NAI1 gene encodes a basic-helix-loop-helix-type putative transcription factor that regulates the formation of an endoplasmic reticulum-derived structure, the ER body. Plant Cell, 16(6):1536-1549.

Mayer, M.P. (2013). Hsp70 chaperone dynamics and molecular mechanism. Trends in Biochemical Science, 38(10):507-514.

McFarlane, H.E., Shin, J.J., Bird, D.A., Samuels, A.L. (2010). *Arabidopsis* ABCG transporters, which are required for export of diverse cuticular lipids, dimerize in different combinations. Plant Cell, 22(9):3066–3075.

Merchante, C., Stepanova, A.N. and Alonso, J. (2017). Translation regulation in plants: an interesting past, an exciting present and a promising future. The Plant Journal, 90(4):628-653.

Molina, I., Ohlrogge, J.B. and Pollard, M. (2008). Deposition and localization of lipid polyester in developing seeds of *Brassica napus* and *Arabidopsis thaliana*. The Plant Journal, 53:437-449.

Moon, J.Y. and Park, J.M. (2016). Cross-talk in viral defense signalling in plants. Frontiers in Microbiology, 7(2068).

Morris, D. and Geballe, A.P. (2000). Upstream open reading frames as regulators of mRNA translation. Molecular and Cellular Biology, 20(23):8635-8642.

Muller, B. and Sheen, J. (2008) Cytokinin and auxin interaction in root stem-cell specification during early embryogenesis. Nature 453(7198):1094-1097.

Nagano, A.J., Fukao, Y., Fujiwara, M., Nishimura, M. and Hara-Nishimura, I. (2008). Antagonistic jacalin-related lectins regulate the size of ER body-type β-glucosidase complexes in *Arabidopsis thaliana*. Plant Cell Physiology, 49(6):969–980.

Nagano, A.J., Matsushima, R. and Hara-Nishimura, I. (2005). Activation of an ER-body-localized beta-glucosidase via a cytosolic binding partner in damaged tissues of *Arabidopsis thaliana*. Plant Cell Physiology, 46(7):1140–1148.

Nakagawa, T., Suzuki, T., Murata, S., Nakamura, S., Hino, T., Maeo, K., Tabata, R., Kawai, T., Tanaka, K., Niwa, Y., Watanabe, Y., Nakamura, K., Kimura, T. and Ishiguro, S. (2007). Improved gateway binary vectors: high-performance vectors for creation of fusion constructs in transgenic analysis of plants. Bioscience, Biotechnology, and Biochemistry, 71(8):2095-2100.

Nakano, R.T., Matsushima, R., Nagano, A.J., Fukao, Y., Fujiwara, M., Kondo, M., Nishimura, M. and Hara-Nishimura, I. (2012). ERMO3/MVP1/GOLD36 is involved in a cell type-specific mechanism for maintaining er morphology in *Arabidopsis thaliana*. PLoSONE, 7(11):e49103.

Nakano, R.T., Piślewska-Bednarek, M., Yamada, K., Edger, P.P., Miyahara, M., Kondo, M., Böttcher, C., Mori, M., Nishimura, M. and Schulze-Lefert, P. (2017). PYK10 myrosinase reveals a functional coordination between endoplasmic reticulum bodies and glucosinolates in *Arabidopsis thaliana*. Plant Journal, 89(2):204–220.

Nakano, R.T., Yamada, K., Bednarek, P., Nishimura, M. and Hara-Nishimura, I. (2014). ER bodies in plants of the Brassicales order: biogenesis and association with innate immunity. Fronteirs in Plant Biology, 5(73):1-17.

Nakazaki, A., Yamada, K., Kunieda, T., Sugiyama, R., Hirai, M.Y., Tamura, K., Hara-Nishimura, I. and Shimada, T. (2019a). Leaf ER bodies identified in *Arabidopsis* rosette leaves are involved in defense against herbivory. Plant Physiology, 179(4):1515–1524.

Nakazaki, A., Yamada, K., Kunieda, T., Tamura, K., Hara-Nishimura, I. and Shimada, T. (2019b). Biogenesis of leaf endoplasmic reticulum body is regulated by both jasmonate-dependent and independent pathways. Plant Signaling and Behavior, 14(8):e1622982.

Ogasawara, K., Yamada, K., Christeller, J.T., Kondo, M., Hatsugai, N., Hara-Nishimura, I. and Nishimura, M. (2009). Constitutive and inducible ER bodies of *Arabidopsis thaliana* accumulate distinct β-glucosidases. Plant Cell and Physiology, 50(3):480-488.

Ohta, M. and Takaiwa, F. (2014). Emerging features of ER resident J-proteins in plants. Plant Signaling and Behaviour, 9:e28194-3.

Öztuna, D., Elhan, A.H. and Tüccar, E. (2006). Investigation of four different normality tests in terms of type 1 error rate and power under different distributions. The Turkish Journal of Medical Sciences, 36(3):171-176.

Pagnussat, G.C., Yu, H.J., Ngo, Q.A., Rajani, S., Mayalagu, S., Johnson, C.S., Capron, A., Xie, L.F., Ye, D. and Sundaresan, V. (2005). Genetic and molecular identification of genes required for female gametophyte development and function in *Arabidopsis*. Development, 132(3):603-614.

Panikashvili, D., Shi, J.X., Schreiber, L. and Aharoni, A. (2011). The *Arabidopsis* ABCG13 transporter is required for flower cuticle secretion and patterning of the petal epidermis. New Phytologist Trust, 190(1):113–124.

Pattanaik, S., Patra, B, Singh, S.K. and Yuan, L. (2014). An overview of the gene regulatory network controlling trichome development in the model plant, *Arabidopsis*. Frontiers in Plant Science, 5:259.

Péret, B., De Rybel, B., Casimiro, I., Benkova, E., Swarup, R., Laplaze, L., Beeckman, T. and Bennett, M.J. (2009). *Arabidopsis* lateral root development: an emerging story. Trends in Plant Science, 14(7):399-408.

Pollard, M., Beisson, F., Li, Y. and Ohlrogge, J.B. (2008). Building lipid barriers: Biosynthesis of cutin and suberin. Trends in Plant Science, 13(5):236-246.

Pruitt, R.E., Vielle-Calzada, J.P., Ploense, S.E., Grossniklaus, U. and Lolle, S.J. (2000). FIDDLEHEAD, a gene required to suppress epidermal cell interactions in *Arabidopsis*, encodes a putative lipid biosynthetic enzyme. Proceedings of the National Academy of Sciences of the United States of America, 97(3):1311-1316.

Rask, L., Andreasson, E., Ekbom, B., Eriksson, S., Pontoppidan, B. and Meijer, J. (2000). Myrosinase: Gene family evolution and herbivore defense in Brassicaceae. Plant Molecular Biology, 42(1):93-113.

Raviv, B., Aghajanyan, L., Granot, G., Makover, V., Frenkel, O., Gutterman, Y. and Grafi, G. (2017). The dead seed coat functions as a long-term storage for active hydrolytic enzymes. PLOS ONE, 12(7):e0181102.

Riederer, M., and Schreiber, L. (2001). Protecting against water loss: analysis of the barrier properties of plant cuticles. Journal of Experimental Botany, 52(363):2023–2032.

Robinson-Beers, K., Pruitt, R.E. and Gasser, C.S. (1992). Ovule development in wild-type *Arabidopsis* and two female-sterile mutants. Plant Cell, 4:1237-1301.

Rojo, E., Zouhar, J., Carter, C., Kovaleva, V. and Raikhel, N.V. (2003). A unique mechanism for protein processing and degradation in *Arabidopsis thaliana*. Proceedings of the National Academy of Sciences of the United States of America, 100(12):7389-7394.

Romanchuk, S.M. (2010). Ultrastructure of the statocytes and cells of the distal elongation zone of *Arabidopsis thaliana* under the conditions of clinorotation. Cytology and Genetics, 44(6):329-333.

Ruberti, C and Brandizzi, F. (2018). Unfolded protein response in Arabidopsis. Methods in Molecular Biology, 1691:231-238.

Samuels, L., Kunst, L. and Jetter, R. (2008). Sealing plant surfaces: cuticular wax formation by epidermal cells. Annual Review of Plant Biology, 59:683-707.

Schellmann, S., Schnittger, A., Kirik, V., Wada, T., Okada, K., Beermann, A., Thumfahrt, J., Jürgens, G. and Hülskamp, M. (2002). TRIPTYCHON and CAPRICE mediate lateral inhibition during trichome and root hair patterning in *Arabidopsis*. EMBO Journal, 21(19):5036-5046.

Schroder, M. and Kaufman, R. J. (2005). The mammalian unfolded protein response. Annual Review of Biochemistry, 74:739–789.

Schweizer, P., Felix, G., Buchala, A., Müller, C. and Métraux, J.P. (1996) Perception of free cutin monomers by plant cells. Plant Journal, 10(2):331–341.

Shental-Bechor, D. and Levy, Y. (2008). Effect of glycosylation on protein folding: A close look at thermodynamic stabilization. Proceedings of the National Academy of Sciences of the United States of America, 105(24):8256-8261.

Sherameti, I., Venus, Y., Drzewiecki, C., Tripathi, S., Dan, V.M., Nitz, I., Varma, A., Grundler, F.M. and Oelmuller, R. (2008). PYK10, a β-glucosidase located in the endoplasmatic reticulum, is crucial for the beneficial interaction between *Arabidopsis thaliana* and the endophytic fungus *Piriformospora indica*. Plant Journal, 54(3):428-439.

Shi, L., Dean, G.H., Zheng, H., Meents, M.J., Haslam, T.M., Haughn, G.W. and Kunst, L. (2019). ECERIFERUM11/C-TERMINAL DOMAIN PHOSPHATASE-LIKE2 affects secretory trafficking. Plant Physiology, 181(3):901-915.

Shirakawa, M. and Hara-Nishimura, I. (2018). Specialized vacuoles of myrosin cells: chemical defense strategy in Brassicales plants. Plant Cell Physiology, 59(7):1309-1316.

Sieber, P., Schorderet, M., Ryser, U., Buchala, A., Kolattukudy, P., Métraux, J.P. and Nawrath., C. (2000). Transgenic *Arabidopsis* plants expressing a fungal cutinase show alterations in the structure and properties of the cuticle and postgenital organ fusions. Plant Cell, 12:721–738.

Siegel, B.A. and Verbeke, J.A. (1989). Diffusible factors essential for epidermal cell redifferentiaion in *Catharanthus roseus*. Science, 244(4904):580-582.

Siegień, I. and Bogatek, R. (2006). Cyanide action in plants - from toxic to regulatory. Acta Physiologiae Plantarum, 28(5):483-497.

Solomonson, L.P. and Barber, M.J. (1990). Assimilatory nitrate reductase: functional properties and regulation. Annual Review of Plant Physiology Plant Molecular Biology, 41(1):225-253.

Srivastava, R., Chen, Y., Deng, Y., Brandizzi, F. and Howell, S.H. (2012). Elements proximal to and within the trans-membrane domain mediate the organelle-to-organelle movement of bZIP28 under ER stress conditions.Plant Journal, 70(6):1033–42.

Srivastava, R., Deng, Y. and Howell, S.H. (2013). Stress sensing in plants by an ER stress sensor/transducer, bZIP28. Frontiers in Plant Science, 5(59):1-6.

Sudre, D., Gutierrez-Carbonell, E., Lattanzio, G., Rellán-Álvarez, R., Gaymard, F., Wohlgemuth, G., Fiehn, O., Alvarez-Fernández, A., Zamarreño, A.M., Bacaicoa, E., Duy, D., García-Mina, J., Abadía, J., Philippar, K., López-Millán, A. and Briat, J. (2013). Iron-dependent modifications of the flower transcriptome, proteome, metabolome, and hormonal content in an *Arabidopsis* ferritin mutant. Journal of Experimental Botany, 64(10):2665-2688.

Sützl, L., Foley, G., Gillam, E.M.J. Bodén, M. and Haltrich, D. (2019). The GMC superfamily of oxidoreductases revisited: analysis and evolution of fungal GMC oxidoreductases. Biotechnology for Biofuels, 12(118):1-18.

Takahashi, S., Yanai, H., Nakamaru, Y., Uchida, A., Nakayama, K. and Satoh, H. (2012). Molecular cloning, characterization and analysis of the intracellular localization of a water-soluble chl-binding protein from brussels sprouts (*Brassica oleracea* var. *gemmifera*). Plant Cell and Physiology, 53(5):879-891.

Theologis, A., Ecker, J.R., Palm, C.J., Federspiel, N.A., Kaul, S., White, O., Alonso, J., Altafi, H., Araujo, R., Bowman, C.L., Brooks, S.Y., Buehler, E., Chan, A., Chao, Q., Chen, H., Cheuk, R.F., Chin, C.W., Chung, M.K., Conn, L., Conway, A.B., Conway, A.R., Creasy, T.H., Dewar, K., Dunn, P., Etgu, P., Feldblyum, T.V., Feng, J., Fong, B., Fujii, C.Y., Gill, J.E., Goldsmith, A.D., Haas, B., Hansen, N.F., Hughes, B., Huizar, L., Hunter, J.L., Jenkins, J., Johnson-Hopson, C., Khan, S., Khaykin, E., Kim, C.J., Koo, H.L., Kremenetskaia, I., Kurtz, D.B., Kwan, A., Lam, B., Langin-Hooper, S., Lee, A., Lee, J.M., Lenz, C.A., Li, J.H., Li, Y., Lin, X., Liu, S.X., Liu, Z.A., Luros, J.S., Maiti, R., Marziali, A., Militscher, J., Miranda, M., Nguyen, M., Nierman, W.C., Osborne, B.I., Pai, G., Peterson, J., Pham, P.K., Rizzo, M., Rooney, T., Rowley, D., Sakano, H., Salzberg, S.L., Schwartz, J.R., Shinn, P., Southwick, A.M., Sun, H., Tallon, L.J., Tambunga, G., Toriumi, M.J., Town, C.D., Utterback, T., Van Aken, S., Vaysberg, M., Vysotskaia, V.S., Walker, M., Wu, D., Yu, G., Fraser, C.M., Venter, J.C. and Davis, R.W. (2000). Sequence and analysis of chromosome 1 of the plant *Arabidopsis thaliana*. Nature, 408(6814): 816-820.

Tokmakov, A.A., Kurotani, A., Takagi, T., Toyama, M., Shirouzu, M., Fukami, Y. and Yokoyama, S. (2012). Multiple post-translational modifications affect heterologous protein synthesis. Journal of Biological Chemistry, 287(32):106-116.

Torrent, M., Llompart, B., Lasserre-Ramassamy, S., Llop-Tous, I., Bastida, M., Marzabal, P., Westerholm-Parvinen, A., Saloheimo, M., Heifetz, P.B. and Ludevid, M.D. (2009). Eukaryotic protein production in designated storage organelles. BioMed Central Biology, 7(5).

Verbeke, J.A. and Walker, D.B. (1986). Morphogenetic factors controlling differentiation and dedifferentiation of epidermal cells in the gynoecium of *Catharanthus roseus*: II. Diffusible morphogens. Planta, 168(1):43-49.

Verbelen, J.P., De Cnodder, T., Le, J., Vissenberg, K. and Baluška, F. (2006). The root apex of *Arabidopsis thaliana* consists of four distinct zones of growth activities: meristematic zone, transition zone, fast elongation zone and growth terminating zone. Plant Signaling and Behaviour, 1(6):296-304.

Vitale, A. and Boston, R.S. (2008). Endoplasmic reticulum quality control and the unfolded protein response: insights from plants. Traffic, 9(10):1581–1588.

Vitale, A. and Ceriotti, A. (2004). Protein quality control mechanisms and protein storage in the endoplasmic reticulum. A conflict of interests? Plant Physiology, 136(3):3420-3426.

von Arnim, A.G., Jia, Q. and Vaughn, J.N. (2014). Regulation of plant translation by upstream open reading frames. Plant Science, 214:1–12.

von Mohl, H. (1847). Untersuchungen der Frage: bildet die cellulose die grundlage sammtlicher vegetabilischen membranen. Botanische Zeitung 5:497–505.

Vrielink, A., Lloyd, L.F. and Blow, D.M. (1991). Crystal structure of cholesterol oxidase from *Brevibacterium sterolicum* refined at 1.8 ˚A resolution. Journal of Molecular Biology, 219:533–554.

Wellesen, K., Durst, F., Pinot, F., Benveniste, I., Nettesheim, K., Wisman, E., Steiner-Lange, S., Saedler, H. and Yephremov, A. (2001). Functional analysis of the *LACERATA* gene of *Arabidopsis* provides evidence for different roles of fatty acid omega-hydroxylation in development. Proceedings of the National Academy of Sciences of the United States of America, 98(17):9694–9699.

Weng, H., Molina, I., Shockey, J. and Browse, J. (2010). Organ fusion and defective cuticle function in a lacs1 lacs2 double mutant of *Arabidopsis*. Planta, 231(5):1089-1100.

Wenzel, C.L., Hester, Q. and Mattsson, J. (2008). Identification of Genes Expressed in Vascular Tissues Using NPA-Induced Vascular Overgrowth in *Arabidopsis*. Plant Cell Physiology, 49(3):457–468.

Wharton, M.J. (1955). The use of tetrazolium test for determining the viability of seeds of the genus Brassica. Proceedings of International Seed Testing Association, 20:81–88.

Williamson, C.D., Wong, D.S., Bozidis, P., Zhang, A. and Colberg-Poley, A.M. (2015). Isolation of endoplasmic reticulum, mitochondria, and mitochondria-associated membrane and detergent resistant membrane fractions from transfected cells and from human cytomegalovirus-infected primary fibroblasts. Current Protocols in Cell Biology, 68:3.27.1-3.27.33.

Wittstock, U. and Halkier, B.A. (2002). Glucosinolate research in the *Arabidopsis* era. Trends in Plant Science, 7(6):263-270.

Xiao, H., Sun, F., Suttapitugsakul, S. and Wu, R. (2019). Global and site-specific analysis of protein glycosylation in complex biological systems with mass spectrometry. Mass Spectrometry Reviews, 38(4-5):356-379.

Xu, Z., Escamilla-Treviño, L., Zeng, L., Lalgondar, M., Bevan, D., Winkel, B., Mohamed, A., Cheng, C., Shih, M., Poulton, J. and Esen, A. (2004). Functional genomic analysis of *Arabidopsis thaliana* glycoside hydrolase family 1. Plant Molecular Biology, 55:343–367.

Xue, Y., Xiao, S., Kim, J., Lung, S.C., Chen, L., Tanner, J.A., Suh, M.C. and Chye, M. (2014). *Arabidopsis* membrane-associated acyl-CoA-binding protein ACBP1 is involved in stem cuticle formation. Journal of Experimental Botany, 65(18):5473–5483.

Yadav, R.K., Tavakkoli, M., Xie, M., Girke, T. and Reddy, G.V. (2014). A high-resolution gene expression map of the *Arabidopsis* shoot meristem stem cell niche. Development, 141(13):2735-2744.

Yamada, K., Goto-Yamada, S., Nakazaki, A., Kunieda, T., Kuwata, K., Nagano, A.J., Nishimura, M. and Hara-Nishimura, I. (2020). Endoplasmic reticulum-derived bodies enable a single-cell chemical defense in Brassicaceae plants. Communications Biology, 3(21):1-10.

Yamada, K., Nagano, A.J, Nishina, M., Hara-Nishimura, I. and Nishimura, M. (2008). NAI2 is an endoplasmic reticulum body component that enables ER body formation in *Arabidopsis thaliana*. The Plant Cell, 20:2529-2540.

Yamada, K., Nagano, A.J, Nishina, M., Hara-Nishimura, I. and Nishimura, M. (2013). Identification of two novel endoplasmic reticulum body-specific integral membrane proteins. Plant Physiology, 161(1):108-120.

Yang, W., Simpson, J.P., Li-Beisson, Y., Beisson, F., Pollard, M. and Ohlrogge, J.B. (2012). A land-plant-specific glycerol-3-phosphate acyltransferase family in *Arabidopsis*: substrate specificity, sn-2 preference, and evolution. Plant Physiology, 160(2):638–652.

Yeats, T.H. and Rose, J.K.C. (2008). The biochemistry and biology of extracellular plant lipid-transfer proteins (LTPs). Protein Science, 17(2):191–198.

Yeats, T.H. and Rose, J.K.C. (2013). The formation and function of plant cuticles. Plant Physiology, 163(1):5-20.

Yeats, T.H., Martin, L.B., Viart, H.M., Isaacson, T., He, Y., Zhao, L., Matas, A.J., Buda, G.J., Domozych, D.S., Clausen, M.H. and Rose, J.K.C. (2012). The identification of cutin synthase: formation of the plant polyester cutin. Natural Chemical Biology, 8:609–611.

Yemm, R.S. and Poulton, J.E. (1986). Isolation and characterization of multiple forms of mandelonitrile lyase from mature black cherry (*Prunus serotina* Ehrh.) seeds. Biochemistry and Biophysics, 247(2):440-445.

Ziv, C., Zhao, Z., Gao, Y.G. and Xia, Y. (2018). Multifunctional roles of plant cuticle during plant-pathogen interactions. Frontiers in Plant Science, 9:1088.

Zwieniecki, M.A., Melcher, P.J. and Holbrook, N.M. (2001). Hydrogel control of xylem hydraulic resistance in plants. Science, 291(5506):1059-1062.

Appendix

Appendix A. The 5’ upstream region and *HOTHEAD* genomic sequence. This genomic DNA was derived from a Col ecotype *A. thaliana* plant and was cloned into the pGWB640 gateway binary vector (Accession: AB543141) (Chang, 2016; Nakagawa et al., 2007).

atgc - 5’ Untranslated region
ATGC - Intron in the *HOTHEAD* gene coding region
ATGC - Exon in the *HOTHEAD* gene coding region
ATGC - 81 bp deletion in the splice variant construct

> *HOTHEAD* (AT1G72970.1) 4.843 kb

taaagaggagagaaacaaagaatcttcttactctccaaaggtttgatctccagttcttgacgtttttttctccttattccctcactcatgagtccaaaacgctgcgtttataggg
acctttttgctctgttttattagaacttctcattatacacacgagtgaattagaattgaaaacgttgtggcatcatttgaatatttttccttcaaataaacaaaaaaaaaaaagatg
aagatgaaaaacaataataaatatatgtacgttctataataactcgtttcatgaaagtggaagcatgggatgagatgccaatcccatgaaaagtgagcaaaaattaat
atttacattaactgctgagtgggtaaagtttaataaccattttctaaaaataacttttattcagaatccaactcatggattggtgtgtgtatttattatcatcatttctatacacatat
ccacccccaataactctgtcaattatacacctcaaaatcactgtaagttataaaaaaatgaatttctacaattaatcaaagaccgtccaaagccttcgtggctaattggtg
ttaaactattcacatttttagtcaagtatttttgcatattatatgagattaattttgccacacaagatcgttaataaactcgacatgatgattctgtttatgtggcttctattaactag
gaaatgaaacaatgtagttatagttgtgactgatatgaagtcagagaaaatggctacgtaatcttatatgaccagaccaacgtacgtgatgcgatgtgacatttttcattc
aacactaaagttaaaaccttgattgtttttgtattacatttggcaactaatccaatatgttttgttagttgttagtactaagtactgactgatgatcacattcacgctcaaccaaat
aaaacggatgatattgtttttggttaggtgaaagaacaattaaattagttgccaaaaacataacccgtgaagatttatgttagtaaccaacctacagtcataattaataag
tttatgactaatagtaattaaatgacttgccaaaaacatggctctgtatagtatagttttagattttggttaggtgaagatgattaattgatacactatgaatctatgaagactt
gatccaacggctaccagatctccgacttcaactgttttcatatcgccattaatgatacagacaagctgtactactatccttttatctctttattgttttatatgattttacagtaata
ctattactaagtactaacaaattgtttttctttgcagctggtcccaaaagtcaaaatcatgggacaaaaaaacgagttattattcttattatcatcaccaaggtaaaaaaat
gtgaaaggaaatccttttaaggcttagtttcaatataaatacaaagatgttatttgatagtgattgttctttgtaacgaagtacttatcattaatttcaatttgcaacaaacaatt
ctgtaacaataagtctaatgtgaggaaagttactagctggtaaaataaattagtaggtaactatttttttatgagtaaatgagggaactattaattgagtaagatgattcatat
gtccttttcatttgctatattcgacagaatgggacacacctaaaatcaaatttacgttttagtgtagaccaccccaacatctctttattacacaacttgtgttttttttttactatatga
ttttttttaccgaatgttgttgtctaaccaaaattcaatgtaccgtataagactataagttatacaactcgtagaaatggttacatatatgtaacaatatatagagacacatgtg
ggtgtaattaatatagttgctctgttggatcgttagtgttatttataggagaagaaaacacacaaaacaaGACCATTCATCAAAAGCCACATAAGAAG
TTGATGCAGAAGCAATAATAACAAAACAAAAAAACATTAAAAAAAAAAGCTCTTCAGTTTTGGTTTCTGCAGTCTC
CAATGGCTCTCAAGCTCTTTCTCTTTGCTCTTCTTCTCTGTCTCCCGACTTCTCTCTCCTCCACTGCCTCTAAAGG
TCACTTCTCTTTCTCTCTTTAAACACAATCCTCCCATTACAAAGTTCTCTCTGTTTTTATCTTTCTCTTGGTCGTTGA
TGATTCTGTCTTGTTTTTAGCTATAGCTCTGTTTTTCGAAACTAGTTACTTATTCATAGACATGATATACATTCATAA
GCTTCTTTTTTATATATTAAAGACTCTGTTTCTTGATCCATCATGACCGAATCTTGAGTAACCAGGACACTAGTGCA
CAGTCCAGTCTTTTTTTAACGCGTAAACTGTTGTGTGTTTTTTGGGTTATGTTCTGCTATAAACACATTAATGGTGT
AATTACTTCTACCAACTACCCATAATTGTTTTATTTATTGAATAGTACAACTAAAAAAAACAATGATTTTGTAGGTAA
AGAGAAGAAGTCGAAGTTTAATCCATACAGATACACATTCATCGATAAAGCAAGCACATTCTCATCATCTTCCTCA
TCTTCATTTTCATCCAACGGTCAAGATTCGTCCTACGACTACATAGTCATCGGAGGTGGAACCGCAGGGTGTCCT
CTCGCCGCAACGTTGTCGCAGAATTTCAGCGTTCTTGTTTTAGAGAGAGGTGGCGTTCCGTTTACAAACGCAAAC
GTTTCTTTCCTCAGGAATTTTCACATCGGACTTGCTGACATTTCAGCTTCTTCCGCGTCTCAAGCGTTTGTTTCCA
CTGACGGCGTTTACAACGCCCGTGCTAGAGTTCTCGGTGGCGGTTCCTGTATTAACGCCGGTTTTTACTCCAGA
GCCGATGCTGCGTAAGTATAATTTTTACCTTTTTAAGACAAGAAAATTATGTTGTTTATTATATACTACTAAAAGGA
TTTATTGGTATAATCGATGCCTCGTGTCCTAGTGGATATGTTACATTTATGAAAACGCACCGAGCGAGAATGTTGT
GTTTTCTTAATAATTTTGGGGGCAATGGTCCGTAAGACTTTTAATTCTCTTTAATTTTTCACACTAATCAACACAAT
ATTTTTAACAAATACTTTTCTTCAGTAAAAATTGCAACCATTTTTTTTTTCTTTTCGAAAAATTGATTTCTTATATAAT
ATTAAAAAAATTCTCGAAAAAACTGATTTACTGTCATAAAAACTATTTTTTTTGTTCAGTAAAATAAGGTAAGAACAA
ATAAATGATTTAAATTGTGACAAAACATTCAGGTTCGTGAAGCGAGCAGGATGGGATCCGAAGCTGGTGAAGGA
GTCGTATCCATGGGTGGAGAGAGAGATTGTTCATCAGCCAAAGTTAACGTTATGGCAGAAAGCTCTCAGAGACA
GTCTTTTAGAGGTTGGAGTCAGACCTTTCAATGGTTTCACTTACGATCACGTTTCCGGAACCAAAATCGGCGGTA
CAATTTTCGACAGATTCGGCCGTCGTCACACCGCGGCGGAGCTTCTCGCTTACGCTAATCCTCAGAAGCTTAGA
GTCTTGATCTACGCCACCGTGCAAAAAATCGTCTTTGACACTTCTGGTACTGATAAATTTTTGTGTCTACCAAATG
TTCGATGAAATTCCTGAGTGAGGAGGTTTTTAACTTTTGTTTTGGTTTTGGATGTAGGAACAAGGCCTCGAGTAAC
AGGAGTAATATTCAAAGATGAGAAAGGTAATCAACACCAGGCTTTACTCTCGAATAGAAAGGGAAGTGAAGTGAT
CTTATCTAGTGGAGCTATTGGGTCACCACAGATGCTGATGTTAAGTGGGATTGGACCTAAGAAGGAGCTTCAGA
GGCTGAAGATTCCTGTGGTTTTAGAGAATGAGCATGTAGGAAAAGGAATGGCTGATAATCCCATGAACACGATCT
TGGTGCCTTCAAAGGCGCCTATAGAGCAGTCACTTATTCAGACTGTTGGAATTACAAAGATGGGTGTGTATGTTG
AAGCCAGTACTGGCTTTGGGCAATCTCCTGAGAGTATTCATACTCACTATGGGATTATGTCGAACAAGGTAACGT
AACTTTGTTGTTGGTGTCTTTGTAGGAGAATGTTGTTTGATGTTAAGGAGATAATGGTCTTTTGATTTTGTATGCA
GAATGAATTGTTTTCCACCATTCCTGCAAAGCAGAGAAGACCAGAAGCAACGCAAGCTTACATCACAAGAAACAA
ATACCAACTTCACGAAGCATTCAATGGAAGTTTCATCTTGGAGAAACTTGCTTACCCGATCTCTAGAGGGCATTT
GAGCTTGGTCAACACAAATGTTGATGACAACCCTTCAGTCACCTTCAATTACTTTAAACACCCGGTGGATCTCCA
ACGCTGTGTTGAAGCCATTCGTCTTGTTTCCAAAGTGGTGACGTCTAACCGTTTCTTAAACTACACGCAGTGTGA
CAAGCAAAACGTACACAAGATGCTTAGCTTAAGCGTCAAGGCAAACATCAATCTAAGGCCAAAGCAACTGAACGA
TACCAAATCAATGGCTCAGTTCTGCAAAGACACTGTTGTCACAATCTGGCACTACCATGGTGGATGTCTTGTGGG
TAAAGTTGTGAGCCCTAACCGCAAAGTTCTTGGTGTCGACAGGCTCAGAGTTATTGATGGTTCAACGTTTGACGA
GTCTCCAGGAACCAACCCGCAAGCTACTATGATGATGATGGGAAGGTAAATCAAAATCATTACCAACATAATGAA
TTGGAGGTTTTCTTTTTAGTTCAATATATAAACAGAGGATTTGTCAATCTTTGCAGATACATGGGAGTCAAGATTCT
TCGGGAGAGACTTGGAAACAAAGCTGGTGTT

Appendix B. The predicted protein sequence of HOTHEAD and its splice variant isoform.

VDLQRCVEAIRLVSKVVTSNRFLNYTQ - peptide missing in AT1G72970.2

KDEL-like sequences

>HOTHEAD (AT1G72970.1), 594 aa, 65.3 kDa

MALKLFLFALLLCLPTSLSSTASKGKEKKSKFNPYRYTFIDKASTFSSSSSSSFSSNGQDSSYDY
IVIGGGTAGCPLAATLSQNFSVLVLERGGVPFTNANVSFLRNFHIGLADISASSASQAFVSTDGV
YNARARVLGGGSCINAGFYSRADAAFVKRAGWDPKLVKESYPWVEREIVHQPKLTLWQKALR
DSLLEVGVRPFNGFTYDHVSGTKIGGTIFDRFGRRHTAAELLAYANPQKLRVLIYATVQKIVFDT
SGTRPRVTGVIFKDEKGNQHQALLSNRKGSEVILSSGAIGSPQMLMLSGIGPKKELQRLKIPVVL
ENEHVGKGMADNPMNTILVPSKAPIEQSLIQTVGITKMGVYVEASTGFGQSPESIHTHYGIMSN
KNELFSTIPAKQRRPEATQAYITRNKYQLHEAFNGSFILEKLAYPISRGHLSLVNTNVDDNPSVT
FNYFKHPVDLQRCVEAIRLVSKVVTSNRFLNYTQCDKQNVHKMLSLSVKANINLRPKQLNDTKS
MAQFCKDTVVTIWHYHGGCLVGKVVSPNRKVLGVDRLRVIDGSTFDESPGTNPQATMMMMG
RYMGVKILRERLGNKAGV

>HOTHEAD (AT1G72970.2), splice variant, 567 aa, 62.2 kDa

MALKLFLFALLLCLPTSLSSTASKGKEKKSKFNPYRYTFIDKASTFSSSSSSSFSSNGQDSSYDY
IVIGGGTAGCPLAATLSQNFSVLVLERGGVPFTNANVSFLRNFHIGLADISASSASQAFVSTDGV
YNARARVLGGGSCINAGFYSRADAAFVKRAGWDPKLVKESYPWVEREIVHQPKLTLWQKALR
DSLLEVGVRPFNGFTYDHVSGTKIGGTIFDRFGRRHTAAELLAYANPQKLRVLIYATVQKIVFDT
SGTRPRVTGVIFKDEKGNQHQALLSNRKGSEVILSSGAIGSPQMLMLSGIGPKKELQRLKIPVVL
ENEHVGKGMADNPMNTILVPSKAPIEQSLIQTVGITKMGVYVEASTGFGQSPESIHTHYGIMSN
KNELFSTIPAKQRRPEATQAYITRNKYQLHEAFNGSFILEKLAYPISRGHLSLVNTNVDDNPSVT
FNYFKHPCDKQNVHKMLSLSVKANINLRPKQLNDTKSMAQFCKDTVVTIWHYHGGCLVGKVVS
PNRKVLGVDRLRVIDGSTFDESPGTNPQATMMMMGRYMGVKILRERLGNKAGV

Appendix C. Micrographs showing HOTHEAD protein expression in response to salt shock. No ER bodies are seen in these images as 6- and 12-hours of exposure to salt shock was too short of a time frame to form HTH-GFP containing iER bodies. See Figure 2.2 for HTH-GFP containing iER bodies in the midrib cells of transgenic rosette leaves.

A. Midrib cells in rosette leaves of a *HTH_{pro}:HTH-GFP* plant transferred from an MS plate to a control MS plate and then returned to the growth chamber for 6-hours. B. Midrib cells in rosette leaves of a *HTH_{pro}:HTH-GFP* plant transferred from an MS plate to an MS plate supplemented with 100 mM NaCl and then returned to the growth chamber for 6-hours. C. Midrib cells in rosette leaves of a *HTH_{pro}:HTH-GFP* plant transferred from an MS plate to a control MS plate and then returned to the growth chamber for 12-hours. D. Midrib cells in rosette leaves of a *HTH_{pro}:HTH-GFP* plant transferred from an MS plate to an MS plate supplemented with 100 mM NaCl and then returned to the growth chamber for 12-hours. E. Midrib cells in rosette leaves of a *HTH_{pro}:HTH-GFP* plant transferred from an MS plate to a control MS plate and then returned to the growth chamber for 24-hours. F. Midrib cells in rosette leaves of a *HTH_{pro}:HTH-GFP* plant transferred from an MS plate to an MS plate supplemented with 100 mM NaCl and then returned to the growth chamber for 24-hours. Fluorescence is shown in white. The yellow arrows indicate ER bodies. Scale bar is 50 μm.

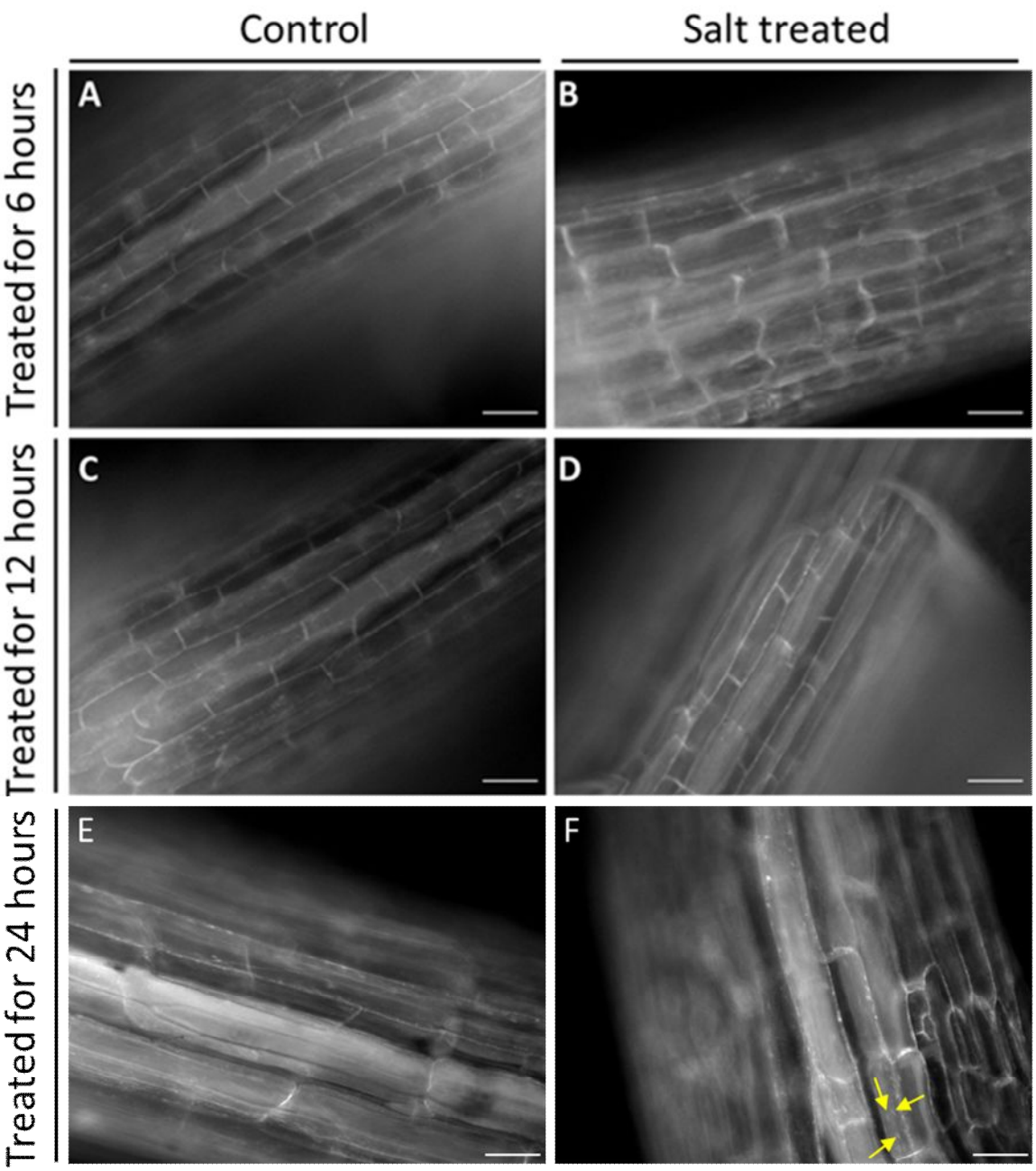
Control
Salt treated
Treated for 6 hours
Treated for 12 hours
Treated for 24 hours
A
B
C
D
E
F

Appendix D. Mandelonitrile lyase activity assays. A. The positive control assay with almond MDL as the enzyme source. B. The effect of diluting the almond MDL enzyme in P1 fraction buffer. C. The positive control assay with almond MDL as the enzyme source. D. Recombinant HTH protein tested for MDL activity. C. and D. were obtained by Le Dreff-Kerwin (2019). The y-axis displays the absorbance (Abs) of benzaldehyde product resulting from the cleavage of mandelonitrile by MDL.

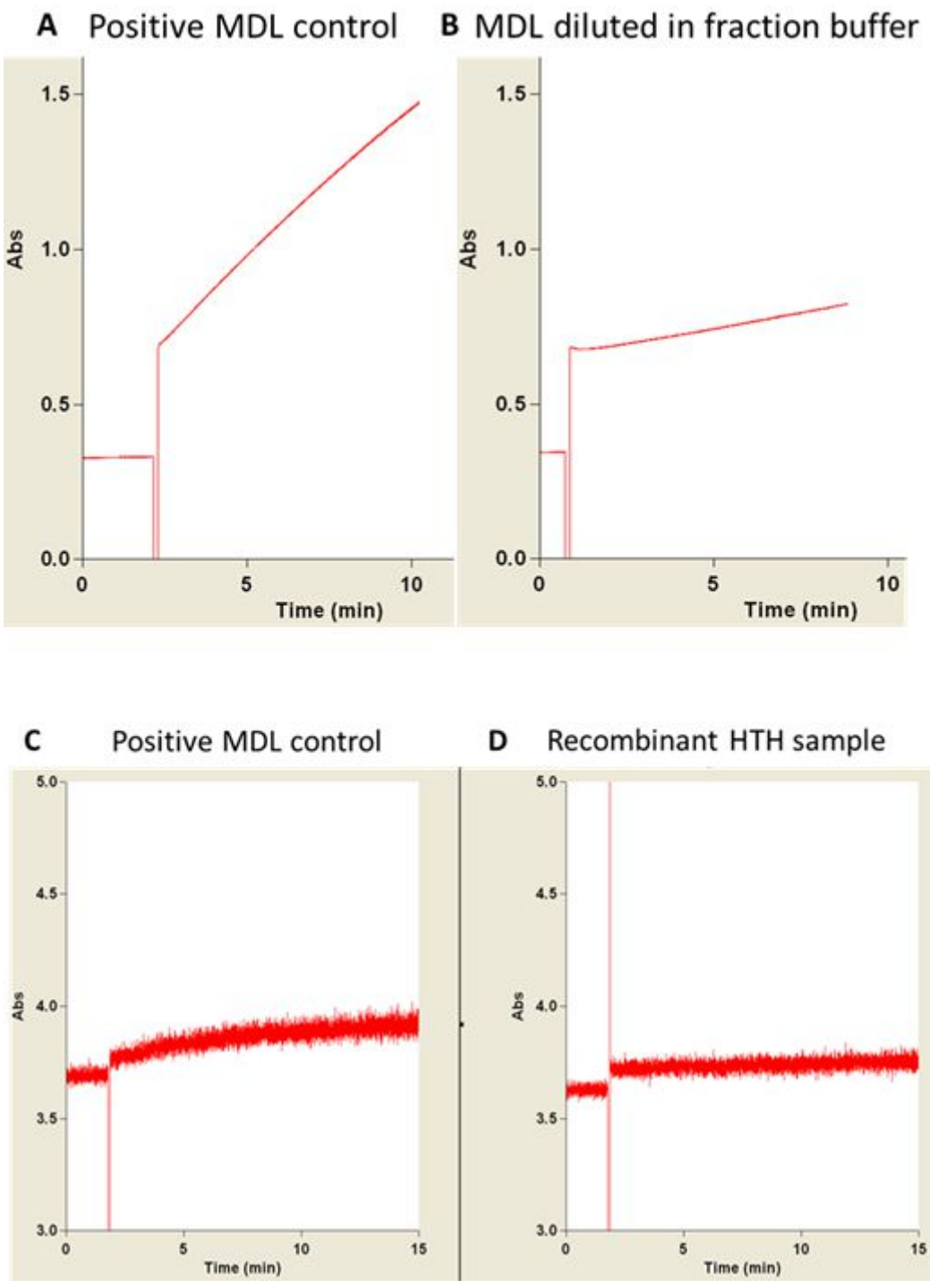
A Positive MDL control
B MDL diluted in fraction buffer
Abs
Time (min)
C Positive MDL control
D Recombinant HTH sample

Appendix E. Cloning the splice variant isoform sequence into the *HTH$_{pro}$:HTH-EYFP* construct. The gateway binary vector pGWB640 with the 5' upstream region and the genomic sequence of *HOTHEAD* cloned into the gateway cassette - *HTH$_{pro}$:HTH-EYFP* - (Chang, 2016) was modified to produce the *HTH$_{pro}$:SV-EYFP* construct (Chapter 3 Materials and Methods 3.2.**2**). *Xho*I and *Sac*I were used to excise a 1.944 kb fragment from *HTH$_{pro}$:HTH-EYFP*. A 1.863 kb fragment, synthesised by Genscript, was cloned into the *Xho*I, *Sac*I digested *HTH$_{pro}$:HTH-EYFP* vector to generate the *HTH$_{pro}$:SV-EYFP* vector. Both *HTH$_{pro}$:HTH-EYFP* and *HTH$_{pro}$:SV-EYFP* vectors have a right and left border (RB and LB); sta, region for stability in Agrobacterium tumefaciens; rep, broad host-range replication; bom, cis-acting element for transfer through conjugation; ori, ColE1 replication origin; aadA, spectinomycin-resistance gene (Spc^r); Pnos, nopaline synthase promoter; bar, bialaphos resistance gene (BASTA^r); Tnos, nopaline synthase terminator; EYFP, enhanced yellow fluorescent protein; L1 and L2, Gateway attL recombination sites for sequence exchange (modified from Nakagawa et al., 2007).

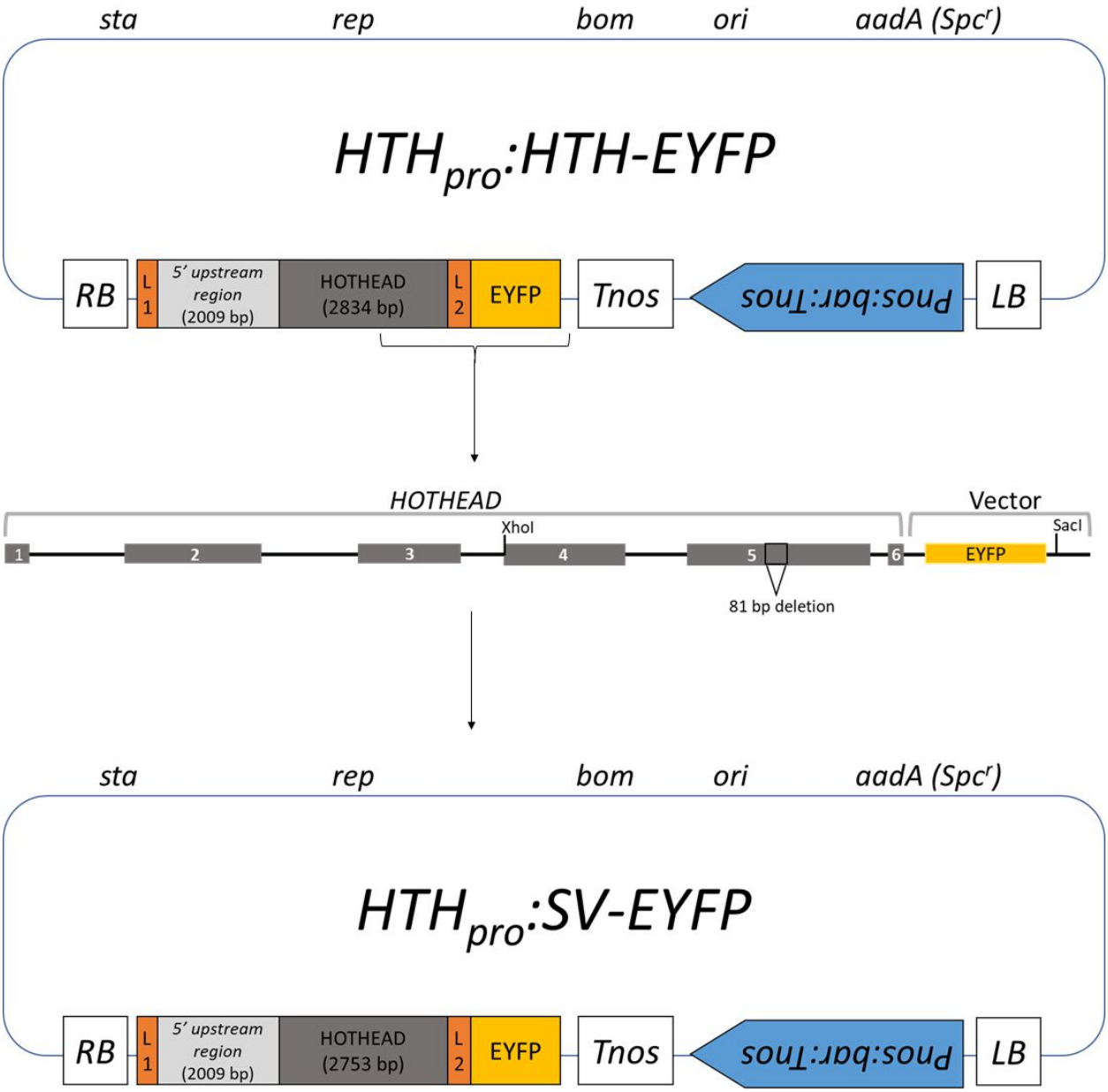
sta
rep
bom
ori
aadA (Spcr)
HTHpro:HTH-EYFP
RB
L1
5′ upstream region (2009 bp)
HOTHEAD (2834 bp)
L2
EYFP
Tnos
Pnos:bar:Tnos
LB
HOTHEAD
Vector
XhoI
SacI
1
2
3
4
5
6
EYFP
81 bp deletion
sta
rep
bom
ori
aadA (Spcr)
HTHpro:SV-EYFP
RB
L1
5′ upstream region (2009 bp)
HOTHEAD (2753 bp)
L2
EYFP
Tnos
Pnos:bar:Tnos
LB

Appendix F. The 1.863 kb fragment synthesised by Genscript. This sequence contains the 81-base pair deletion within the 5th exon of *HOTHEAD* resulting in the splice variant isoform.

ATGC - *Xho*I restriction enzyme cut site
ATGC - Exons in the *HOTHEAD* gene coding region
ATGC - Introns in the *HOTHEAD* gene coding region
ATGC - 81 bp deletion in the splice variant construct
ATGC - Vector sequence
ATGC - *Sac*I restriction enzyme cut site

> Genscript 1.863 kb fragment

CTCGAGTAACAGGAGTAATATTCAAAGATGAGAAAGGTAATCAACACCAGGCTTTACTCTC
GAATAGAAAGGGAAGTGAAGTGATCTTATCTAGTGGAGCTATTGGGTCACCACAGATGCTG
ATGTTAAGTGGGATTGGACCTAAGAAGGAGCTTCAGAGGCTGAAGATTCCTGTGGTTTTAG
AGAATGAGCATGTAGGAAAAGGAATGGCTGATAATCCCATGAACACGATCTTGGTGCCTTC
AAAGGCGCCTATAGAGCAGTCACTTATTCAGACTGTTGGAATTACAAAGATGGGTGTGTAT
GTTGAAGCCAGTACTGGCTTTGGGCAATCTCCTGAGAGTATTCATACTCACTATGGGATTA
TGTCGAACAAGGTAACGTAACTTTGTTGTTGGTGTCTTTGTAGGAGAATGTTGTTTGATGTT
AAGGAGATAATGGTCTTTTGATTTTGTATGCAGAATGAATTGTTTTCCACCATTCCTGCAAA
GCAGAGAAGACCAGAAGCAACGCAAGCTTACATCACAAGAAACAAATACCAACTTCACGAA
GCATTCAATGGAAGTTTCATCTTGGAGAAACTTGCTTACCCGATCTCTAGAGGGCATTTGA
GCTTGGTCAACACAAATGTTGATGACAACCCTTCAGTCACCTTCAATTACTTTAAACACCCG
TGTGACAAGCAAAACGTACACAAGATGCTTAGCTTAAGCGTCAAGGCAAACATCAATCTAA
GGCCAAAGCAACTGAACGATACCAAATCAATGGCTCAGTTCTGCAAAGACACTGTTGTCAC
AATCTGGCACTACCATGGTGGATGTCTTGTGGGTAAAGTTGTGAGCCCTAACCGCAAAGTT
CTTGGTGTCGACAGGCTCAGAGTTATTGATGGTTCAACGTTTGACGAGTCTCCAGGAACCA
ACCCGCAAGCTACTATGATGATGATGGGAAGGTAAATCAAAATCATTACCAACATAATGAAT
TGGAGGTTTTCTTTTTAGTTCAATATATAAACAGAGGATTTGTCAATCTTTGCAGATACATGG
GAGTCAAGATTCTTCGGGAGAGACTTGGAAACAAAGCTGGTGTTAAGGGCGAATTCGACC
CAGCTTTCTTGTACAAAGTGGTTGATAACAGCATGGTGAGCAAGGGCGAGGAGCTGTTCA
CCGGGGTGGTGCCCATCCTGGTCGAGCTGGACGGCGACGTAAACGGCCACAAGTTCAGC
GTGTCCGGCGAGGGCGAGGGCGATGCCACCTACGGCAAGCTGACCCTGAAGTTCATCTG
CACCACCGGCAAGCTGCCCGTGCCCTGGCCCACCCTCGTGACCACCTTCGGCTACGGCC
TGCAGTGCTTCGCCCGCTACCCCGACCACATGAAGCAGCACGACTTCTTCAAGTCCGCCA
TGCCCGAAGGCTACGTCCAGGAGCGCACCATCTTCTTCAAGGACGACGGCAACTACAAGA
CCCGCGCCGAGGTGAAGTTCGAGGGCGACACCCTGGTGAACCGCATCGAGCTGAAGGGC
ATCGACTTCAAGGAGGACGGCAACATCCTGGGGCACAAGCTGGAGTACAACTACAACAGC
CACAACGTCTATATCATGGCCGACAAGCAGAAGAACGGCATCAAGGTGAACTTCAAGATCC
GCCACAACATCGAGGACGGCAGCGTGCAGCTCGCCGACCACTACCAGCAGAACACCCCC
ATCGGCGACGGCCCCGTGCTGCTGCCCGACAACCACTACCTGAGCTACCAGTCCGCCCT
GAGCAAAGACCCCAACGAGAAGCGCGATCACATGGTCCTGCTGGAGTTCGTGACCGCCG
CCGGGATCACTCTCGGCATGGACGAGCTGTACAAGGCTTAGAGCTC

Appendix G. Micrographs showing SV-EYFP localization in the developing trichomes on an emerging leaf of an 11-day-old transgenic plant. A. SV-EYFP fluorescence is shown in yellow. B. Autofluorescence is shown in red. C. Merged fluorescence and autofluorescence. D. Brightfield image of the trichomes on an emerging leaf. Imaged was acquired by Erica Cushnie (an undergraduate thesis student). Scale bar is 100 μm.

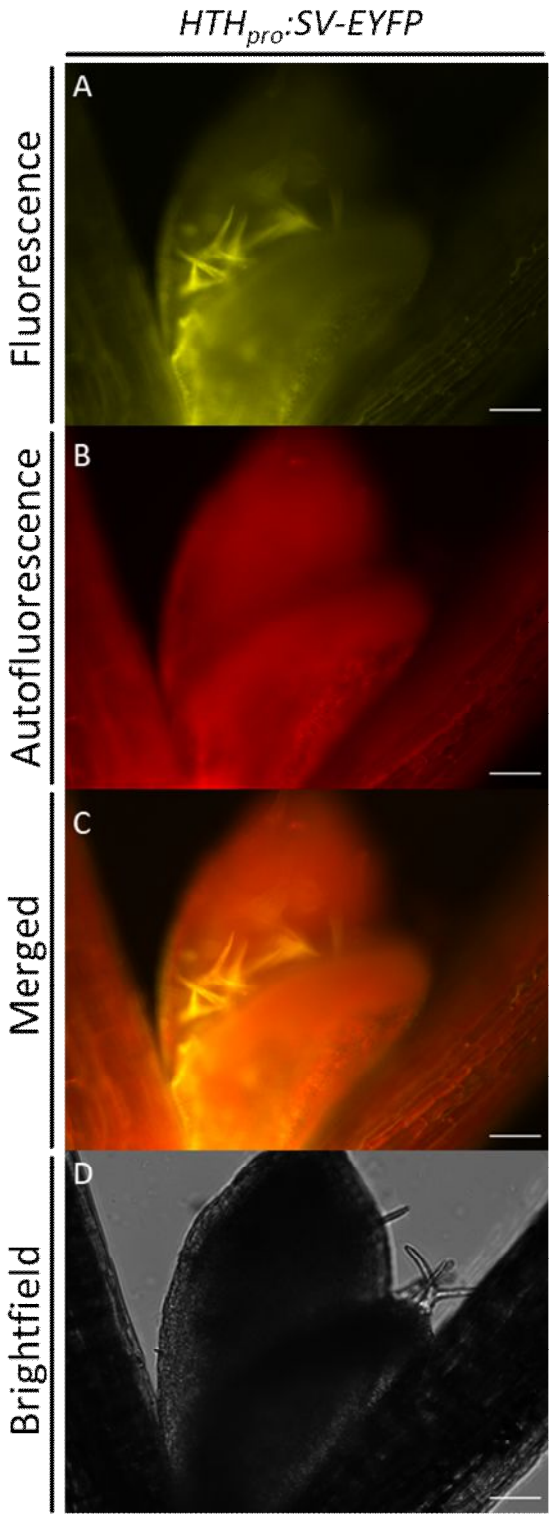
HTH$_{pro}$:SV-EYFP
Fluorescence
Autofluorescence
Merged
Brightfield
A
B
C
D

Appendix H. Ribbon diagrams showing hypothetical three-dimensional structures of HOTHEAD and the HOTHEAD splice variant. Models were generated using PHYRE2 and PYMOL.

A. Hypothetical structure of the full-length HTH protein modeled onto pyranose dehydrogenase AmPDH (PDB: 4H7U). The black arrow indicates the random coil that will refold to an alpha helix in the splice variant model.

B. Hypothetical structure of the splice variant HTH isoform modeled onto pyranose dehydrogenase AmPDH (PDB: 4H7U). The black arrow indicates the conserved alpha helix structure that was deleted and formed from what would normally be a random coil.

C. Hypothetical structure of the full-length HTH protein modeled onto mandelonitrile lyase PdMDL2 (PDB: 1JU2). The black arrow indicates the random coil that will refold to an alpha helix in the splice variant model.

D. Hypothetical structure of the splice variant HTH isoform modeled onto mandelonitrile lyase PdMDL2 (PDB: 1JU2). The black arrow indicates the conserved alpha helix structure that was deleted and formed from what would normally be a random coil.

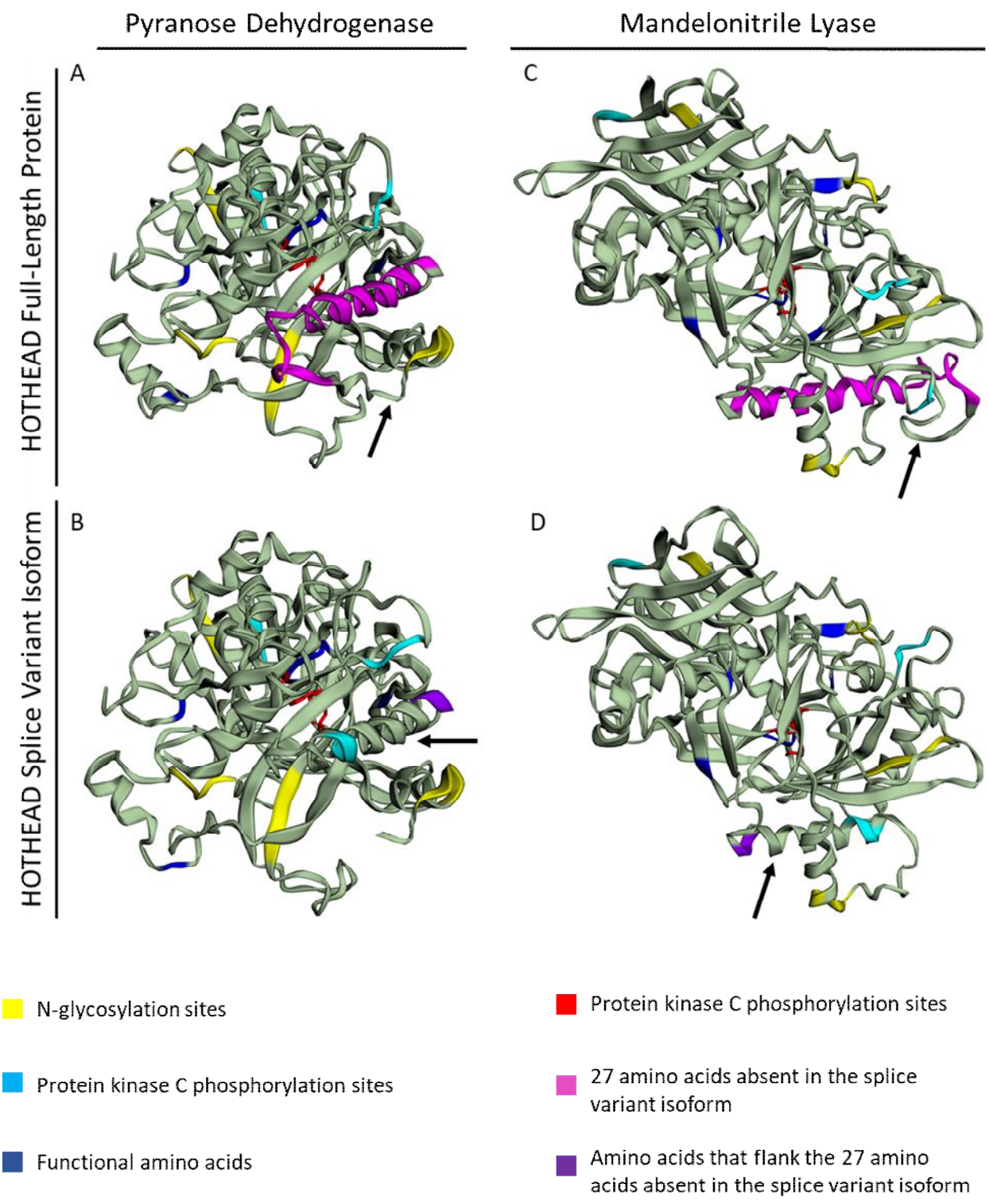
Pyranose Dehydrogenase
Mandelonitrile Lyase
HOTHEAD Full-Length Protein
HOTHEAD Splice Variant Isoform
A
B
C
D
N-glycosylation sites
Protein kinase C phosphorylation sites
Functional amino acids
Protein kinase C phosphorylation sites
27 amino acids absent in the splice variant isoform
Amino acids that flank the 27 amino acids absent in the splice variant isoform

Appendix I. Immunoblot analysis of HTH-EYFP and SV-EYFP in rosette leaves, floral buds, and siliques of transgenic plants.

A. and B. Ponceau stains confirm protein transfer from 10% SDS-polyacrylamide gel to PVDF. Ponceau stain of total protein derived from A.(right) rosette leaves, A.(left) floral buds, and B. siliques.

C. and D. PVDF blots probed with an anti-GFP antibody to detect HTH-EYFP. HTH-EYFP is ~105 kDa in weight. C. No immunoreactive protein bands were detected in protein extracts from HTH-EYFP, empty vector, or SV-EYFP rosette leaves (right); immunoreactive protein bands were detected in protein extracts from HTH-EYFP floral buds (left) but not from empty vector and SV-EYFP floral buds (left). D. Immunoreactive protein bands were detected in protein extracts obtained from HTH-EYFP siliques but not from empty vector and SV-EYFP siliques.

HTH-EYFP is expected to weigh 105 kDa but a protein band of this weight was not detected in this experiment, likely due to protein degredation. The Empty vector-EYFP transgenic plant contained no fluorescently tagged proteins and was used as a negative control. Two independently transformed from Ws and *hth-9* HTH_{pro}*:HTH-EYFP* transgenic lines were probed for the presence of SV-EYFP. As there was no SV-EYFP detected in this immunoblot, no conclusions on SV-EYFP expression can be made. The protein bands on this blot were visualized using a general ECL reagent. HTH-EYFP is ~105 kDa, SV-EYFP is ~102 kDa. Marker (M) is in kDa.

This blot was not repeated due to the shutdown of the University of Waterloo during the 2020 global covid-19 pandemic.

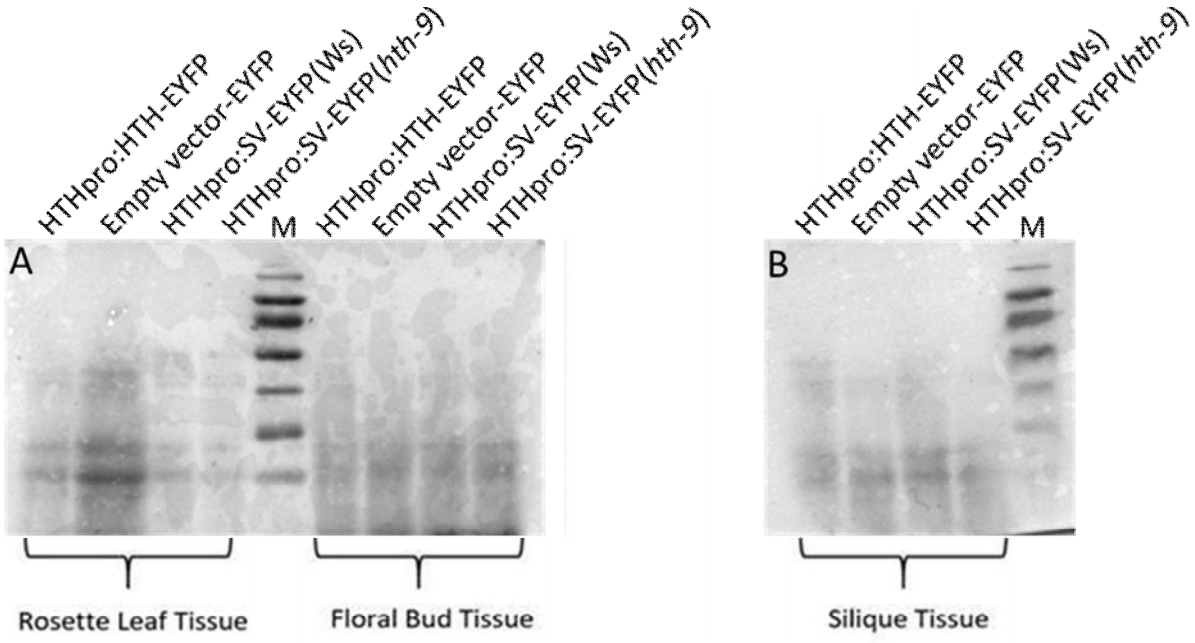
HTHpro:HTH-EYFP
Empty vector-EYFP
HTHpro:SV-EYFP(Ws)
HTHpro:SV-EYFP(hth-9)
M
A
Rosette Leaf Tissue
Floral Bud Tissue
B
Silique Tissue

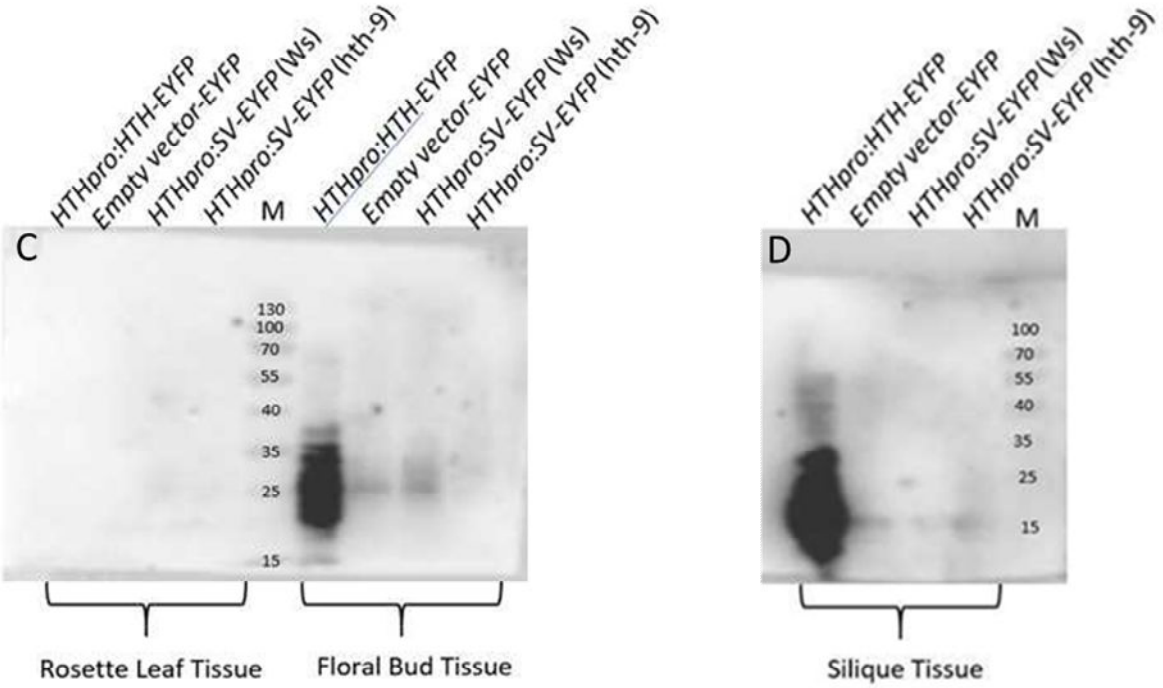
HTHpro:HTH-EYFP
Empty vector-EYFP
HTHpro:SV-EYFP(Ws)
HTHpro:SV-EYFP(hth-9)
M
C
130
100
70
55
40
35
25
15
Rosette Leaf Tissue
Floral Bud Tissue
D
100
70
55
40
35
25
15
Silique Tissue

Appendix J. A comparison of the two HTH protein isoforms within each plant line used in this study.

A. A representation of the *HTH* genomic DNA transcription and translation into either the full-length HTH or the HTH splice variant isoform. The HTH genomic DNA consists of six exons (colored boxes separated by a black line (introns)). For the full-length HTH protein, all six exons are transcribed and translated (colored boxes). For the splice variant HTH protein, five exons are transcribed and translated as above (blue, orange, pink, yellow, purple boxes), however, the fifth exon is altered by a deletion of 27 amino acids (represented by a change of the red fifth box to green).

B. A representation of the HTH protein isoforms expressed in the wild-type, mutant, and transgenic plant lines used in this study. In Ws plants, expression of the SV-EYFP transgene may result in a higher endogenous splice variant isoform protein titre than in wild-type plants, while *hth-9* mutant plants expressing the SV-EYFP transgene should express lower titres. Full-length HTH protein is denoted by the presence of the red box, the splice variant HTH protein is denoted by the presence of the green box. Transgenic versions of these proteins are tagged with enhanced yellow fluorescent protein (EYFP).

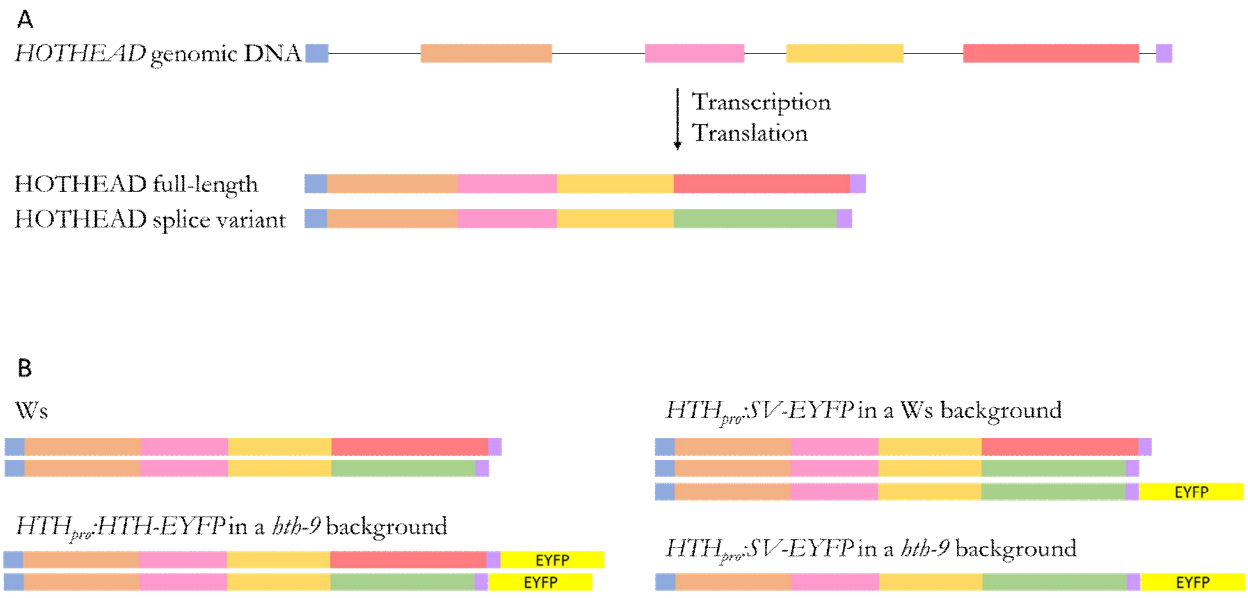
A
HOTHEAD genomic DNA
Transcription
Translation
HOTHEAD full-length
HOTHEAD splice variant
B
Ws
HTH_pro:HTH-EYFP in a hth-9 background
EYFP
EYFP
HTH_pro:SV-EYFP in a Ws background
EYFP
HTH_pro:SV-EYFP in a hth-9 background
EYFP